Miniaturized Chemistry: from Synthesis in Nanoliters to Purification and High-Throughput Screening

Zur Erlangung des akademischen Grades eines

DOKTORS DER NATURWISSENSCHAFTEN

(Dr. rer. nat.)

von der KIT-Fakultät für Chemie und Biowissenschaften

des Karlsruher Instituts für Technologie (KIT)

genehmigte

DISSERTATION

von

Janne Jasmin Wiedmann

aus Marburg

Dekan: Prof. Dr. Hans-Achim Wagenknecht

Referent: Prof. Dr. Pavel Levkin

Korreferent: Prof. Dr. Carsten Hopf

Tag der mündlichen Prüfung: 17.07.2023

“Great things are done by a series of small things brought together.”

Vincent Van Gogh

Miniaturisierte Chemie: Von der Synthese in Nanolitern zu Reinigung und Hochdurchsatz-Screening

Kurzfassung

Neue Krankheiten, wachsende Resistenzen und das Gesamtwohl einer stetig alternden Weltbevölkerung erfordern dringend die Entwicklung neuer Wirkstoffe. Dieser Entwicklungsprozess kann allerdings bis zu 12 Jahre dauern und 2.6 Mrd. Dollar kosten, wobei die Erfolgsrate in den finalen klinischen Tests im Mittel nur bei 12% liegt. Eine Optimierungsmöglichkeit, um neue Medikamente einfacher zugänglich zu machen, liegt im frühen Stadium des Entwicklungsprozesses, in welchem große Bibliotheken möglicher Wirkstoffe hergestellt und auf ihre biologische Aktivität getestet werden. Indem diese Schritte miniaturisiert und parallel durchgeführt werden, werden Zeit und teure Reagenzien eingespart. Zusätzlich könnte die Integration aller Schritte auf eine einzelne Plattform eine automatisierte und hocheffiziente Identifizierung möglicher Wirkstoffanwärter ermöglichen. Eine Lösung hierfür bietet der *Droplet-Microarray,* welcher die Handhabung hunderter nanolitergroßer Tropfen als abgegrenzte Reservoire ermöglicht.

Diese Arbeit ist in zwei Teile unterteilt. Im ersten Teil wurde eine Plattform für organische Synthese in Kombination mit enzymatischem Screening und massenspektrometrischer Charakterisierung auf Basis des *Droplet Microarray* etabliert. Hierfür wurde eine Detektionsmethode für das Fluoreszenzsignal des enzymatischen Assays in 1152 100 nL Tröpfchen entwickelt. Hierbei wurde zum ersten Mal ein miniaturisierter enzymatischer Assay in den Tropfen durchgeführt und gezeigt, dass eine vorangegangene Amid-Synthese hiermit kompatibel ist. Dies ermöglicht ein direktes Screening einer miniaturisiert synthetisierten Amid-Bibliothek über die Enzym-Inhibition mit zusätzlicher Charakterisierung der synthetisierten Strukturen über massenspektrometrische Analytik.

Außerdem wurde auf der gleichen Plattform eine Hochdurchsatz-Flüssig-Flüssig-Extraktion zur Trennung von Stoffgemischen in 400 nL pro Tropfen entwickelt. Diese Methode wurde hinsichtlich der Auftrennung von Stoffgemischen und den Einfluss der Umgebungsbedingungen mit Hilfe neuer Detektionsmethoden untersucht. Zudem wurde eine neue Art der Flüssig-Flüssig Extraktion gezeigt, welche durch die hohe Stabilität von Wassertropfen auf den hydrophilen Flächen beim Eintauchen in eine organische Phase basiert.

Der hohe Grad der Miniaturisierung und Parallelisierung, sowie die Integration einzelner Arbeitsschritte konnten die Flexibilität des *Droplet Microarray* demonstrieren. Synthese, Screening, Trennung und Charakterisierung auf einer Platte vereinend kann der *Droplet Microarray* den Beginn der Revolutionierung der Wirkstoffentwicklung darstellen.

Abstract

New diseases, growing resistances and the aim of wellbeing of a steadily aging population, demand the development of new drugs. However, the whole process from identifying a possible target to the FDA or EMA approval can take 12 years and cost up to 2.6 billion dollars with a success rate of 12% in the final clinical studies. One possible way to enhance the efficiency and speed of the drug development pipeline is to accelerate the first step in the drug development pipeline of synthesizing large libraries of possible drug candidates and screening for their biological activity. Miniaturization and parallelization of all steps of synthesis and screening allow us to save time and costly reagents. Integrating all steps on one single platform would make the whole process even more efficient and would allow a fully automated and seamless identification of possible hit candidates. As a solution for this challenge, the Droplet Microarray was introduced. This platform enables the creation and manipulation of small droplets in nanoliter size as single reservoirs, separated by hydrophobic borders. Although mainly used for miniaturized cell culture, some applications of chemical synthesis have been already presented.

This thesis is separated in two main chapters. In the first part, the Droplet Microarray was used to develop an integrated platform uniting organic synthesis, enzymatic screening and mass-spectrometry-based analytics. Therefore, a readout method was established and adapted for an array of 18 × 64 100 nL droplets based on a fluorescent signal from an enzymatic assay. This was the first time of performing this highly miniaturized enzymatic assay on the Droplet Microarray. Furthermore, the compatibility with an amide-coupling reaction was demonstrated, to allow the direct screening of a miniaturized synthesized library of amides for enzyme inhibition, as well as structure identification by mass-spectrometry right after synthesis.

In addition, a new separation method was developed on the same platform by performing high-throughput liquid-liquid extraction with 400 nL per droplet. The method was investigated in terms of separation performance and environmental impacts with newly established readout methods. Furthermore, a completely new liquid-liquid extraction method was developed, which was enabled by the high stability of an array of aqueous droplets on the hydrophilic spots upon immersion in an organic solvent.

Highly miniaturized and parallel experiments and the integration of different working steps in one workflow could demonstrate the versatility of the Droplet Microarray. Uniting synthesis, screening, separation and characterization on one chip, this combined platform can be the first step of revolutionizing drug discovery.

Preface

This Thesis is based on results of my research in the group of PROF. DR. PAVEL LEVKIN between March 2020 and July 2023 at the INSTITUTE OF BIOLOGICAL AND CHEMICAL SYSTEMS – FUNCTIONAL MATERIAL SYSTEMS (IBCS-FMS) at KARLSRUHE INSTITUTE OF TECHNOLOGY (KIT).

The results in Chapter 3.1 were obtained in a collaboration with SANOFI

Parts of the results were presented at the following conference as poster:
ELRIG DRUG DISCOVERY 2022 (4^{th}-5^{th} October 2022, London, UK)

Parts of this thesis in chapter 3.2 are based on a concept developed by YELDA DEMIRDÖGEN in a previous Master Thesis[1] in our group and have been published in *small* with shared first authorship.[2] The part done in the Master Thesis will be indicated, as well as any contributions by other co-authors.

Parts of the results were presented at the following conference in a conference talk:
SLAS2022 INTERNATIONAL CONFERENCE & EXHIBITION (05^{th}-9^{th} February 2022, Boston, USA)

The research was funded by the MINISTERIUM FÜR WISSENSCHAFT, FORSCHUNG UND KUNST BADEN-WÜRTTEMBERG within the project MALDIDROPSCREEN2.

The project MALDIDROPSCREEN2 was conducted as a collaboration between the group of PROF. DR. PAVEL LEVKIN at KIT and the group of PROF. DR. CARSTEN HOPF at the CENTER FOR MASS SPECTROMETRY AND OPTICAL SPECTROSCOPY (CEMOS), UNIVERSITY OF APPLIED SCIENCE in Mannheim.

Hiermit versichere ich, diese Arbeit selbstständig verfasst zu haben, dass ich keine anderen als die angegebenen Quellen und Hilfsmittel benutzt habe, dass ich die wörtlich oder inhaltlich übernommenen Stellen als solche kenntlich gemacht habe und die Satzung des KIT zur Sicherung guter wissenschaftlicher Praxis in der jeweils gültigen Fassung beachtet habe.

Karlsruhe, den 13.06.2023

Table of Contents

1 Introduction

With a steadily growing and aging population, there is an urgent demand for developing new treatments for new upcoming diseases. In addition, the growing resistance of bacteria against commonly used antibiotics can currently lead to infections without any conventional treatment options. Moreover, the outbreak of the COVID 19 pandemics, which arrived in Germany at the beginning of this work in spring 2020, drastically demonstrated the need for accelerated drug development processes.[3] A huge challenge is the high costs and time effort for the development of a new approved drug. With a 12% success rate in a final clinical trial,[4] approximated costs of 2.6 billion USD and around 12 years of development from the target identification to an FDA approved drug,[5] the whole process needs to be optimized to ensure accessible drugs for every patient. There are already a few approaches suggested to lower the costs and time in the early-stage drug development process with the synthesis and screening of large compound libraries for possible drug candidates. Target-guided synthesis and computational models can be a solution to reduce the number of tested compounds,[6] but they also requires large amount of time, and high computing capacity.[7] Furthermore, the system must be understood very well to make exact predictions, which is a huge drawback for the development of orphan drugs for rare diseases. On the other hand, the chance to find an unpredicted hit is increasing with the number of screened compounds.[8] One possibility to save valuable resources like chemicals, biological material and time and still covering a large chemical space is miniaturization, parallelization and integration of all single steps in early drug discovery on one platform.[9]

1.1 Combining Miniaturized Chemical Synthesis with Biological Evaluation

So far, libraries of drug candidates need to be synthesized in laborious work by chemists in the lab. Every compound needs to be synthesized, purified and characterized before it can be screened in a biological assay. The biological activity can be evaluated either by a cell-based assay, enzymatic inhibition or binding assay. This all is extremely costly in terms of time and manpower, but also of material consumption for the bulk synthesis and the cells or proteins. However, in biology and biochemistry the idea of miniaturization and parallelization came up more than seventy years ago, when the 96-well plate was invented.[9,10] Until today, high interest in saving those rare ingredients promoted the development and wide application of highly miniaturized high-throughput microtiter plates in biological and biochemical experiments, with 1536 single wells holding 3 – 10 µL of sample solution. Furthermore, highly complex liquid handling robots were developed to enable the handling and manipulation of those small

volumes in an automated and high-throughput way. Somehow, this mindset of miniaturization and parallelization was barely taken into account by the chemical world for a long time, even though only a miniaturized, parallelized and integrated way of synthesis and screening for new compounds can finally allow the ultimate goal of affordable and efficient drug discovery.

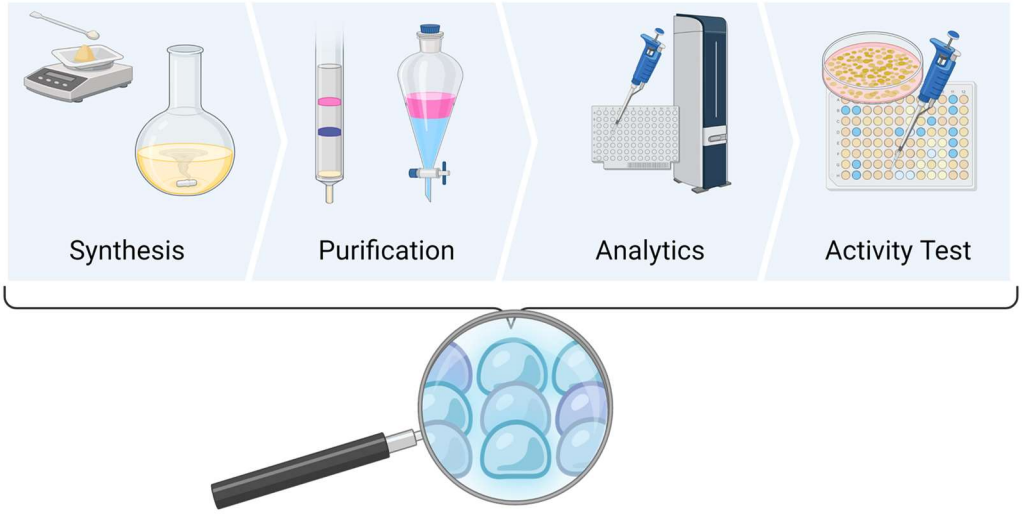

Figure 1: Miniaturization and combination of all steps in early-stage drug discovery to enable an efficient and sustainable workflow.

1.1.1 Small Scale High-Throughput Synthesis and Workup

The most established method for miniaturized, high-throughput organic synthesis is the solid phase synthesis (SPS). Here, a chemical linker moiety is used to attach the starting materials to a solid support. The reaction is carried out by addition of the required reagents in excess, which can be easily removed together with most unwanted side products by a washing step. The solid support can consist of beads, which can be transferred to different reaction vessels, like it is done in the split and mix approach.[11,12] For increased throughput and lower reagent consumption, this procedure was transferred to microtiter format with robotic sample handling.[12] Despite the comparably easy handling and purification of the compounds to the beads, the one-bead-one-compound libraries require an additional tag, like in DNA-encoded libraries to identify the synthesized structure afterwards[13] FRANK *et al.* transferred this system to an array format by developing the SPOT synthesis. In this case, a membrane is used as solid support and the reagents are added in a droplet format.[14] Especially for synthesis of oligomers like peptides or oligonucleotides, these solid phase approach has been commercially established to create customized peptide or nucleotide microarrays (JPT PEPTIDE TECHNOLOGIES, PEPPERCHIP, ARRAYSTAR INC, MICROARRAYS INC).

Downscaling of a reaction in solution phase was first used to screen for optimal reaction conditions for a certain set of limited starting materials.[9] SANTANILLA *et al*. showed the optimization of Pd-catalyzed cross couplings in a 1536 well plate.[9] All solutions were handled with an automated pipetting robot MOSQUITO, which allows aspiration and mixing within the needle before dispensing the already well mixed reaction solution in a single droplet. The reaction was done in high boiling and plastic-compatible solvents like dimethyl sulfoxide (DMSO) and N-methyl-2-pyrrolidone (NMP) and the readout was performed in a multiplexed way with liquid chromatography-mass spectrometry (LC-MS) after quenching of the reaction mixture. Hits were confirmed with ultra-performance liquid chromatography-MS (UPLC-MS). In this case, the focus was set on the reaction optimization, without any further use of the synthesized product except for determination of the reaction yield. The system of miniaturized reactions in microtiter plates was further developed by MAHJOUR *et al.*, where a special glass 1536-well microtiter plate was used to enable heating and sonication as well as less plastic-compatible solvents like dimethyl formamide (DMF) to broaden the scope of possible reactions.[15] Furthermore, the group implemented a biochemical binding assay by adding a protein directly to the crude reaction mixture for affinity-selection mass spectrometry (ASMS).[15]

Besides cross coupling reactions mentioned above, which are widely used in medicinal chemistry, multicomponent reactions are perfectly suited to create large and diverse libraries out of a limited number of starting materials. Hence, the optimization of reactions like the Ugi three- and four-component reaction are often investigated to analyze structure-related reactivity profiles, but also to create highly diverse libraries for screenings based on a limited amount of starting materials.[16,17]

With a more complex setup, SUTANTO *et al*.[17] were able to synthesize and purify a library in a parallel manner. Here, a highly diverse library of acryl amides was synthesized by the Ugi four-component and a Passerini three-component reaction in 96-well glass plates in 1.5 mL. For reaction workup, the product was precipitated and in a complex, in-house built filtration system filtered and washed to gain pure product. The comparably high amount of 0.5 mmol product allowed analytics with nuclear magnetic resonance spectroscopy (NMR) to confirm the purity. In the following next miniaturization step, the same reactions were performed in a 384 well plate using an acoustic droplet ejection liquid dispenser. At this scale, the purification by precipitation was not possible anymore, but the synthesis could be confirmed by direct injection of the crude mixture into a mass spectrometer.

Another example to mention is the work of GAO *et al*., who used 384-well plates to perform different multicomponent reactions in a 10 µL scale using 300-500 nmol of starting material. While stock solutions were prepared in the high-boiling solvent ethylene glycol to be dispensed in low volumes with the ECHO acoustic dispenser, the main reaction solvent was added with multichannel pipettes. Using solvents with lower boiling points like dichloromethane (DCM) and methanol (MeOH), the well plates were sealed for incubation at room temperature without significant loss. Those libraries consisting of several multicomponent reactions were not further used for biological screening, as the focus was set to compare different multicomponent reactions and their yield. The synthesized products were analyzed in a chemoinformatic approach to evaluate and compare their biophysical properties to FDA approved drugs.[18]

For reaction workup in bulk synthesis, Liquid-Liquid Extraction (LLE) is a fast method to remove unwanted compounds in the crude reaction mixture by their affinity to organic or aqueous phases.[19] It is widely used in laboratory and industrial workup procedures, but its miniaturization is challenging due to the complex solvent handling requirements. PENG *et al*. developed an automated liquid handling workstation to perform LLE in 96-well plates in 3.2 mL in total per well to remove amines from crude mixtures.[20] Another approach is the single-drop microextraction (SDME), where small droplets of an organic solvent are presented on the tip of a syringe to extract components from another phase. This allows the extraction into small droplets of microliters.[21] Despite the high level of miniaturization, this method requires a complex setup and is challenging if performed in high-throughput for the parallel purification of an array of samples.[22]

1.1.2 Small Scale Analytics

As described in the chapter before, LC-MS is in most cases the analytical method of choice, as it can be used to separate a crude reaction mixture in the chromatography step. The retention time and number of peaks in the chromatogram gives information about the amount and polarity of the compounds, for example how much starting material is left or if a side reaction is occurring. More important, the purified sample is directly injected into a mass spectrometer to gain further insight into the chemical structure.[23] This can be used to clearly identify if the expected product was synthesized or to identify side reactions. This method shows high sensitivity already for low concentration and low amounts of sample and it can be easily automated with already integrated autosamplers.[24] The samples are diluted in a solvent, which can be acetonitrile or an aqueous buffer, which means that the samples can be directly taken after the reaction and might only require an additional dilution step. However, a single run can

take up to 10-20 min, which is a huge drawback in terms of analyzing large libraries in a short time.[25] Further developments like the multiple injections in a single experiment run (MISER) method allow to reduce the measurement time,[9,26] as well as supercritical fluid chromatography (SFC-MS), which can be run with higher flow rates enabling a measurement time of 2 min per sample.[27] UPLC describes the further developed high-performance liquid chromatography (HPLC) method with increased performance in regard of separation efficiency, sensitivity or throughput with smaller column particle sizes and increased pressure.[28] Still, the multidimensional data obtained from a single run, containing retention times and in case of LC-MS mass spectra for each time point, results in a high load for data evaluation, in addition to comparably long measurement times.

In contrast to any analytical tool that contains a chromatography step like LC-MS, direct mass spectrometry represents a rapid alternative approach. Within the field of this highly sensitive analytical method, the surface-based matrix assisted laser desorption ionization mass spectrometry (MALDI-MS) has a huge advantage.[29] As it can be used to image a two-dimensional biological sample for mapping different biological markers, the method allows the fast screening of large arrays of compounds with comparably low sample preparation effort. A low amount of sample is added to a conductive target plate and co-crystallized with a matrix. The matrix consists of small molecules that can be excited by laser irradiation and transfer this energy onto analyte to achieve a soft ionization.[30] For quantitative readouts, standard compounds are required, as the signal intensity strongly depends on the crystallization and other compounds from the reaction present in the sample.[31] This high-throughput measurement method allowed the analysis of 1536 different reactions within 11 min to test the impact of different functional groups for different catalysis in a C-N coupling reaction by LIN *et al*.[31]

With the self-assembled monolayer desorption ionization (SAMDI) ASMS, the company SAMDI TECH INC. presents a high-throughput platform for MALDI-MS-based detection of molecules bound to an immobilized target on 1536-well format.[32] These could be exemplarily used to identify binders of the human rhinovirus 3C protease. However, initial binding was performed in well plates and the samples were transferred to the SAMDI-plates for analysis.[33]

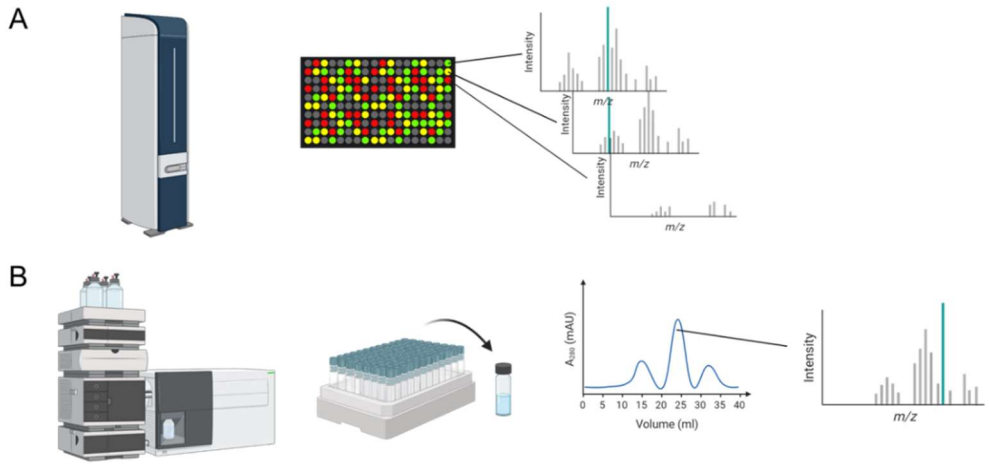

Figure 2: Analytical Methods and their throughput. A) MALDI-MS is measuring samples form a source plate to give the mass spectra for every spot. B) LC-MS is analyzing samples one-by-one and gives a chromatogram with all components present in the sample and mass spectra for every single compound within that sample.

One commonly used technique to determine the purity, but also structural information about new compounds is NMR. This method requires on the one hand quite long measurement times, and on the other hand, a high amount of highly concentrated sample in the milligram range. Furthermore, the solvent needs to be exchanged to deuterated solvents, which would require additional handling steps and the measurement needs to be performed in a certain glass tube, which requires a transferring step. Due to that, NMR is usually used to analyze potential leads, which are resynthesized in bulk in higher amounts.

In general, the analytics are often performed during the optimization step and only for several representative samples instead of analyzing the whole library. For detailed identification and characterization of the synthesized molecules, the hit candidates are synthesized in an upscaled reaction and analyzed after purification in the next step.[34]

1.1.3 Screening Methods Combined with Synthesis Steps

HABESHIAN *et al*. published a method for miniaturized amide coupling with following enzymatic screening in 2022.[34] In addition, the authors miniaturized first the synthesis of complex precursors via solid phase synthesis in 96-well plates and used an acoustic dispenser to create 80 nL reaction droplets in DMSO on the bottom of a 384-well plate in the following step. The reaction was quenched by addition of buffer and subsequently diluted to perform an enzymatic activity assay in 15 µL total volume with fluorescence readout by a plate reader. The reaction additives were still present in the assay, but showed no significant impact. Despite this example of an integrated synthesis and screening platform, samples needed to be transferred by a pipetting robot to target plates to confirm the structures via MALDI-MS. Another protein-

based assay was presented by SUTANTO *et al*.,[17] who screened their synthesized crude library obtained from multicomponent reactions with high-throughput protein crystallography.

A combination of synthesis with directly following cellular readout was presented by GEHRTZ *et al*., who performed a copper-mediated azide-alkyne click reaction in a water/DMSO mixture in 384-well plates. The crude library was tested directly after synthesis, however, only a small amount of the reaction mixture was transferred to a second plate for the in-cell western assay.[35]

A completely different approach was developed with the idea of protein templated reactions. Here, the synthesis and assay are even combined in one step, as the protein is used to catalyze the reaction itself. The most prominent example is the azide-alkyne cycloaddition, where the triazole is only formed if both starting materials are binding in close proximity to the protein. In this way, only those structures are synthesized, which are also binding to the protein.[36]

Despite all the developments described above, there is still the challenge to unify all aspects of early-stage drug discovery on one universal platform. Furthermore, most applications are using the microtiter plate, consisting of a polymer which is not compatible to some organic solvents, and also not suitable for example for a MALDI-MS-based readout. In all cases, for exact hit validation, a bulk synthesis and purification step is required, to perform dose-dependent binding assays or characterize the molecular interaction with the protein of interest without any interfering compounds and an exactly determined concentration.

1.1.4 Challenges and Opportunities of Miniaturized, Parallel and Integrated Systems

Comparing the different approaches for combined, miniaturized synthesis and screening, there can be found some challenges to be overcome.

The first challenge to solve is the array format, as the chemical reaction as well as biological/biochemical assay need a vessel with different requirements. For the chemical reaction, the platform needs to be stable against different organic solvents with the possibility to avoid evaporation. Here, the state of the art in most synthetic labs is still in the range of either round bottom flasks of glass vials for reactions in the scale of hundreds to single milliliters, where every reaction is performed individually. For the screening, the platform needs to be suitable for a certain readout, in most cases colorimetric or fluorescence-based assays require a transparent setup and a suitable geometry for the analytical device. For the last point, microtiter plates have been developed, which can be transparent, are organized in a unified format and can be closed by a lid or sealed with a thin film to avoid evaporation. Furthermore, there have been investigations towards more stable polymers like polypropylene or polystyrene with

cyclooctane copolymer or even glass to ensure stability in contact with organic solvents.[15,31] Microtiter plates are available in scales from 96 wells with 400 µL reservoirs up to 3456 well-plates, which can be used for 1-5 µL.[37] Thinking about volume reduction from several milliliters to microliters, there is still a lot of room for further miniaturization compared to microfluidic reactors, where picoliter droplets are created in an oil layer for chemical synthesis[38] as well as biological experiments.[39] Furthermore, a huge drawback is the compatibility of microtiter plates with analytical methods. While there are autosamplers for LC-MS devices, which can handle 384-well plates, the samples still need to be spotted by a liquid handler to target plates for MALDI-MS measurements, which is the optimal method for high-throughput structural analytics.

Another challenge in miniaturization of the handled volumes is the larger impact of evaporation for smaller volumes on the one hand and open platforms in comparison with reaction vials, which can be sealed tightly, heated and, if necessary, prevent the presence of water or oxygen on the other hand. For tackling the evaporation of solvents during a reaction, most methods are based on reactions that occur at room temperature, which is in addition often required by the plastic reaction reservoir. In addition, often highly volatile solvents like methanol or dichloromethane are avoided and high-boiling point solvents such as DMSO are used, which are also stable as small droplets at room temperature and atmospheric pressure. Furthermore, there are already special sealing films developed for microtiter plates, which can be also used to run reactions in methanol, when the volume of the organic solvent is comparably high[15] and the plate is sealed directly after dispensing.[31] Some more sophisticated setups have been described by LIN *et al*., where a sealing block was used to heat a reaction mixture up to 100°C in a 1536-well-plate. Developed and customized for this application, the aluminum blocks are now commercially available by ANALYTICAL SALES AND SERVICES.[9] For the handling of air-sensitive catalysts in cross coupling reactions, the whole pipeline with dispensing robots and plates were placed in a glove box to work under nitrogen atmosphere.[9] One completely different approach was the idea to avoid solvents and perform a reaction in a solid matrix material, which is melting upon laser irradiation.[40]

In addition to a successful synthesis of the product of choice, a huge challenge for the combined synthesis and screening is the purity of the synthesized and analyzed compounds. While in large scale synthesis crude reaction mixtures are usually purified via chromatography (flash chromatography, HPLC, preparative thin layer chromatography), crystallization or liquid-liquid extraction, the handling of nanomoles of compounds and the parallelization of purification

methods becomes very difficult. Therefore, most of the samples are analyzed as crude mixtures if the impact of the additional reagents to the assay can be excluded.[34,35] Still, there are examples where UPLC methods were developed to purify large libraries before screening them and the approach of precipitation was performed in a parallelized way in 96-well format.[17] For most approaches, the reactions are chosen based on a high expected yield and atom economy, resulting in low amounts of starting material or side products present.[17] One example, where a copper-mediated azide-alkyne reaction was performed and directly used in a cell-based assay show that for a first readout the purification might not be strictly necessary.[35] Nevertheless, an additional dispensing step was used to dilute the synthesized product to a suiting concentration for the assay in a new microtiter plate. While biochemical or biological assays often require low concentrations of potential active small molecules, the chemical reaction is favored in higher concentrations. Hence, most of the synthesized compounds need to be transferred to new plates to perform the dilution step, which is time and material consuming and requires precise robotics for sample uptake and release of low volumes. One solution to that was presented by HABESHIAN *et al*., where the chemical reaction was performed in DMSO in a more than 150 times lower volume compared to the following assay. In this case, the assay could be started by simply adding the reagents to the same wells.[34] For exact hit validation, a bulk synthesis and purification step is required in most steps, to perform dose-dependent binding assays or characterize the molecular interaction with the protein of interest without any interfering compounds and an exactly determined concentration. If this can be performed with a small selection of the best hits from the high-throughput screening, the whole pipeline is much more sustainable and cheaper.

The future of medicinal chemistry and screenings in ultra-high throughput in miniaturized, parallelized batches would not only increase the possibilities to find hits in the performed assay while covering larger chemical space, but also creates high amount of experimental data, which can be used for machine learning. In addition, the use of tiny amounts of often costly starting and screening materials can lower the costs drastically. With machine learning algorithms used in the experimental planning, a fully automated pipeline could be applied to many biological questions resulting in a revolutionized drug discovery, which can be applied to rare diseases as well as even personalized optimized treatments. In addition, the results of the screenings can be used to answer more fundamental questions about biological processes, without investing millions of dollars for one single application.

1.2 The Droplet Microarray as Miniaturized Platform

1.2.1 A (super)hydrophilic/(super)hydrophobic Patterned Glass Slide

When thinking about further miniaturization and integration, microtiter plates are comparably large, using microliters of solutions to perform 384 or 1536 experiments on an area of 127 × 85 mm. Furthermore, the solid walls might be necessary to prevent cross-contamination of neighboring solutions, but they also lead to high adsorption, capillary effects and prevent the sample from direct contact with a second target placed on top. However, the array format allows the direct targeting of distinct samples and the sample information is encoded in the position on the array. JOKINEN *et al*. analyzed the behavior of aqueous droplets on superhydrophobic/hydrophilic patterned silicon surfaces. They described that a droplet can be maintained within a hydrophilic area if the difference in wettability is high enough. If a droplet gets in contact with a hydrophilic area, it will be retained by superhydrophobic borders. Furthermore, the difference in wettability could be controlled in a photolithographic step, which allows precisely formed geometries.[41]

With this technique, a powerful platform beyond the dimensions of microtiter plates was introduced through the Droplet Microarray (DMA) by the LEVKIN group in 2011 (Figure 3).[42] The DMA consists of a microscope glass slide with the dimensions of 76 × 25 mm, which is compatible with many adaptors available. Instead of solid walls, repellant hydrophobic borders are maintaining a droplet in a certain geometry. This can be used to form aqueous of volumes down to 20 nL in up to 2187 spots on one single glass slide.[43] The transparent glass slide allows the characterization of the cultured and treated cells by microscopy, while the open and flat format allows new possibilities in case of sample manipulation and miniaturization.

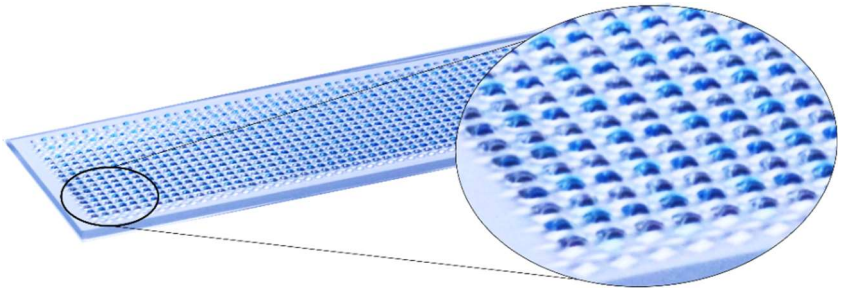

Figure 3: Photo of a Droplet Microarray containing 1152 100 nL droplets of dyed water. The square spots have a side length of 900 µm.

Each DMA is based on the modification of the microscope glass to create a reactive layer, which can react in a photoinduced reaction step with different thiols to create either hydrophobic or superhydrophobic surfaces if *1H,1H',2H,2H'*-perfluorodecanethiol (PFDT, **04b**) is used, or induce a hydrophilic characteristic using thiols with more polar groups, such as amines or

alcohols. This can be controlled photolithographically by applying photomasks during the first irradiation step. Afterwards, the remaining reactive groups covered by the photomask in the prior step can react with the second thiol. This can be used to create patterns of various geometries in an easy, two-step process.[44] In the Levkin group, several different methods have been developed to create this special reactive layer, which are presented schematically in Figure 4. All modifications are based on different principles by using a porous polymer layer, a nanoparticle coating or building dendritic structures attached to the glass slide. Therefore, they result in different special properties of the DMA slide, which will be described in the following chapter.

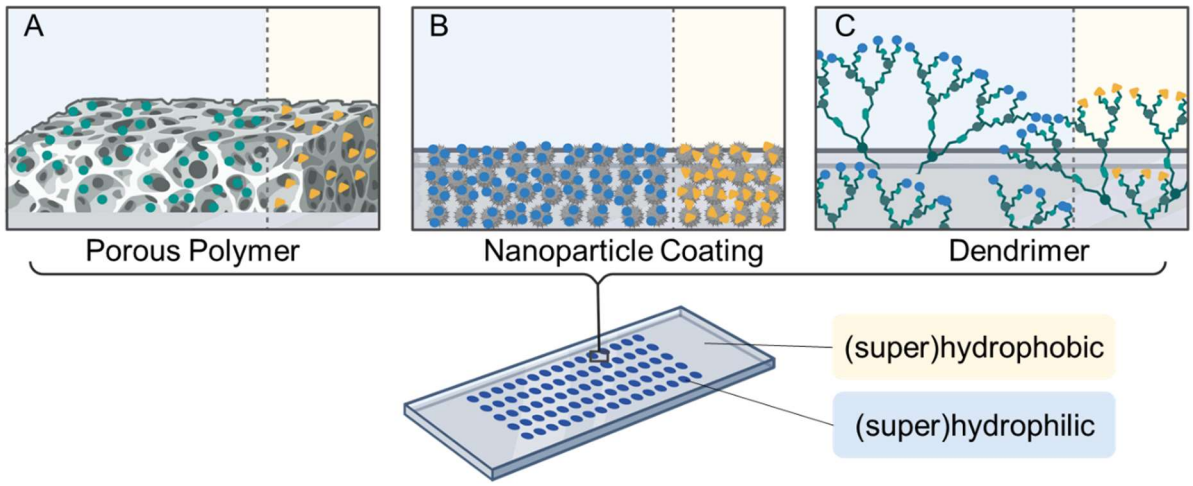

Figure 4: Different surface modifications (top) to create a patterned surface (bottom). The dashed line mimics the border of surface properties between hydrophilic (green/blue) and hydrophobic (yellow) created by a photolithographic step with the respective reagents. A) A porous polymer layer on top of the glass slides enables the surface functionalization on top and in the pores of HEMA-EDMA slides. B) The glass slide is coated with nanoparticles, which can be modified afterwards to become hydrophilic or hydrophobic to create Z-DMAs. C) A dendritic structure is chemically attached to the glass slide and grown for three generations to create the stable Dendrimer slides.

1.2.2 Surface Functionalizations

The HEMA-EDMA-Slide

The first microarray proposed by the Levkin group 12 years ago was based on a porous polymer film based on 2-hydroxyethyl methacrylate (HEMA) with ethylene dimethacrylate (EDMA) as crosslinker, the HEMA-*co*-EDMA polymer. In the first approach, the pattern was created by a second polymerization step with the hydrophobic 2,2,3,3,3-pentafluoropropyl methacrylate monomer to create the hydrophobic borders.[42] Few years later, the thiol-yne click reaction was utilized to achieve the hydrophilic-hydrophobic pattern in two irradiation steps with UV light as shown in Figure 5.[44] For that, the hydroxy groups of the polymer layer **(01)** first undergo

an esterification step with 4-pentynoic **(02)** acid to create the reactive triple bonds for the patterning *via* thiol-yne reaction (Figure 5).

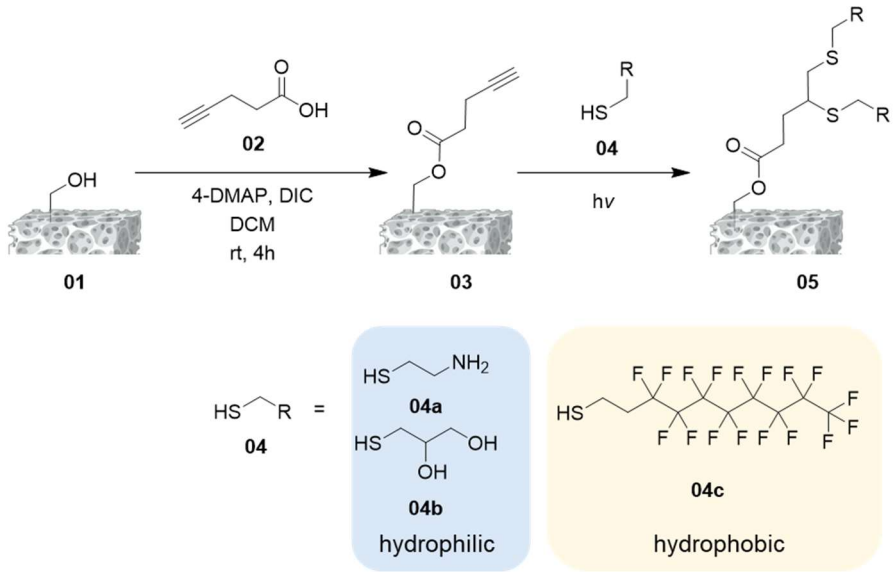

Figure 5: Surface modification of the HEMA-EDMA polymer (grey) with the esterification step and the thiol-yne click reaction. R can either contain an amine or alcohol group for hydrophilic spots (blue), or a fluorinated chain to create the hydrophobic borders (yellow). The grey squares represent schematically the HEMA-*co*-EDMA polymer.

The porous polymer (Figure 4A) creates a rough surface, which on the one hand increases the hydrophobicity to create a superhydrophobic surface. On the other hand, using cysteamine to modify the hydrophilic spots, the porous polymer can be used as solid support for solid phase synthesis. By attaching a photocleavable linker to the polymer, reactions can be carried out by addition of reagents to the different spots with an easy washing step of the whole slide to remove reagents.[45] The slide showed in addition good biocompatibility and was used in several cell-based assays. The drawbacks are the inhomogeneous surface of the polymer, which only turns transparent after addition of liquids and tends to adsorb compounds so that higher concentration of drugs need to be used to achieve same impact on the cells.

The Z-Slide

In order to optimize the surface for cell culture, the so-called Z-Slides were developed by DR. ZHEQIN DONG (unpublished). The surface modification is based on nanoparticles, which are deposited on the glass slide via spin-coating. With a vinyl group attached to the nanoparticle, they can be modified afterwards by a thiol-ene click reaction in a similar manner as the HEMA-EDMA slides. The surface of Z-DMA slides is optimized for aqueous solutions like cell medium for cell culture. The extremely repellant borders allow high volumes and extremely high stability of the droplets, also when the slide is moved or placed upside down.[46] In contrast,

organic liquids with lower surface tension tend to leak and do not form stable droplets of higher volumes. The simple preparation on the other hand also results in major drawbacks, such as reduced mechanical stability of the coating due to the weak attachment to the glass surface. Therefore, the slides can be only cleaned by rinsing as the pattern can be destroyed by simply touching the surface.

The Dendrimer-Slide

As omniphilic/omniphobic counterpart to the Z-Slide, the Dendrimer DMA was developed most recently.[47] Based on the principle of dendritic growth to increase the density of functional groups on the surface, the modification starts with chemically linking triethoxyvinylsilane to the surface. Using the thiol-ene click reaction with thioglycerol (**04b**), the number of reactive groups is doubled and an esterification reaction with 4-pentenoic acid (**08**) creates again the vinyl groups for the next cycle (Figure 6). With those orthogonal steps, the number of dendrimer generation can be controlled, while the last layer of vinyl groups is used for the thiol-ene based photopatterning.

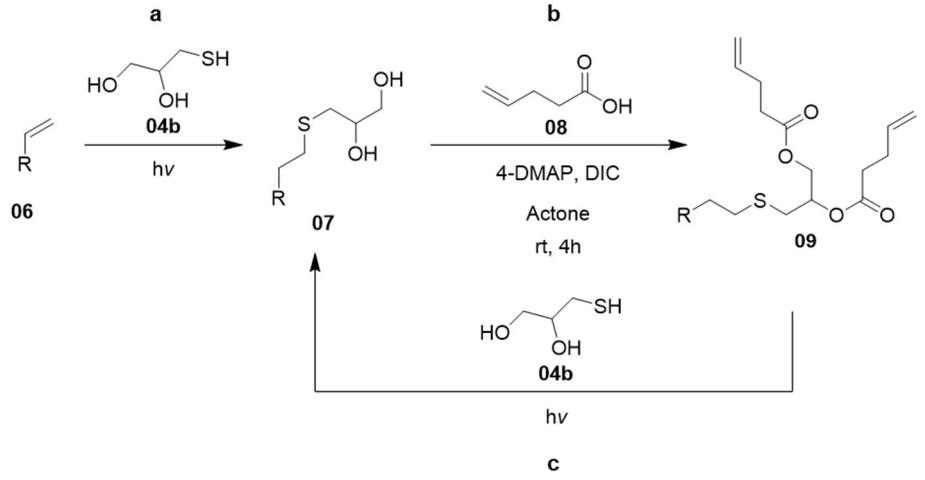

Figure 6: Creation of the dendritic structure by repeating the thiol-ene photoreaction (a, c) and an esterification step (b) starting from the surface bound silane (R = $Si(OEt)_3$) to an increasing number of thioether generations.

This modification shows advantages, as the surface properties were described as omniphilic/omniphobic, meaning that droplets can be formed from aqueous as well as organic, low surface tension liquids. Compared to the Z-DMA, optimized for aqueous solutions, the performance with aqueous buffers is slightly weaker, leading to lower maximum volumes of buffers or cell culture medium that can be handled on the dendrimer DMA. Still, stable droplets of cell culture medium can be formed and used for cell culture on those slides. In addition, the surface stays completely transparent during the whole manufacturing process. The chemical modification procedure is the most time consuming one, taking three days from a bare glass

slide to the patterned one, but the covalent chemical bonds enable a stable surface modification which is stable during washing steps with soap and a soft brush as well as during autoclaving steps. This results in a powerful surface, suitable for chemical reactions in various solvents as well as the following biological screening and sustainable due to the possibility of reusing after cleaning.[47]

1.2.3 Applications of the Droplet Microarray

The DMA was initially developed for miniaturized, high-throughput cell screenings to reduce the consumption of rare materials while creating a large dataset in cell-based screenings. In the first publication, a patterned HEMA-*co*-EDMA slide was placed in a petri dish, completely covered by cell suspension.[42] It was shown that the cells attached to the surface and were retained by the superhydrophobic borders to prevent cross contamination between the cell compartments (Figure 7 A). After showing the compatibility for Hepa, HEK293 and rat mammary carcinoma cells, the cells were seeded on slides with preprinted and evaporated transfection mixtures resulting in different fluorescent signal expression for the respective spots. With this procedure, an array of 50 400 square spots with a side length of 335 µm, separated by 60 µm thick borders was created.[42] This is on the one hand a very high number of single spots, on the other hand, there was a risk of cross contamination over the cell medium. This last point was used for investigations on cell-cell interactions between different cell types by manually pipetting the cells to certain hydrophilic regions. After attaching to the surface, the DMA was washed to remove non-adherent cells and placed in a large reservoir of cell medium to investigate the response of one cell line to the signal produced by a second cell line on a different spot.[48]

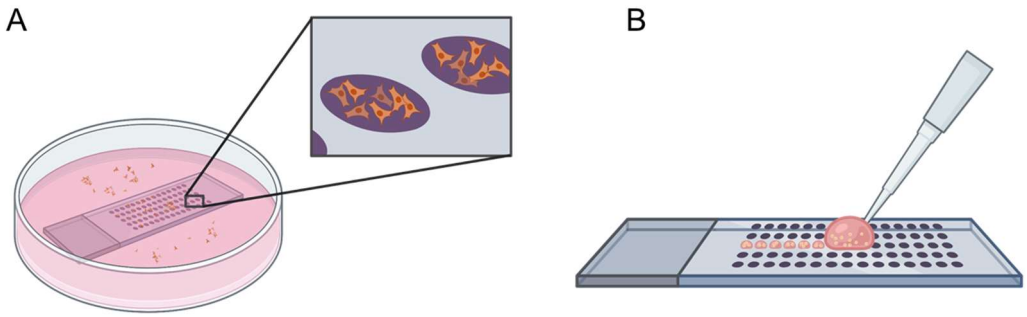

Figure 7: Schematic representations of different cell culture methods with an immersed DMA in cell suspension (A) and creation of single droplets by discontinuous dewetting (B).

To overcome the limitation of contamination, the principle of discontinuous dewetting was established.[49] Here, a large droplet containing cell suspension or reagent solution is pulled over the whole DMA. On every hydrophilic spot which gets in contact with this reservoir, a

small part is retained and forms an individual droplet (Figure 7 B). This method creates an array of single droplets containing cells, which can be cultured and treated independently. Furthermore, the so-called sandwiching-technique enabled the simultaneous addition of a compound library to the different cell-containing spots. Here, a special adapter was created to precisely align two slides facing each other. By adjusting the distance between those two slides, the two opposite spots with droplets could be connected and compounds can be transferred by diffusion.[50] With this setup, arrays of adherent cell lines,[51] down to a single cell per spot,[52] stem cells,[53] suspension cells[54] and spheroids[55] were cultured and used for drug sensitivity tests with fluorescent staining and microscopic imaging as readout. In addition to cell lines, an array of zebrafish embryos was cultured in 108 single square spots on one DMA. The eggs were cultured in 5 µL, could be treated with an array of peptoids and were then pooled in one petri dish for hatching.[56] This demonstrated a powerful miniaturized platform for screenings with low amount of consumables and a handling method, that does not require a complex setup if the compounds to screen or for staining were provided on the platform. All steps during cell culture could be in theory performed in any biological lab without the need of expensive devices.

As mentioned before, the miniaturized platform could be used to culture human derived pluripotent stem cells. Providing a platform for increased maintenance of pluripotency,[57] the DMA was used to test the impact of proteins and combination of protein mixtures for maintaining the pluripotency.[58] This is a great example of enabling a large screening of costly compounds with rare cells. Another example of using the low volumes for rare material samples is the drug sensitivity and resistance test of patient derived tumor cells from chronic lymphocytic leukemia, which were tested for different FDA approved cancer drugs.[59] With this application, the DMA shows its efficacy as a possible new standard platform for precision medicine.

For increased precision, noncontact liquid dispensers were used to address every single spot on the DMA. This was used to further manipulate cultured cells by combining several droplets after the formation of spheroids.[46] Furthermore, a colorimetric assay was established to estimate the cell viability using a document scanner.[60] This method was applied to a screening of multidrug-resistant bacteria against 2826 compounds provided by the COMPOUND PLATFORM.[61]

For a cellular readout on the molecular level of a cell, a transcriptomic analysis of cells cultured on the different DMAs and commercially available microtiter plates and in different volumes was performed. Cells were seeded on the different surfaces and several droplets were pooled together to get enough material to perform RNA isolation and sequencing.[62] It was shown that the phenotypic characterization performed by microscopic imaging was confirmed by analyzing the transcriptome. There were no significant differences observed between the different surfaces or droplet volumes, most of the genes were expressed at the same level. The largest differences were detected for the dendritic surface structure, while down to 9 nL droplets the expression was not changed depending on the volume.[62] In the next step, the whole procedure from cell culture, cell lysis, mRNA isolation to the transcription to cDNA was performed on the DMA in 200 nL droplets.[63] Subsequently, the gene expression was analyzed qualitatively by gel electrophoresis as well as quantitatively by real time polymerase chain reaction (PCR) up to a single cell per droplet.[63]

Another possibility to analyze cells on a molecular level is MALDI-MS.[64] This method requires a flat, conductive surface to give information about masses of analytes with high sensitivity and has found already broad applications in biological analysis of cellular components[65] as well as product identification after chemical synthesis.[66] To get access to this analytical method, the glass slide with its flat topography needs to become conductive. This was achieved by using Indium-Tin Oxide (ITO) coated glass slides, which have a conductive surface while maintaining the transparency for additional microscopic analytics. The cell based application was shown by analyzing a lung cancer cell line cultured in 40 nL droplets on an ITO-Z-DMA.[67] After culturing, the spots were dried and matrix applied by spray-coating. The MALDI-MSI analysis showed clear signals within the spots with a sensitivity down to a single cell per spot. Furthermore, a dose dependent curve of signal intensity of a fatty acid in an inhibition assay of the fatty acid synthase did provide a quantitative readout.[67] Showing this certain substrate independency, another possibility is to create an eDMA, a droplet microarray on an array of electrochemical cells.[68] With this setup, single droplets could be addressed and the redox signal of the solution contained at this specific position was measured. This shows the potential for an electrochemical readout for biological or biochemical applications.[68]

Not only limited to the biological applications, the DMA further was used for material development by creating an array of hydrogels with different compositions, followed by screening for their photodegradability.[69] With the idea of combining the drug response test directly with the synthesis of new drugs, the HEMA-EDMA slide was used by BREHM *et al.* to

establish a SPS platform.[45] The porous polymer containing amine groups in the hydrophilic spots was used to attach a photocleavable linker directly to the DMA. The first reaction presented was a combinatorial synthesis of tripeptides by addition of four different amino acids to different spots to synthesize 16 different compounds.[45] The release by irradiation with 365 nm uv light was shown exemplarily with doxorubicin, resulting in a time dependent release upon irradiation. Furthermore, cells were cultured on the DMA containing the bound model drug and showed a significant decrease of viability when the drug was released.[70] To show the potential in combinatorial drug synthesis, the Ugi 4 component reaction was used to synthesize a library of 588 products on one DMA. For analysis of the product, larger droplets were combined for LC-MS analysis and the whole library was detected with MALDI-MS after transferring the samples via sandwiching from the HEMA-EDMA slide to an non-patterned ITO glass slide[70]

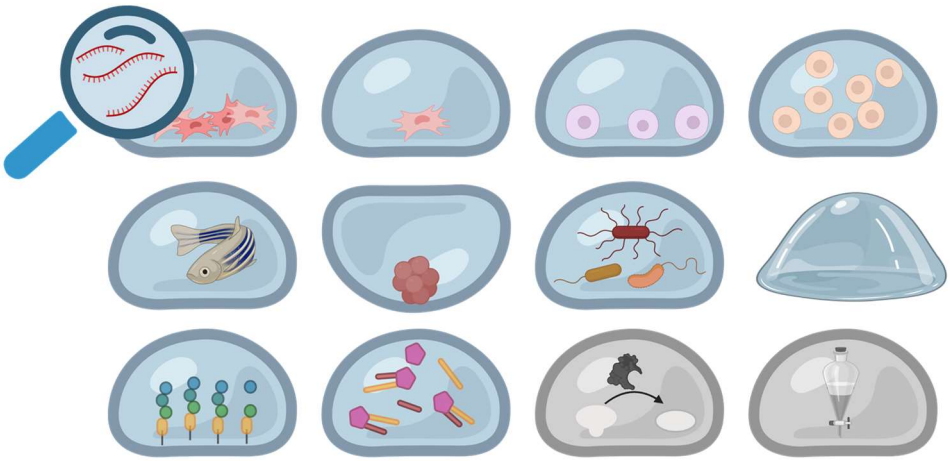

Figure 8: Overview of applications of the Droplet Microarray. From top left to bottom right: transcriptomics, cell culture, single-cell culture, stem-cell culture, suspension-cell culture, zebrafish assay, spheroid formation, bacterial screening, hydrogel formation, solid-phase synthesis, solution-phase synthesis. No enzymatic screen or extraction step was performed on the DMA.

Combining chemical synthesis with a biological screening, BENZ *et al.* presented the synthesis of a small library of lipidoids with following screening for transfection efficiency.[71] In the first approach, two differently prepared DMA slides were used, the first able to maintain organic liquids for the synthesis[72] and as second slide, a HEMA-EDMA slide was used for testing the prepared compounds in aqueous media for transfection efficiency. In a second approach, the Dendrimer DMA was introduced as optimized platform for solution-phase synthesis. The synthesis was performed in solution phase on 3 mm diameter spots by combining two different starting materials via the sandwiching method. The reaction was carried out at room temperature and characterized by UV/Vis, IR-Spectroscopy and MALDI-MS on the same

platform. Furthermore, high sensitivity up to 0.1 femtomoles on a 500 µm square spot was shown in the MALDI-MS measurements.[47] Also in this case, cells were cultured on 3 mm diameter spots, but without performing the on-chip transfection reaction.[47]

In the last 12 years, the DMA platform was continuously developed further to enable new applications. This resulted in the different surface modifications presented in chapter 1.2.2, showing different advantages for different fields. As an overview, a tabular summary of the different kinds of surface modifications to create a DMA can be found in Table 1 including the surface properties and major applications.

Table 1: Summary and Comparison of the established Droplet Microarrays. If not mentioned otherwise, the source of information is stated in the header. Missing information is stated as N/A (or was measured for this work). [a] based on experience of the author

	HEMA-EDMA[44]	Z-Slide[73]	Dendrimer[47]
$\theta_{stat}(H_2O)$ hydrophilic	4.4°	<10°	24°
$\theta_{stat}(H_2O)$ hydrophobic	170°	154°	116°
$V_{max}(H_2O)$ 900 µm spot	200	150	125
V_{max}(DMF) 900 µm spot	150	50	80
Stability	Brittle polymer, can be detached by physical force[a]	Pattern can be destroyed by touching the surface[a]	Stable against wiping with a soft brush[a]
Application biology	Cell culture[52], fish embryos[56]	Cell culture (stem cells,[58] spheroids[46]), bacteria,[74] sequencing	Cell culture (5 µL)
Application chemistry	Solid-phase synthesis[45,70]	Hydrogel synthesis	Solution-phase synthesis
MALDI-MS measurements	Weak signals[75]	Clear signals, high sensitivity[67]	Clear signals, high sensitivity

Showing the broad application of the DMA, there is still an urgent need in investigating on the possibilities of this universal platform to unite all needed steps in early-stage drug discovery. This includes the solution-phase synthesis of new compounds, a possibility to separate a crude mixture of different analytes as well as the chemical and biological evaluation of the synthesized compounds. Even if some basic investigations have been already made focusing on spots with a diameter of 3 mm and volumes of 5-10 µL,[47,71] the most important factor using the DMA is the downscaling to submillimeter and sub-microliter scale.

Despite the opportunities of all biological applications presented in this chapter, the cell-based screenings are very sensitive models with a certain chance of misleading results due to "unhappy cells". In addition, the mostly used phenotypic readout by microscopy gives only a final result after treatment without learning about the detailed mode of action of the tested compound, especially if the live/dead staining is used, while genotypic analytics are also in small scale costly and time consuming. What is still missing is an established biochemical readout to analyze a library of on-chip synthesized potential new inhibitors.

2 Motivation

While there is a huge demand for new drugs, their development is highly time and material consuming and therefore expensive and risky. Miniaturization, parallelization and integration of all steps in early drug discovery is a promising solution to accelerate identification of potential leads, while reducing the amount of material needed. Showing certain biological activities, the lead structures are further optimized to result in new possible drug candidates. First approaches have been published about microliter-sized synthesis with following analytics or screenings, but there is still a high demand for small-scale and integrated platforms.

The aim of this work was therefore the further miniaturization and integration of solution-based chemistry, including reaction optimization, purification and analytics, and an activity-based readout on the Droplet Microarray for accelerated drug discovery in a high-throughput and parallel format.

The work was divided in two main chapters, establishing first the combination of on-chip solution-based chemical synthesis with an enzymatic assay, and secondly describing a new method of on-chip, parallel extraction for separation of mixtures in nanoliter scale.

In the first part, a library of potential inhibitors for the low molecular-weight protein tyrosine phosphatase should be synthesized on-chip in 50 nL droplets *via* an amide coupling reaction. By varying the starting materials based on a known core structure and the reaction conditions, this multiplexed library should be then analyzed in an enzymatic inhibition assay. In this case, the inhibition rate could not only be used to identify the best inhibiting compound, but also to find the best reaction condition for each of the compounds. In addition, MALDI-MS screening of the synthesized library should be used to characterize the synthesized compounds.

While focusing in the first part on synthesis, analytics and screening, the second part describes possibilities of separating mixtures in nanoliter droplets by liquid-liquid extraction. Here, the work is based on a recently developed method of merging an aqueous and organic droplet for parallel, miniaturized extraction. The system should be further investigated to understand the process and methods developed to characterize it. In addition, a second way of high-throughput extraction should be developed based on the stability of aqueous droplets in contact with an organic phase.

All steps should be optimized to be performed on a Dendrimer-Droplet Microarray slide containing 1152 spots with a diameter of 900 µm to show all aspects required for accelerated drug discovery: miniaturization, parallelization and integration.

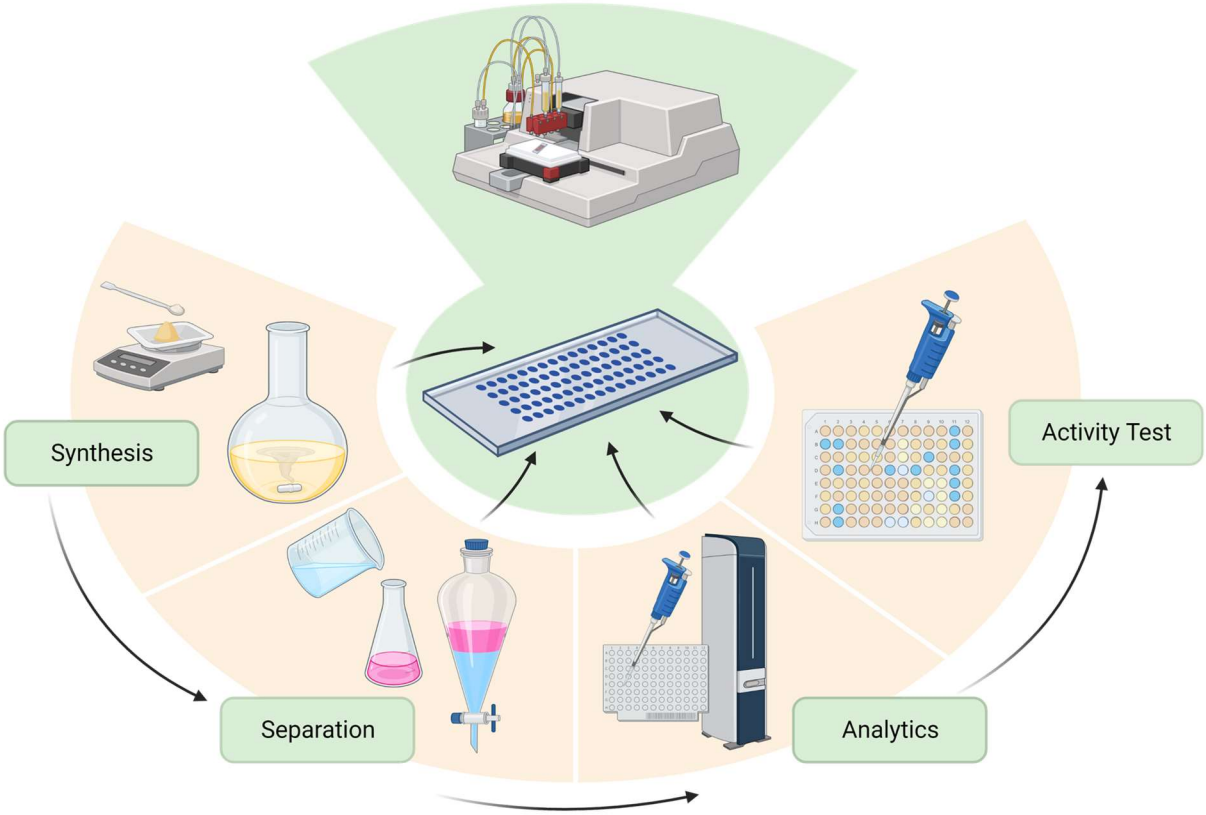

Figure 9: Overview about miniaturization and integration of an early drug discover pipeline on the Droplet Microarray. All steps from synthesis, separation to mass spectrometry for chemical analytics and biological activity tests combined on the DMA (center) by using a single liquid dispenser without additional handling steps.

3 Results and Discussion

3.1 Combining Miniaturized Synthesis with Enzymatic Readout

For highly efficient identification of new possible hits in drug discovery, miniaturization and parallelization, as well as integration of the synthesis, screening and analytics in one workflow on the same platform is required to allow a fast and economical workflow. For hit identification, protein-based assays offer a reliable and fast readout for the direct interaction of the protein of interest with some drug candidates. The possibility to combine the chemical synthesis and activity assay on the same platform can be used to accelerate and simplify first screenings for hit candidates.

3.1.1 Project Idea and Background

In a phenotypic, cell-based screening, where cell lines are treated with the compounds, the viability or shape of the cells are evaluated (Figure 10A). In this case the impact of the treatment on the whole system is analyzed. As consequence, the mode of action of the treatment might not be clear and side effects might lead to false assumptions. Compared to that, all possibly interfering pathways are removed in an enzymatic assay (Figure 10B).

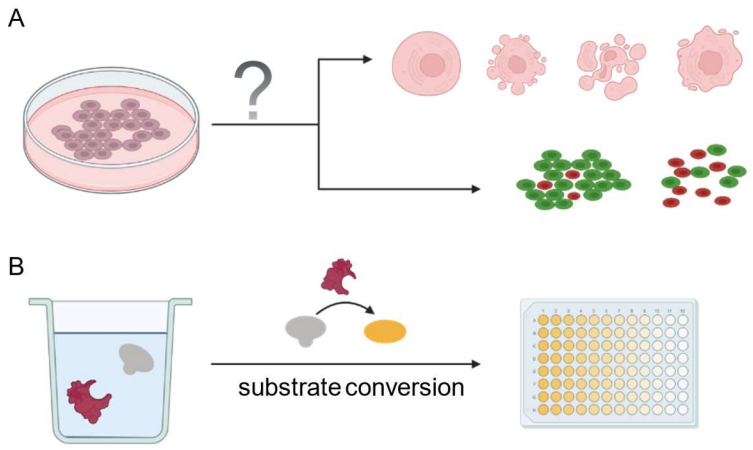

Figure 10: Cell-based and enzymatic assays. A) Cell-based assays offer a phenotypic readout of the overall system, resulting for example in cell shape analysis (top) or live-dead staining (bottom) to determine the viability. B) Enzymatic assays contain only the protein of interest and its substrate. This conversion is then measured as indicator of the enzymatic activity.

Here, the protein of interest is isolated and a buffer composition is used to maintain physiological conditions. For the readout, a model substrate is usually used, which is converted by the active protein and detected in the end. Often, the substrate changes its color[76] or fluorescence,[77] but there are also radioactive[78] or mass-dependent[79] readouts available. This simple setup results in a reliable readout to compare different potential drugs upon their interaction with the protein of interest. The main drawbacks for this kind of assays are that the

protein and its mode of action needs to be known on the one hand and available as purified and stable compound on the other hand. Furthermore, there is a need of a suitable substrate for the readout. Even if the protein of interest can be expressed in cell lines or bacteria, it is very costly. This shows the need of miniaturization for high-throughput screenings to make sure that large libraries of drug candidates can be investigated with low amounts of protein in a reproducible way.

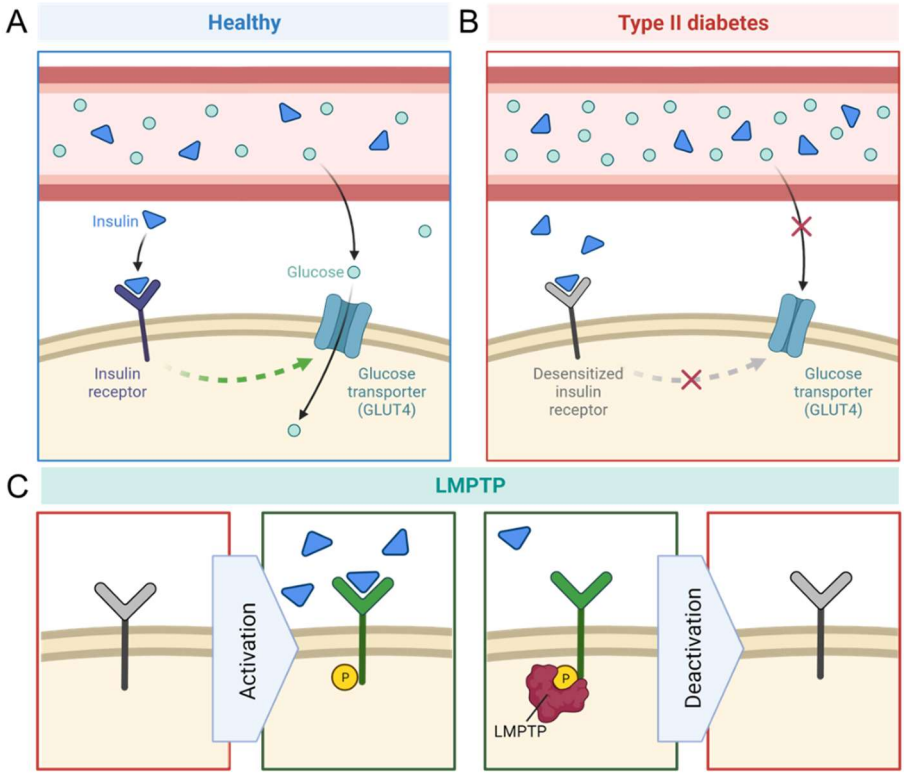

Figure 11: Insulin pathway, Type II diabetes and the role of LMPTP. A) in healthy cells, the insulin receptor is activated by insulin binding and induces glucose uptake form the blood by the glucose transporter GLUT4. B) Type II diabetes insulin receptors are desensitized against insulin and are not activated. Therefore, there is also no glucose uptake taking place. C) Activation of the insulin receptor by autophosphorylation. D) Deactivation of the insulin receptor for regulation of the glucose uptake by the enzyme LMPTP (Low molecular weight protein tyrosine phosphatase).

The target molecule of this work, the low-molecular protein tyrosine phosphatase plays a role in the insulin signaling pathway.[80] Activated by insulin binding, the insulin receptor autophosphorylates and starts a signaling pathway resulting in glucose uptake of the cell *via* the GLUT4 glucose transporter (Figure 11A) to regulate the glucose level in the blood.[81] As its antagonist, LMPTP deactivates the receptor by dephosphorylation to regulate the level of glucose uptake (Figure 11C).[82] In type 2 diabetes, insulin resistance of the insulin receptor leads to reduced glucose uptake, which can lead to severe health issues (Figure 11B).[82] LMPTP is known as a target against type 2 diabetes and thereby to prevent high-fat diet induced obesity, which is part of the metabolic syndrome.[83] STANFORD *et al.* could show that mice without

LMPTP activity could be protected from insulin resistance.[84] With a small molecule acting as uncompetitive inhibitor, the phosphorylation of insulin receptors in the liver could be increased and the high-fat diet-induced diabetes reversed.[84] This indicates a new possible treatment for diabetes type 2.[85] In addition, these inhibitors were used to prevent lipotoxicity in the liver-based HepG2 cell line after overdose of fatty acids in the context of treatment of non-alcoholic fatty liver disease.[86] This well-studied system with a core structure with known inhibitory activity[85] should be used in this work for a screening for improved inhibitors.

Due to the catalytic activity of the enzyme, the resulting signal of a small amount and concentration of the enzyme as well as the inhibiting compound can be used to analyze the substrate transfer with a colorimetric or fluorescent readout. Furthermore, the conversion rate is strongly dependent on the activity of the enzyme and can be therefore used to indicate the inhibitory activity of the compound. When compared to a starting material, a library of varied molecules can be added to different spots and the best inhibiting compound can be easily detected. Thinking further, a whole library could be synthesized and directly analyzed if the impact of the starting material, reagents and solvent on the enzyme can be excluded in a control assay. If the activity of the enzyme can be maintained even though some additional chemicals are present in the buffer, this combined synthesis and assay could not only save a lot of time and resources by avoiding transfer steps between synthesis and assay, but also serve as a readout of the chemical yield when comparing different reaction conditions with the same starting material.

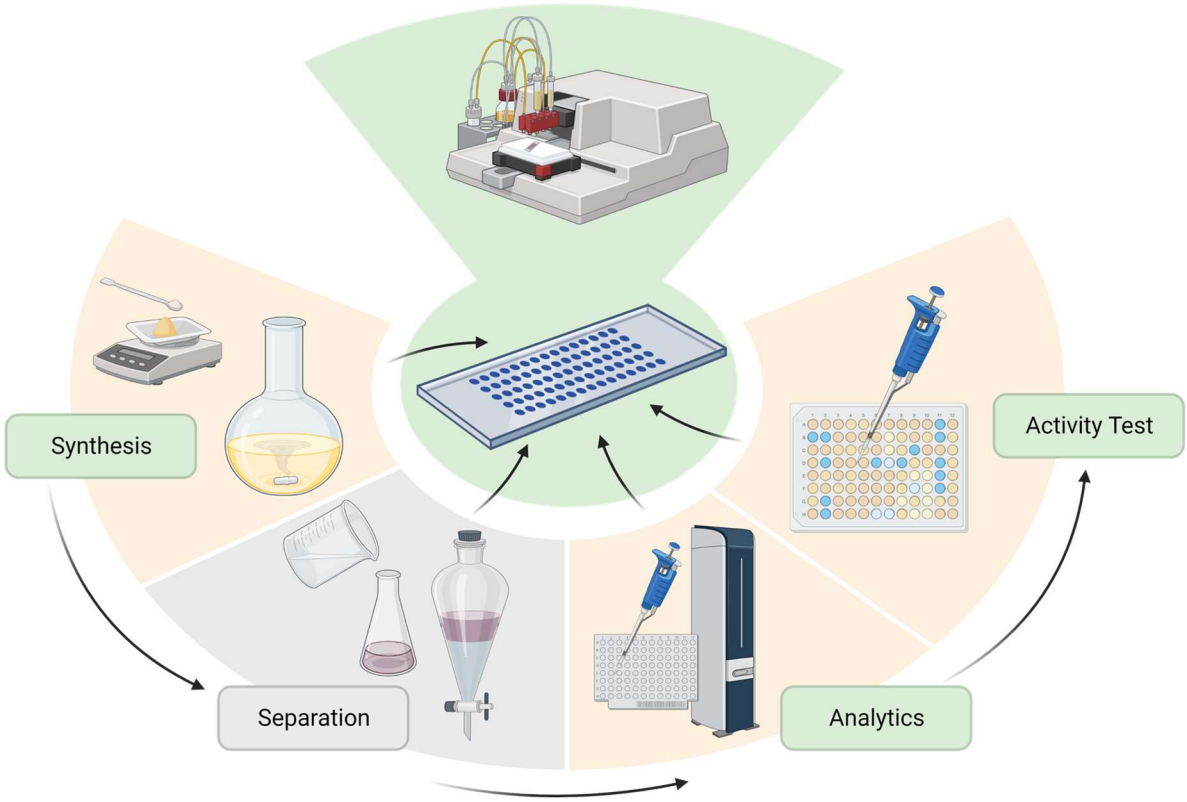

Figure 12: Goal of the project was to combine a synthesis, characterization and activity testing step on the DMA to miniaturize the whole screening process and reduce unnecessary transferring steps by simply adding reagents with a liquid dispenser.

The aim of this project was to transfer and combine the whole pipeline for the first inhibitor screening to the miniaturized DMA platform and is summarized in Figure 12. This screening includes first the synthesis of a library of possible inhibitors based on the known core structure and a following enzymatic assay to test the inhibitory activity of the synthesized compound. In addition, MALDI-MS should be investigated as structural analysis tool in small scale and high-throughput format.

The biochemical screening was adapted from a procedure performed at SANOFI based on STANFORD *et al.*[84] At SANOFI, several potential inhibitors were synthesized with an O-(7-Azabenzotriazol-1-yl)-N,N,N',N'-tetramethyluronium-hexafluoro phosphate (HATU) - mediated amide coupling step in 1 mL batches with 0.1 mmol of the acid **10** as starting material and purified by HPLC. Two model inhibitors (**12a, 12b**) based on acid **10a** were provided by SANOFI as pure compounds and were used as control reagents in this work.

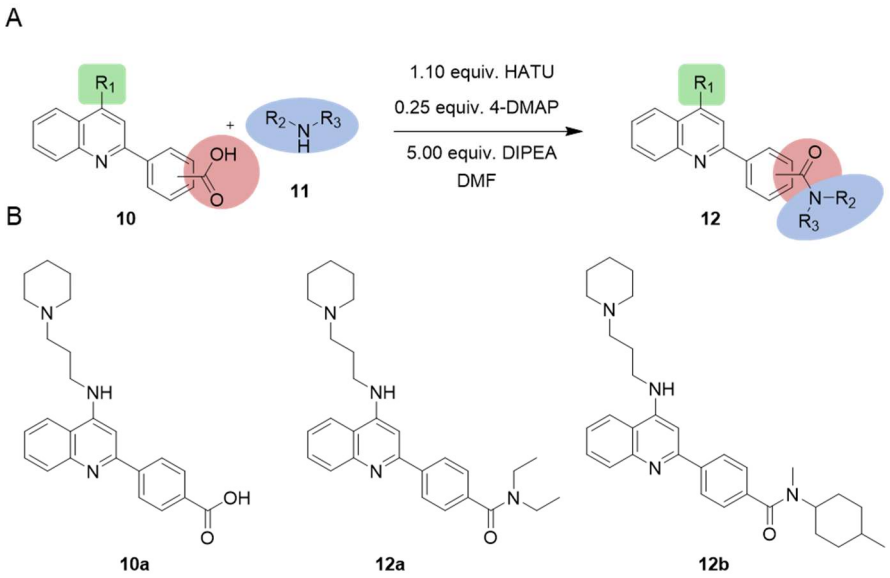

Figure 13: Reaction scheme performed at SANOFI. A) The acid could be used with varied head group (green) and with the acid group in either para or ortho position (red) with different amines (blue) to create a library. Amines were used in 1.50 equiv. or higher excess for volatile amines. Reaction scale was 0.10 mmol with 0.1 M acid concentration. B) Core structure of the acid **10a** and two amides **12a** and **12b** which were used for synthesis and assay optimization.

The pure compounds were dissolved to give a 10 mM stock solution in DMSO and added to a 1536 well plate for the enzymatic assay in the original workflow at the SANOFI lab. 5 nL of the 10 mM of a stock solution was added to each well and the assay was performed using 4 µL of buffer containing enzyme and substrate with a fluorescent readout using 8,6-difluoro-4-methylumbelliferyl phosphate (DiFMUP).

3.1.2 The First Enzymatic Assay on the Droplet Microarray

After having used the DMA for several biological applications like culturing of cells,[51,59] zebrafish[56] and bacteria,[61] a biochemical readout was still missing. Therefore, the first step in the project was to perform the first enzymatic assay on a DMA. With the overall aim of combining chemistry and biology, the dendrimer DMA was chosen, as it showed good compatibility with organic solvents in chemical reactions as well as with aqueous solutions. In the first step, the assay should be transferred from the microtiter plate to the DMA, including a suitable readout method.

The assay was first performed on spots with a diameter of 2.83 mm to test the proof of principle. The 5 × 16 spots were arranged on the 7.5 × 2.5 mm glass slide in the same format as wells in a 384 well plate and volumes between 1.5 to 6 µL could be added manually with a pipette. The *p*-nitrophenyl phosphate (*p*-NPP) assay protocol was adapted from STANFORD *et al.*,[84] which is based on a colorless substrate *p*-NPP (**13**), which is dephosphorylated by the active

phosphatase to *p*-nitrophenol (**15a**)(Figure 14). This can then be transformed into a yellow dye *p*-nitrophenolate (**15b**) by addition of 1.0 M sodium hydroxide (NaOH) solution to increase the pH value after the incubation with the protein.[87] This end-point assay has the advantage that the enzymatic reaction is stopped at a certain time point before the readout. The yellow dye can be detected by measuring the absorbance at 405 nm. If the protein is inhibited by an inhibitor, the substrate is not transferred and the phosphorylated compound stays colorless upon pH change.

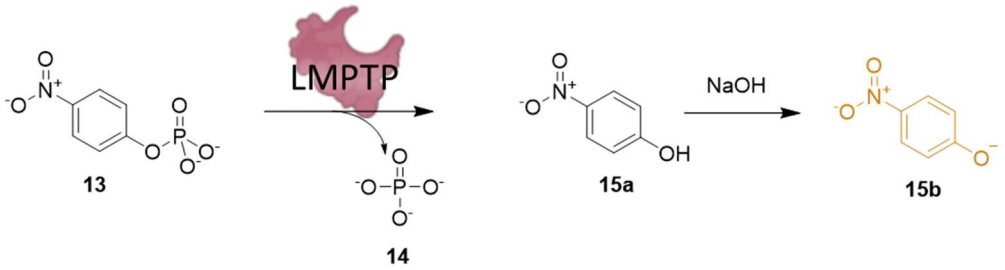

Figure 14: *P*-NPP-based phosphatase assay. A) The colorless substrate *p*-NPP (**13**) is converted by the phosphatase (LMPTP) into the dephosphorylated *p*-nitrophenol (**15a**). This it then transformed into the yellow *p*-nitrophenolate (**15b**) anion by addition of 1.0 M sodium hydroxide solution resulting in a strong absorbance at 405 nm.

For the first experiment, volumes were slightly reduced compared to a microtiter plate by adding first 1.5 µL of enzyme buffer to the DMA and after 30 min incubation 1.5 µL of the substrate buffer. This mixture was further incubated for 60 min at room temperature in a closed petri dish, before the reaction was stopped by addition of 3 µL 1.0 M aqueous NaOH solution. All volumes were added with the liquid dispenser CERTUS FLEX. To image the assay, an adapter created for this application by DR. MAXIMILIAN BENZ was used. In this adapter, two slides could be sandwiched in the center of a plate with the dimensions of a standard microtiter plate. This setup showed several beneficial features. On one hand, this could be used to quench the assay slide in a single step by sandwiching with a slide containing 3 µL 1.0 M NaOH droplets. Furthermore, the merging of the droplets results in a liquid bridge between the two slides with a constant distance and flat surface given by the patterned spots on the transparent glass slides as it is schematically shown in Figure 15B. With this setup, the DMA could be analyzed by a conventional plate reader in a 384-well format and the absorbance at 405 nm was measured. Figure 15A shows the adapter containing two slides with 6 µL droplets in-between when loaded to a plate reader.

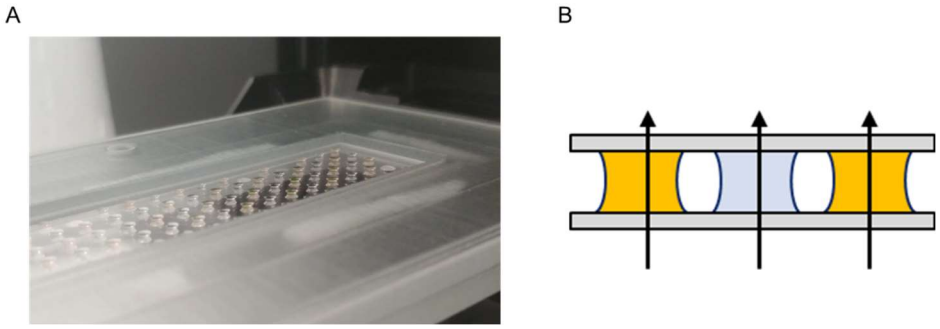

Figure 15: Analyzing a Droplet Microarray with the plate reader. A) Image of two sandwiched slides in the 3D-printed adaptor before analyzed with the plate reader. B) Scheme of the profile of droplets between two glass slides, which is used to form a plane solution film with a constant distance. The adaptor is adjusting the spots in the same position as in a 384 well plate.

As the plate reader was developed for microtiter plates, the scanning unit is limited for microtiter plate frames. Furthermore, for a reliable readout a flat surface and fixed height are required. Therefore, this readout method was not suitable for further miniaturization down to 900 µm diameter spots, which are not comparable to any microtiter plate format. For colorimetric readouts, a new method had been developed based on the use of a document scanner.[60] The slide is imaged in color mode with variable light intensity as presented in Figure 16.

Figure 16: Document scanner as imaging option for Droplet Microarrays. Adapted from WIEDMANN *et al.*[2]

The colored image was subsequently analyzed by MARCEL SCHILLING in the group of PROF. MARKUS REISCHL with a preliminary version of the GRID SCREENER as described in Figure 17. The spots were detected in the center of each droplet to avoid the dark borders of each droplet. After that, the mean color was determined for every spot and transferred into a value ranging from zero for colorless droplets to 0.07 for yellow-colored droplets.

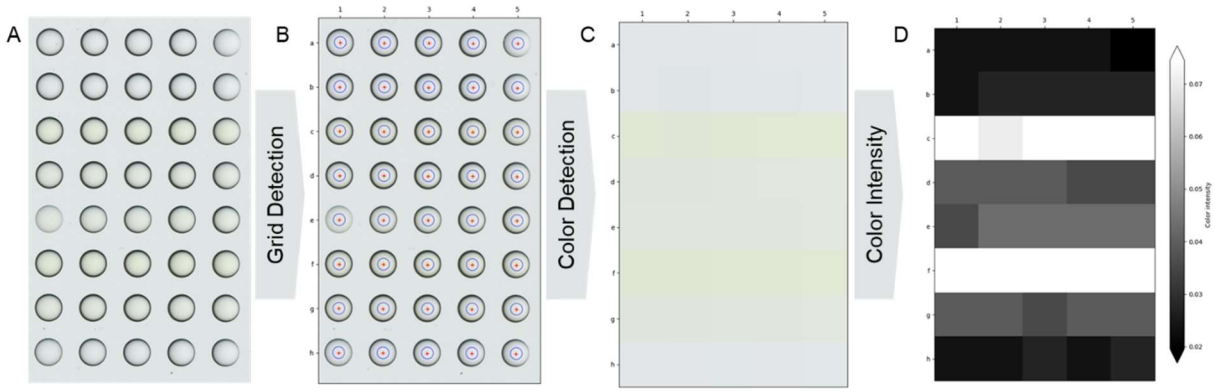

Figure 17: Image Analysis after Scanning. A) Scanned image of the slide with 2.83 mm diameter spots. B) Grid detection for following image analysis. C) Color detected for every spot. D) Color intensity detected for every spot on a scale from zero to 0.07.

The first results of an enzymatic assay performed on the DMA are presented in Figure 18. For a variation of enzyme and substrate concentration, the color intensity is given in artificial units with different scale bars for the scanner (red, left) and plate reader (green, right). The low control is containing only substrate without enzyme and shows negligibly higher signal intensity than the buffer control, indicating that the color change upon substrate conversion solely takes place in presence of the enzyme (Figure 18B).

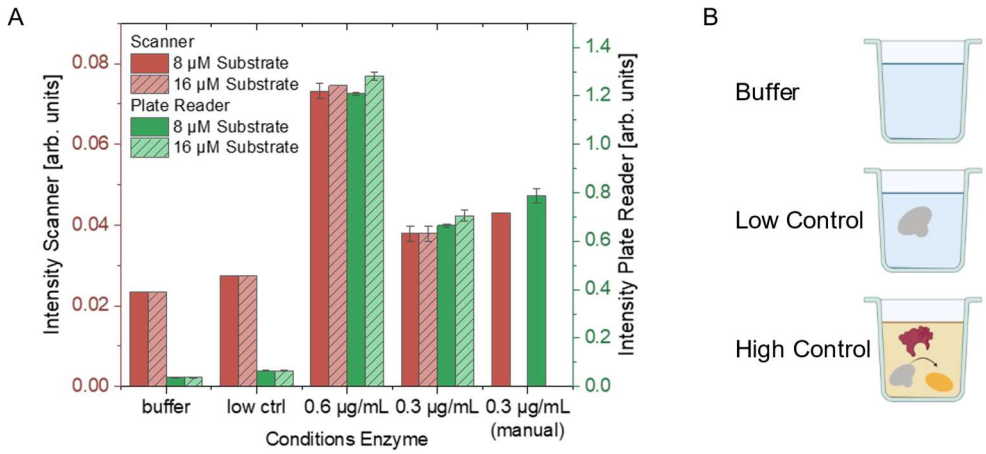

Figure 18: Results of different detection methods for the *p*-NPP assay on 2.83 mm spots on the DMA. A) Intensity values detected by the Scanner (red) and Plate Reader at 405 nm (green) for different assay conditions (right). The substrate concentration was set to 8 µM (blank) or 16 µM (hatched) and the enzyme concentration was changed as indicated on the x-axis. The solutions were added with the liquid dispenser except for the "manual" spot, where the solution was pipetted manually. The same slide was first analyzed with the plate reader and imaged by the scanner. B) Schematic description of different setups and the expected assay result.

As expected, the increase of the enzyme concentration leads to an increased signal, while the substrate concentration did not significantly increase the intensity. This can be explained by a high initial substrate concentration of 8 µM to focus on a non-competitive inhibition mechanism. Despite the two different scale bars, the difference between buffer, low and high controls are

much higher for the scanner, which shows that the sensitivity is higher for the plate reader. This can be also described by the Z' value, which was described by ZHANG *et al.*[88] and classifies the performance of the assay based on the difference between high and low control in relation to the standard deviation (Equation I). For the high enzyme concentration, the Z' value is higher than 0.95 for the plate reader and 0.88 for the results obtained by the scanner. Both are classified as excellent assay according to Table 2. For 0.3 µg/mL enzyme concentration, the Z' value for the plate reader evaluation is still higher than 0.83, while it is 0.47 for the scanner method, indicating that the assay performance is only in the acceptable range. Though, the value would be high enough to use this readout for further experiments.

$$Z' = 1 - \frac{(3 * SD_{Hig\ \ Control} + 3 * SD_{Low\ Control})}{\left|mean_{High\ Control} - mean_{Low\ Control}\right|}$$

I

Table 2: Classification of Z' values in assays by ZHANg *et al.*[88]

Z' value	Classification
z' = 1	Ideal assay
1 > z' > 0.5	Excellent assay
0.5 > z' > 0	Acceptable
z' = 0	Yes/no type
z' < 0	Screening impossible

Having the miniaturization and high-throughput application in mind, the reagents were added with the liquid dispenser CERTUS FLEX. To avoid protein loss during dispensing due to hydrophobic interactions and attachment to the valve and reservoir, the system was incubated for 15-20 min with the buffer containing additional bovine serum albumin (BSA) and then flushed with pure buffer before addition of the enzyme. As control, the solutions were added manually to five spots. Only slightly lower signal intensity compared to the dispensed buffers proves that the dispensing process does neither reduce significantly the protein activity nor its concentration.

3.1.3 Downscaling and Readout Development

After successfully performing an enzymatic assay on the dendrimer modified glass plate, the next step was to reduce the spot size and thereby increase the throughput and decrease the material consumption drastically. Therefore, a new photomask was used to create an array of 16 × 64 round spots with a diameter of 900 µm. This allows to have 1152 spots on a 2.5 × 7.5 cm

glass slide and results in 840 single reaction or assay experiments when the two outer rows are subtracted for buffer or solvent reservoirs due to the fast evaporation.

The assay was performed with the same conditions as described above, but the volume was reduced by the factor 50 to 120 nL in total. Even though there was no color development observed by eye, the slide was imaged with the document scanner. After color evaluation by MARCEL SCHILLING and PROF MARKUS REISCHL, the intensity values did not vary significantly, which lead to the conclusion that the sensitivity of this method for small volumes is not sufficient. These results were confirmed with Z' values in the negative range, which clearly shows that the readout is not suitable for this assay.

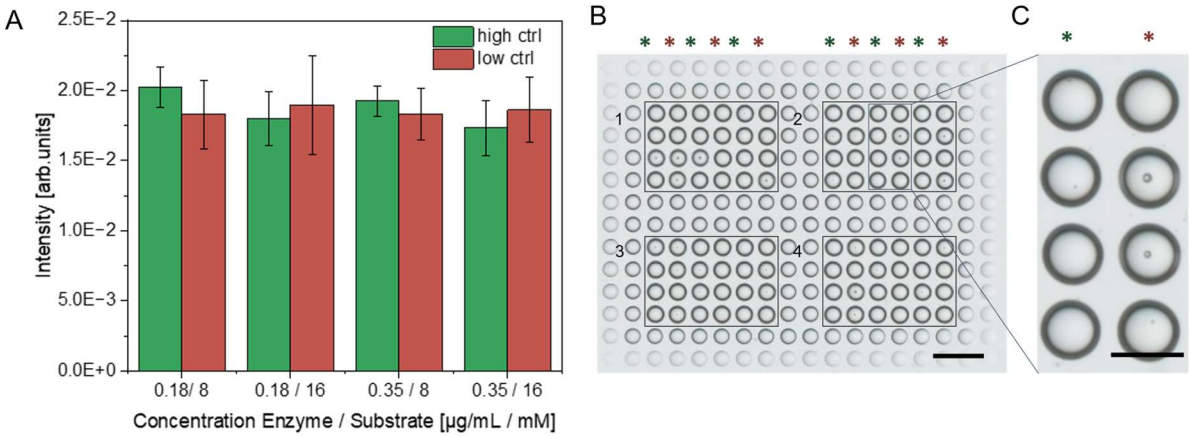

Figure 19: *P*-NPP assay on 900 µm spots. A) The calculated signal intensity is presented for samples containing enzyme (green) and without (red) for different concentrations of enzyme and substrate described on the x-axis. The values are calculated as mean values from 12 different spots with standard deviation. B) Scanned image of the analyzed part of a slide with columns of high (green) and low (red) control, within one square the conditions are used as following: (1) 0.18 µg/mL enzyme, 8 mM substrate, (2) 0.18 µg/mL enzyme, 16 mM buffer, (3) 0.35 µg/mL enzyme, 8 mM substrate, (4) 0.35 µg/mL enzyme, 16 mM substrate. Scale bar is 3 mm. C) Zoomed region of square 2 with a high (left) and low control (right) row. Scale bar is 1 mm.

To achieve higher sensitivity, a new readout method had to be developed. As another well-known phosphatase substrate, DiFMUP (**16**) can be transformed from colorless to a fluorescent molecule **17** with an excitation wavelength at 360 nm and emission at 460 nm (Figure 20). This corresponds to the "blue" channel of a fluorescence microscope. The substrate is converted by proteases with higher efficiency, thus, the substrate and enzyme concentrations can be reduced compared to *p*-NPP-based assays to 0.029 µg/mL enzyme and 200 µM DiFMUP.[89]

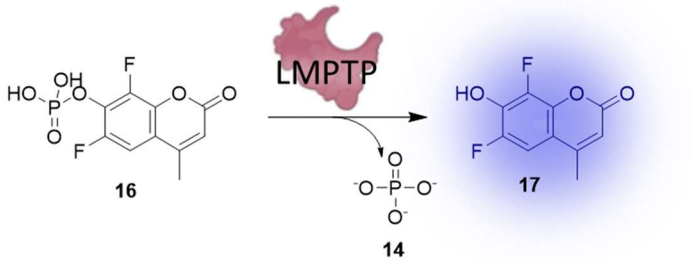

Figure 20: DiFMUP-based phosphatase assay. A) The colorless DiFMUP (**16**) is dephosphorylated by the active LMPTP, resulting in a fluorescent dye **17** with λ_{ex} = 360 nm, λ_{em} = 460 nm.

Images of the resulting fluorescent droplets are presented in Figure 21. There images were taken with a digital microscope, which can be used to image three-dimensional objects like droplets. This effect can be visualized best by imaging with a tilted objective in Figure 21A. Because of the special setup, the uv light source can only be placed next to the sample, which can result in variation of intensities depending on the position of a slide.

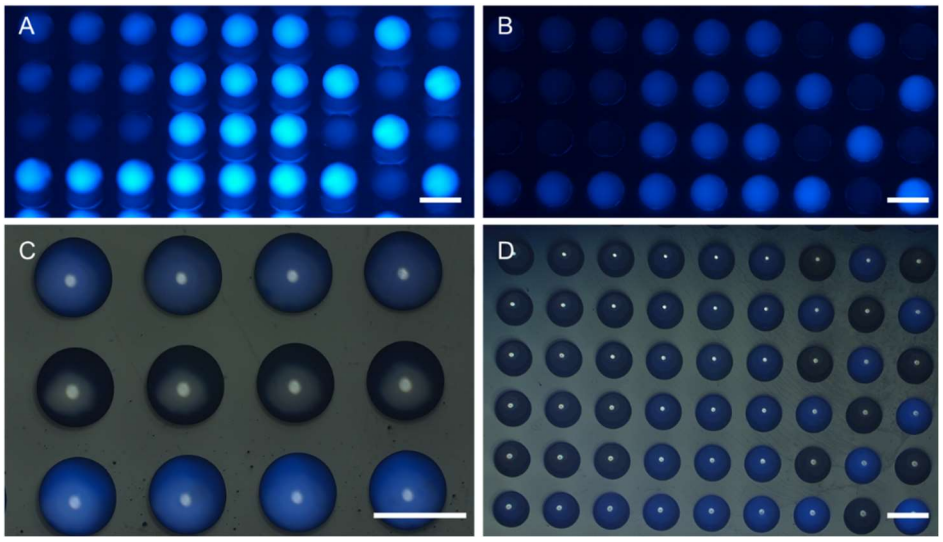

Figure 21: Fluorescent droplets on the Droplet Microarray. The DiFMUP-based assay performed in 100 nL on 900 µm spots. The slide was imaged with a digital microscope with (bottom) and without (top) additional light source and with tilted microscope head (A) and from top (B-D). Scale bar is 1 mm for all images.

Therefore, a confocal fluorescence microscope was used to image the assay on the DMA for further evaluation. For improved reproducibility, the focus was set on the border of the droplets on the glass slide, resulting in a ring at the border of the droplets representing the fluorescence of the droplet (Figure 22A). Using the GRID SCREENER, the spots were detected using the overlay image of the brightfield and blue channel and the mean signal intensity of the respective fluorescence channel was determined as presented in Figure 22.

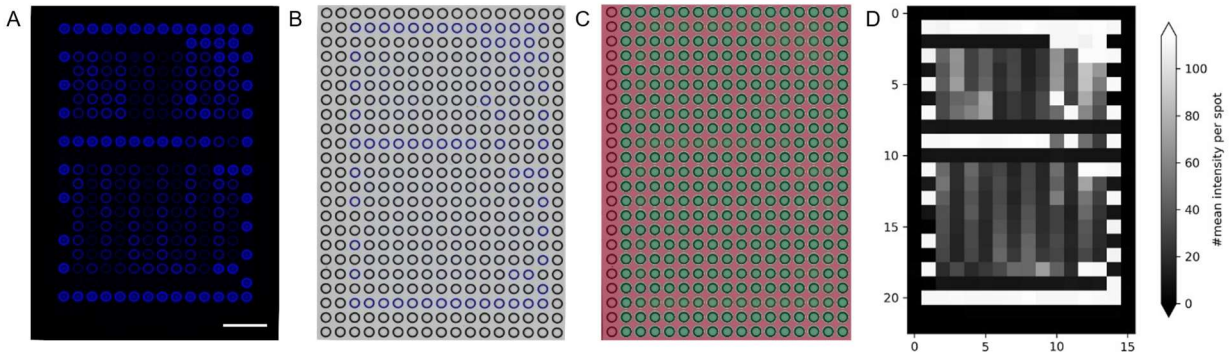

Figure 22: Assay detection and image processing using DiFMUP. A) Blue fluorescence channel of a part of a slide containing high and low controls as well as inhibitors in different concentrations. B) Overlay of fluorescent and brightfield channel. C) Detected grid by Grid Screener. D) Intensity evaluated by the fluorescence detection tool of the GRID SCREENER. Scale bar is 2 mm.

At low concentrations, evaporation becomes more and more crucial, especially for the fluorescence analysis of the droplets. The initial setup for incubation of the assay on the DMA was a closed petri dish with a water-soaked tissue sticking to the lid and 5 mL of water distributed on the bottom of the dish (Figure 23A). The slide was placed inside the petri dish after addition of the enzyme and the lid was exchanged with a new one for microscope imaging. Despite those measures, the outer droplets showed significant evaporation effects, even the ones within the two outer rows of buffer as shown in Figure 23D.

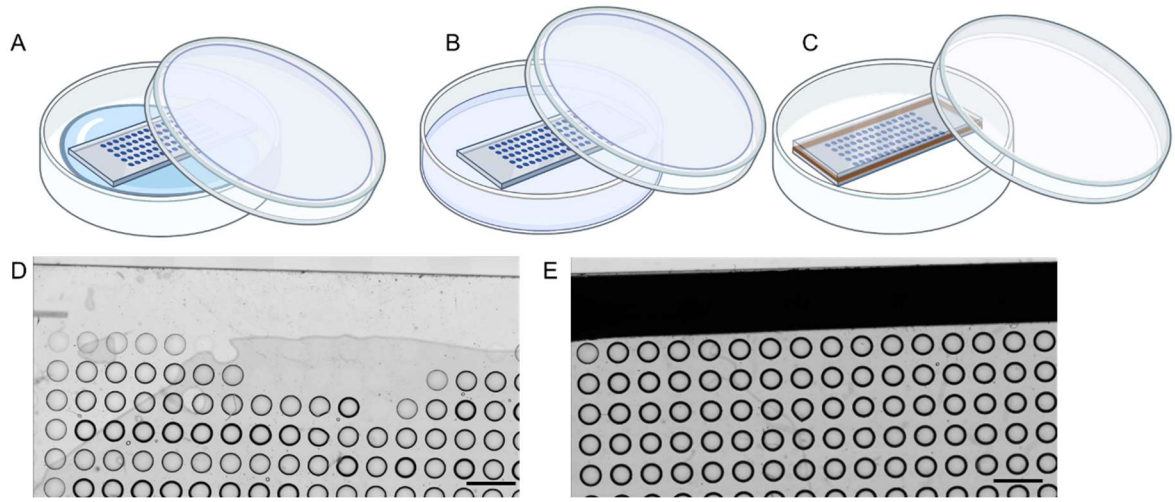

Figure 23: Setup for assay incubation on the DMA. A) Scheme of initial setup with tissue sticking to the lid and water added to the bottom part. B) Petri dish with soaked tissues on the bottom and the lid. C) Setup for microscopy with the sticky chamber. D) Slide imaged after incubated in a chamber described in A). E) Slide imaged after incubation described in B) and C). Scale bar is 1 mm.

To overcome this, a second tissue was placed on the bottom of the petri dish and both were soaked with 8-10 mL buffer solution to ensure that the whole atmosphere is saturated with the assay buffer (Figure 23B). For imaging, the slide was placed in a fresh petri dish and a so-called sticky chamber consisting of a second glass slide and a thin, sticky polymer band was used to

cover the surface without touching the droplets (Figure 23C). This reduced the evaporation effect to a negligible level as shown in Figure 23E, especially when the replicates were distributed over the whole DMA to compensate slightly higher evaporation in the outer regions.

3.1.4 Reaction Readout with the Enzymatic Assay

The first aim was to make sure that the controls are resulting in a bright fluorescence for the active enzyme in the high control without high background noise to result in a good Z' value. To favor a non-competitive inhibition mechanism, the substrate was used in comparably high concentrations, which was known to cause background signals. In addition, all reagents used in the synthesis step to create the library of amides were tested if they showed an impact on the assay. In most established screenings, the new compounds are first synthesized and then purified by chromatography to gain a pure analyte. This purification step requires a complex setup, handling of the reagents and can only be done for one compound at a time. Therefore, the assay was planned to be performed directly after the synthesis without any manual purification step. After ending the reaction, the solvent should be removed under reduced pressure, but other reagents as the coupling reagent HATU and its byproducts, the base diisopropylethylamine (DIPEA) and the additive 4-dimethylaminopyridine (4-DMAP) as well as side products like the urea obtained from the coupling step and some starting material were still present on the spot. For assay development, the control inhibitor **12a** and acid **10a** (Figure 13B) were used. Stock solutions of the compounds were diluted in DMF and then dispensed, but without addition of amine to test the reaction solution without product formation. As shown in Figure 24A, all reagents used in the reaction were dispensed on separate droplets or in mixtures to test their possible impact on the enzymatic activity or on the substrate conversion. The latter one was shown by adding the reagents to the low control, without having any enzyme present.

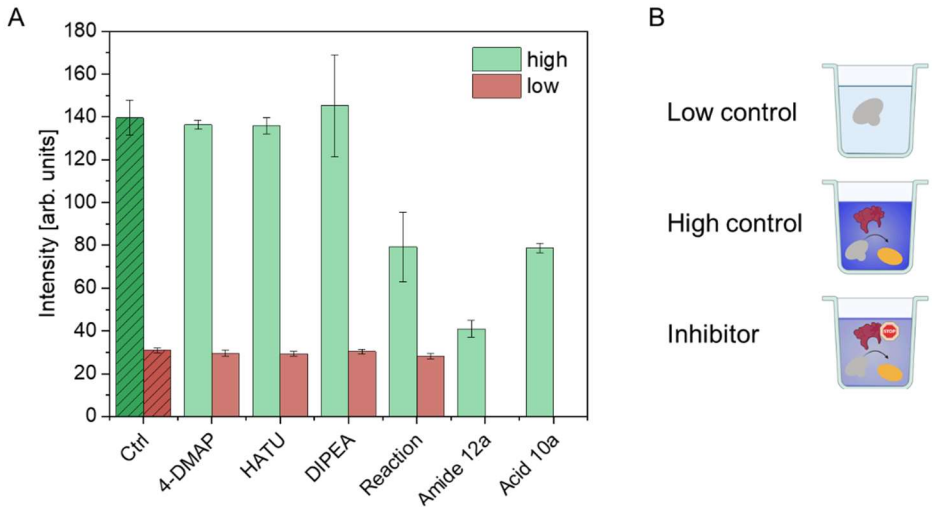

Figure 24: Fluorescence-based assay with reaction controls. The signal intensity for high (dark green, hatched) and low (dark red, hatched) control for an enzymatic assay with 0.029 µg/mL LMPTP and 400 µM DiFMUP are shown. In addition, the different reagents were added in the respective concentrations to the different spots and the signal intensity after addition of enzyme and substrate (light green) or only substrate (light red) were imaged after 1 h incubation. Acid **10a** 12.5 µM (1.00 equiv.), HATU: 13.75 µM (1.10 equiv.), DIPEA: 62.5 µM (5.00 equiv.), 3.13 µM 4-DMAP (0.25 equiv.), reaction: mixture of all mentioned compounds, amide **12a** 12.5 µM B) Schematic representation of expected fluorescence signals for the different controls.

The first two bars in Figure 24A represent the high and low control and showed a high signal difference with a Z' value of 0.733, which is defined as excellent assay. This highlights that the enzyme is active also in the miniaturized format in 100 nL droplets and can be used for evaluation of different inhibitors with the suitable readout. The low signal from the low control without enzyme confirms that the signal is based solely on the enzymatic activity and that there is no crosstalk between highly fluorescent droplets and ones without fluorescent dyes, despite the absence of any non-transparent physical barrier compared to microtiter plates optimized for enzymatic assays.

Compared to the high and low control without addition of any reagents, the signal intensity did not change significantly for the spots with the reagents and therefore main side effects by the chemicals on the assay performance could be excluded. The only compound that clearly showed an inhibitory effect was the acid **10a** as starting material. Due to the core structure, which was known to show some inhibitory effects,[84] this was no surprising finding. To determine the yield of a reaction by measuring the amount of synthesized inhibitor, this initial inhibition for zero percent reaction yield therefore needed to be included in the analysis.

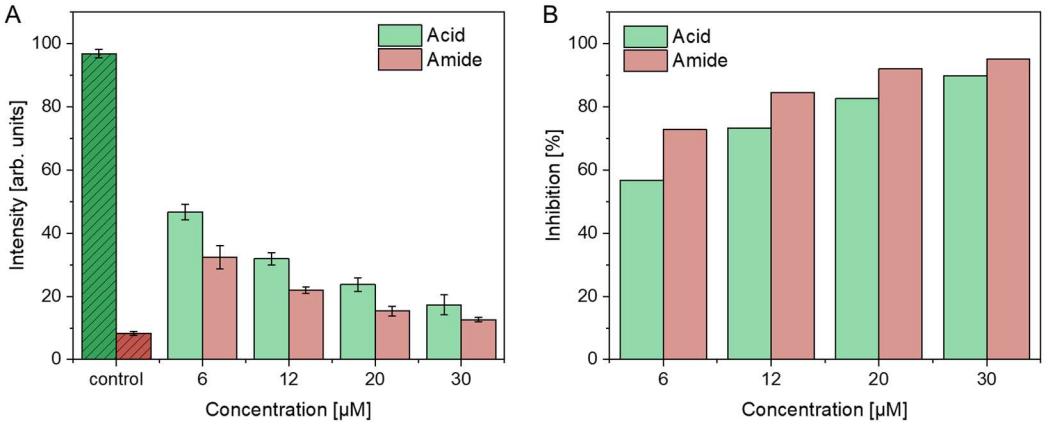

Figure 25: Enzymatic assay with two different inhibitors. A) The signal intensity calculated from the fluorescence image for high (dark green, hatched) and low (dark red, hatched) control. Acid **10a** (light green) and Amide **12a** (light red) were added in different concentrations as indicated on the x-axis. B) Inhibition calculated from the Intensity. High and low control are not presented as they are used in the calculation.

The results of the next assay, investigating on the relation of the inhibitory activity of starting material acid **10a** and product **12a** are presented in Figure 25. The model inhibitor amide **12a** and the respective starting material acid **10a** were added in different concentrations to analyze their difference in inhibitory activity. As expected, the signal intensity was decreasing with increased inhibitor concentration for both compounds. For better visualization, the inhibition rate was calculated based on following equation II:

$$\%\ Inhibition = 100 - \left(\frac{compound - mean_{low\ control}}{mean_{high\ control} - mean_{low\ control}} * 100\right) \qquad \text{II}$$

Despite the fact that the acid shows weaker inhibition, resulting in a higher signal intensity compared to the amide at same concentrations, this difference decreases with increasing inhibitor concentration. The challenge that arose from those results was the low difference in signal intensity between the starting material and product to use the assay as readout for the reaction yield. To compare not only the signal intensity of starting material and product, a so-called artificial yield was prepared and screened with the assay. For that, the two compounds were mixed in different ratios as described schematically in Figure 26B, mimicking a reaction with less than 100% conversion.

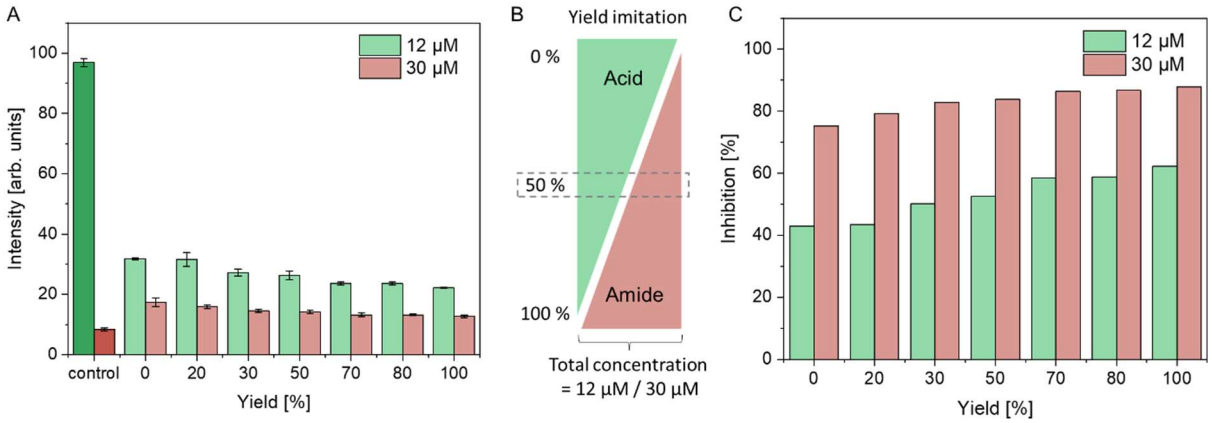

Figure 26: Yield estimation for the enzymatic assay. A) The signal intensity is given for inhibitor mixtures representing different artificially obtained yields for two different total concentrations (red/green). Percentage of amide **12a** is shown on the x-axis. B) Scheme explaining the idea of artificial yield by mixing the starting material (acid **10a**, green) and product (amide **12a**, red) in different ratios by maintaining the total amount of material per spot. C) Inhibition is given for different percentages of amide in the mixture with acid.

These low differences for yields higher than 50% in the assay with 30 µM inhibitor, but also for a lower concentration showed that this setup was not suitable for reaction optimization to identify not only the best hit, but also the best reaction condition to synthesize the hit compound. Hence, the conditions for the assay itself was varied to achieve an increased sensitivity to differentiate between the different ratios of amide to acid.

As a possible solution for that problem, the incubation time after addition of substrate was increased to aim for higher differences between the partially inhibited enzymatic activity. Therefore, the assay was prepared with three different concentrations of acid **10a** as starting material and amide **12a** as potential product and the slide was imaged after one, two and three hours. The results are summarized in Figure 27, showing a total increase in signal intensity after one hour based on the fact, that in general more substrate was converted. A higher signal intensity was observed for all spots containing enzyme, so that the signal intensity difference between acid and amide samples was not substantially increased. To analyze that, the differences of signal intensities were calculated as absolute values and in relation to the signal intensity of the acid, which does not show a high increase after prolonged incubation. Furthermore, the aspect of evaporation needs to be taken into account for longer incubation times. With increasing incubation time, even a low evaporation rate can lead to major side effects and reduce the reliability of the readout. Therefore, the drawbacks in comparison to the low increase in signal difference were too high.

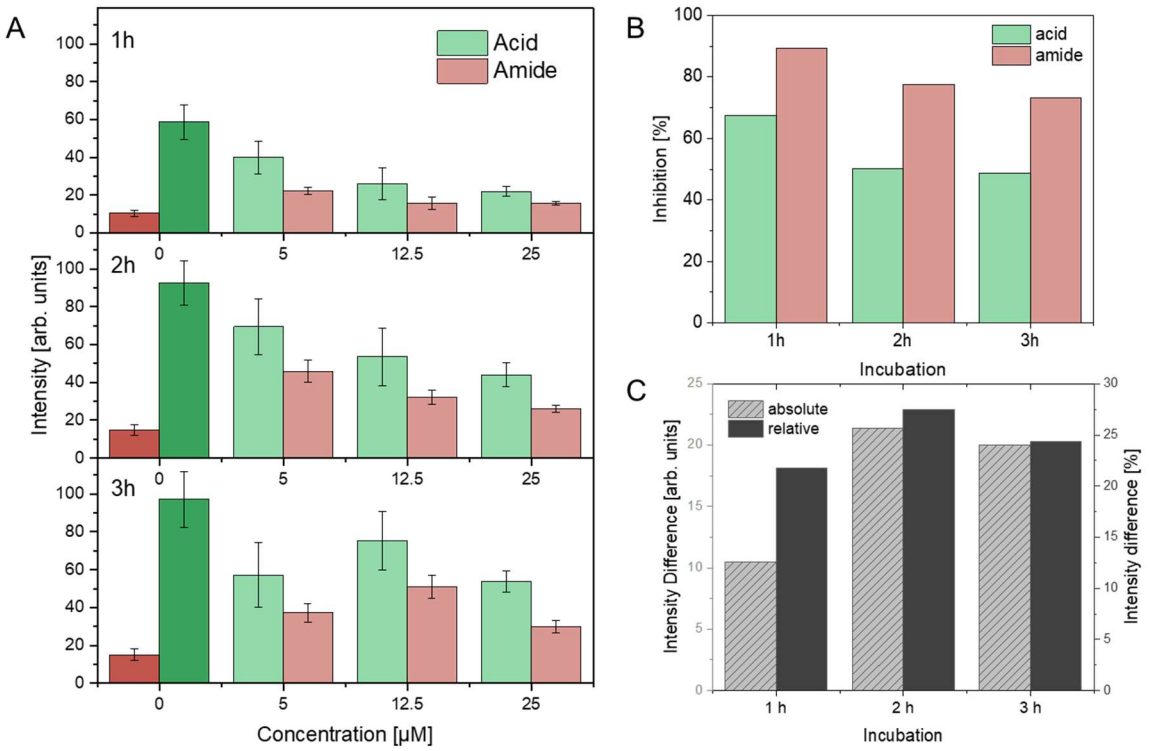

Figure 27: Increasing the incubation time. A) The Signal intensity obtained from an assay with 0.029 µg/mL enzyme and 200 µM substrate per spot. Acid **10a** (light green) and amide **12a** (light red) were added in the given concentrations and the DMA slide was imaged after 1, 2 and 3 hours after addition of substrate. For 0 µM inhibitor, the high (dark green) and low (dark red) controls are represented. B) For 12.5 µM inhibitor, the inhibition was calculated for acid (green) and amide (red). C) For 12.5 µM inhibitor, the difference between acid and amide signal was determined in absolute arb. units (hatched, left) and relative (black, right) by dividing the difference by the inhibition of the amide.

The next approach for a higher signal difference between acid **10a** as exemplary starting material and amide **12a** as possible product, the concentration of enzyme was increased. For maintaining the excess of substrate, the concentration of DiFMUP was increased in the same ratio. As shown in Figure 28A, the difference in inhibition was increasing with higher concentrations of enzyme.

The idea of increasing the enzyme concentration might counteract the idea of miniaturization, but still, with the volume decrease by factor 40, an increase in enzyme concentration can be tolerated. The best compromise of signal difference and used amount of enzyme was found to be at a final concentration of 0.145 µg/mL LMPTP. Despite increasing the enzyme concentration by the factor five, the miniaturized format leads to reduced usage of eight time less enzyme.

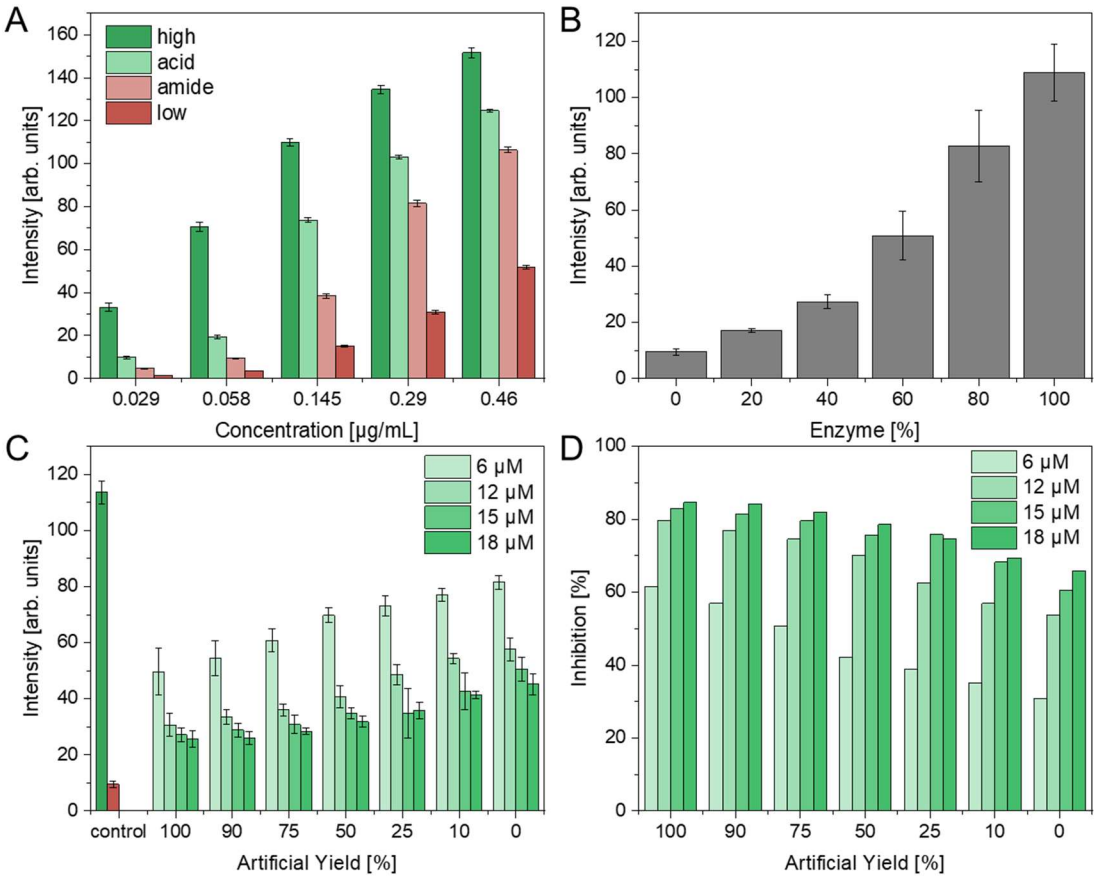

Figure 28: Increasing the enzyme concentration. A) Variation of enzyme concentration. The intensity for high (dark green) and low (dark red) control as well as 12.5 µM acid **10a** (light green) and amide **12a** (light red) in an assay with different enzyme concentrations. The concentration of substrate was increased by the same factor compared to the enzyme. B) Variation of enzyme content with maintained substrate concentration of 0.145 µg/mL assay. C) Assay with 0.145 µg/mL enzyme with inhibitors. Signal intensity for low (red) and high (dark green) control as well as for different ratios of amide **12a** and acid **10a** (x-axis) at different overall concentrations (light to dark green). D) Inhibition calculated from the results from C).

With this assay setup, first the dose-dependent signal intensity was tested by dispensing a dilution series of the enzyme with the same amount of substrate (Figure 28B). The decrease of signal intensity in correlation with the reduced amount of enzyme, shows that the assay can be used as readout for the amount of active enzyme in the droplet at this concentration. Next, the artificial yield was tested again as described before by mixing acid **10a** and amide **12a** in different ratios. This was performed for different overall concentrations of 6, 12, 15 and 18 µM. The results obtained from this assay are presented in Figure 28C and D. When comparing the inhibition for 12 µM concentrations, the inhibition ranges from 80% for 100% amide **12a** to 54% for 0% yield, allowing a much better distinction of intermediate yields compared to the assays with 0.029 µg/mL enzyme in Figure 26. What can be also seen in Figure 28D is the fact, that the difference of inhibition for different artificial yields strongly depends on the concentration of the inhibitors, resulting in the lowest difference between 84% and 65% for

18 µM concentration with 22% inhibition reduction, while the inhibition for 6 µM is decreased by 50% from 61% for amide **12a** to 30% for the acid **10a**. This means, that the higher enzyme concentration allows a better distinction between a starting material and product. Furthermore, a reduction in analyte concentration leads to better readouts. The problem behind this is the fact, that the reaction is performed on the same spot, in the amount that will be used in this assay. As higher concentrations are required in general in the reaction solution, the reaction was performed in 50 nL, while for the assay 100 nL of buffer was used. With that, a 1:2 dilution effect was achieved without taking manually parts of the compound from the spot. A higher degree of dilution was not possible due to the technical restrictions of a maximal buffer volume of 100 nL that could be used on the droplets without merging. For the reaction volume, the minimal volume of 10 nL was set by the liquid dispenser. To mix several different solutions and avoid evaporation during the dispensing steps, 50 nL was used as minimal volume for the reaction.

Finally, the enzymatic assay could be used as readout for a small screening of reaction conditions for the on-chip synthesis of amide **12a**. To this end, the acid was dispensed with 1.00 pmol per spot, resulting in a reaction concentration of 20 µM in 50 nL DMF and an assay concentration of 10 µM in 100 nL. DIPEA was added with 5.00 and 10.00 equiv., HATU in three amounts of 2.00, 2.50 and 3.00 equiv., 4-DMAP was used with 0.25 equiv. for all reaction steps and diethylammonium hydrochloride (**18b**, see following chapter for elucidation) was added with 1.50 and 3.00 equiv.. DIPEA,4-DMAP and HATU were premixed in the required ratios and acid was added separately. After 20 min incubation in a petri dish with DMF saturated atmosphere to avoid evaporation, the amine was added in different amounts and the slide was placed back and incubated overnight at room temperature in the petri dish. Afterwards, the solvent was evaporated, additional controls were dispensed and, after a second evaporation step, the assay was performed with the 0.145 µg/mL concentrated enzyme and 1 h incubation after addition of 1.00 mM substrate. All following results presented in Figure 29 were obtained from one single experiment.

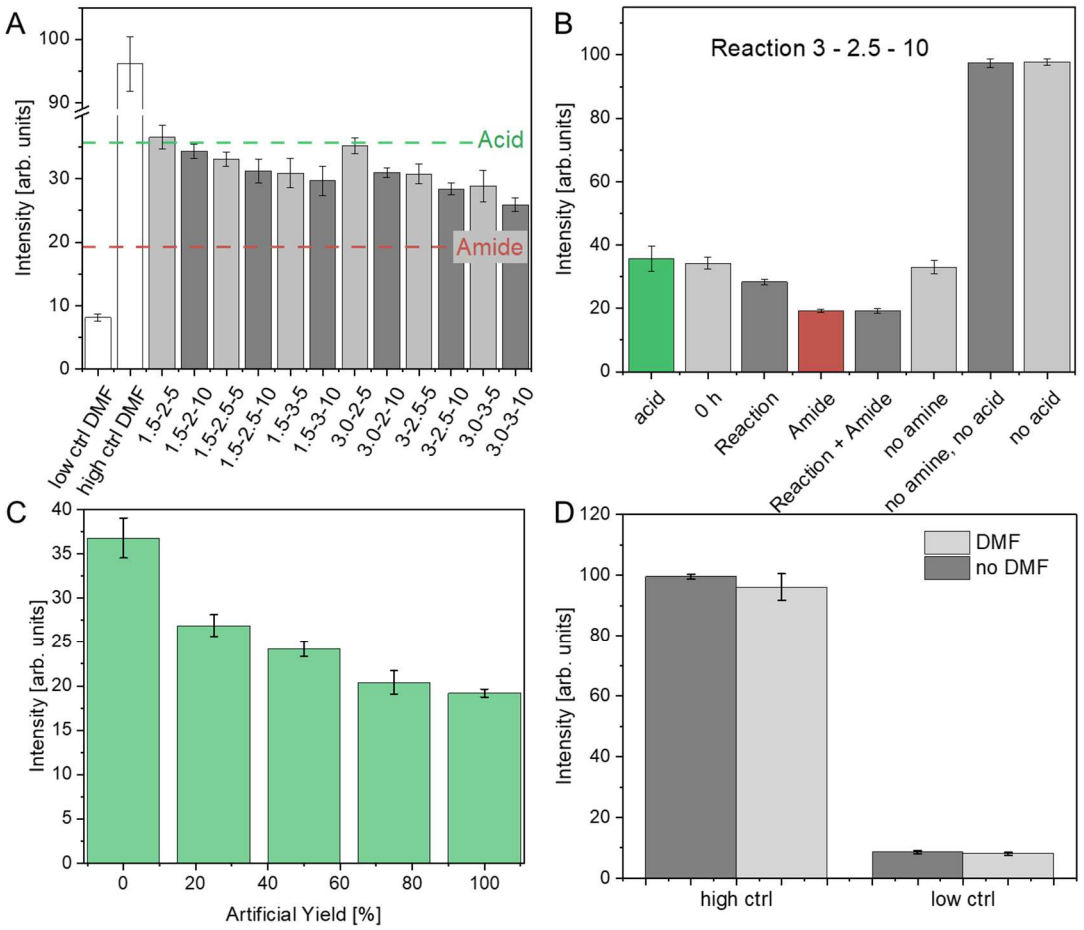

Figure 29: Reaction test with enzymatic readout. A) Signal intensity from the assay is given for different reaction conditions. The reaction was performed with 20 µM acid **10a** in 50 nL, resulting in 10 µM acid/amide mixture in the assay. The equivalents of amine – HATU – and DIPEA are given on the x-axis, 0.25 equiv. 4-DMAP were added to all reaction spots. B) Example of different controls for a reaction using 3.00 equiv. amine **18b**, 2.50 equiv. amide and 10.0 equiv. DIPEA. The pure acid **10a** (green) and amide **12a** (red) are highlighted. The reaction is shown without (0 h) or overnight incubation, and the reaction mixture was additionally dispensed with the amide instead of the acid (reaction + amide) and as described on the graph. C) Signal intensity for artificial yield, given as % of amide **12a**. D) Control spots with evaporated DMF or without any treatment.

In Figure 29A, the signal intensity for the different reaction conditions is shown. The signal intensity from the acid **10a** control is shown as green line at 35.7 arb. units, indicating no significant product formation and the red line at 19.3 arb. units represents the signal intensity of 10 µM amide **12a**, which would indicate 100% conversion of acid **10a** to the product **12a**. The signal intensities of all reaction steps can be found in between those two lines, which indicates that the assay readout showed reliable results. Also, the significant reduction in signal intensity for increasing concentration of the base DIPEA as well as coupling reagent HATU shows that the reaction gives higher yields for higher concentrations of reagents. Though, the yield seemed to be quite low, as the signal intensity for the best conditions of 3.00 equiv. amine, 3.00 equiv. of HATU and 10.0 equiv. of DIPEA is at 25.9 arb. units, which correlates with a yield of 25-50% in the control spots (Figure 29C). That the enzyme inhibition is not caused by

any side effect of the reaction, but is solely based on the product formation is again shown for one example in Figure 29B. There, the starting material, highlighted in green, is compared with a reaction that was stopped by evaporation of the solvent immediately after dispensing, the reaction solution and the pure inhibitor. In addition, the reaction was dispensed without addition of amine, without the addition of acid and without acid and amine. The high intensity for the last two samples shows that the main inhibition is caused by the acid and not by any additional side reaction of the coupling reagents. The intensity for the sample without amine is slightly lower than the acid only, which could indicate that there might be a side reaction of the acid with other compounds in the reaction mixture, resulting in a slightly more potent inhibitor compared to the acid. For the reaction, also all empty spots are covered by DMF to prevent evaporation. By leaving several spots free, the high and low controls were compared to those where DMF was added and evaporated before. There is no significant difference between those controls, indicating that the solvent can be completely removed by evaporation and does not show any impact on the assay results.

The enzymatic assay was herewith successfully transferred to the DMA, miniaturized to 100 nL droplets in an 18 × 64 array on a microscope glass slide and used as readout for a chemical reaction from a carboxylic acid to an amide. By the decrease of enzymatic activity, the improvement of the inhibitory potential of the new compound could be analyzed, if compared to the acid without modification. Furthermore, if the same compound is synthesized on several spots with different reaction conditions, the highest yield can be identified by comparing those different spots resulting in the same product, as shown in Figure 29. Still, this assay can only give an information about the increase in inhibitory activity and therefore, some additional methods were required to characterize the chemical reaction.

3.1.5 Reaction Optimization Using LC-MS

After establishing the enzymatic readout to estimate the yield of the amide synthesis, this reaction was investigated more detailed. A useful possibility to analyze low amounts of crude reaction mixtures in regard of their components and their ratio is LC-MS. The mixture is separated in a reversed phase column and the retention time can be used to identify a compound in comparison to a control analyzed under the same conditions, which is in addition analyzed by a mass detector. Furthermore, the peak area corresponds to the amount of analyte and can therefore be used to estimate the ratio between structurally similar compounds.

Due to limited sensitivity of LC-MS, the first reaction tests were performed in 5 µL on a dendrimer DMA slide with 2.83 mm round spots. Adapted from the original protocol, a 10 mM reaction mixture of acid **10a**, containing 1.50 equiv. of the amine **18**, 1.10 equiv. HATU, 5.00 equiv. DIPEA and 0.25 equiv, 4-DMAP. The amine was first pipetted to five spots in the first row and the reaction solution containing all remaining compounds was added to those spots and three additional neighboring rows (Figure 30A, green/grey). The DMA slide was placed in a closed petri dish to prevent evaporation and incubated over night at room temperature. Two spots were collected for LC-MS measurements, the spots were washed with additional DMF and diluted with water. For evaluation, the peak areas in the total ion chromatogram were compared.

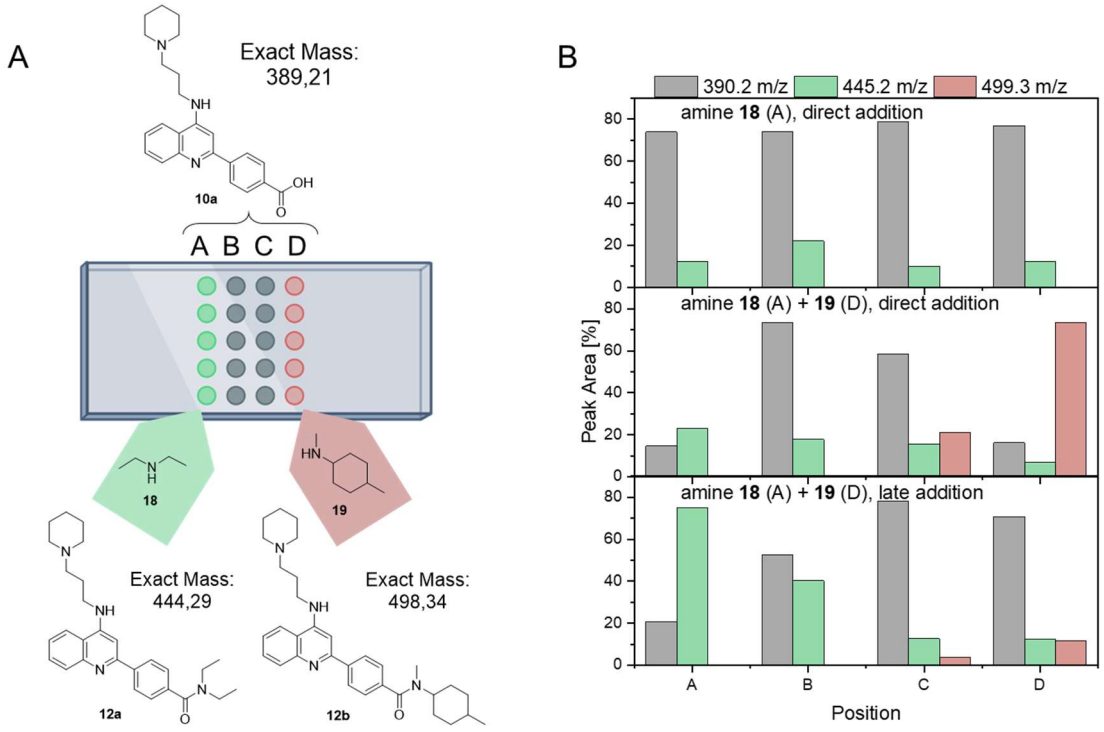

Figure 30: LC-MS analysis of amine impact. A) schematic description of the experimental setup. Reaction solution containing acid **10a**, DIPEA, HATU and 4-DMAP was added to four rows of 2.83 mm spots on the DMA. To the first row (A), diethylamine (**18**) was added, to the last one (D) N,4-dimethylcyclohexan-1-amine (**19b**) was added and the reaction was incubated. B) Peak area of the different m/z signals for acid **10a** (grey), Amide **12a** (green) and Amide **12b** (red) obtained from the TLC are given for two spots collected from each row (x-axis). The three diagrams represent different reaction conditions, where only amine **18** was used, without addition of amine **19** (top), where both amines were added together with the reaction solution in the respective spots (centre) and where the amines were added after 15 min (bottom).

As shown in the first chart in Figure 30B, the product **12a** was detected at the spot from row A, showing a signal at 445.2 m/z in the mass spectrum of a peak after 3.64 min ($[M+H]^+$). The conversion seemed to be quite low, as the peak of the starting material **10a** (m/z = 390.2, $[M+H]^+$) at 3.16 min was very high. This ratio between acid **10a** and amide **12a** was also

confirmed by the absorbance chromatogram, which showed lower sensitivity and was therefore not used for final comparison. Interestingly, the product mass was also found on all neighboring spots in rows B-D, where the amine was not added. This can be explained by the high volatility of diethylamine (**18**) (see Table 3), as the reaction spots were spatially separated by the omniphobic borders, but still in close proximity and without any physical barrier which could prevent gas exchange.

To further investigate on the effect of contamination, the second amine **19** was added in addition to the last row of the 4 × 5 array as described in the scheme in Figure 30A. The results are shown in Figure 30B in the second graph. The product signal of amide **12b** (m/z = 499.3, $[M+H]^+$) after 4.12 min could be clearly identified as main peak in row D, with some starting material left. But even in this case, there were traces of amide **12a** detected, as on every spot. Also in the third row, the amide **12b** was synthesized, indicating also a contamination with amine **19** despite its lower volatility with a boiling point at 166 °C.

Table 3: Amines used for the reaction and their boiling points.

Boiling point [°C]	Free amine	HCl salt
Diethylamine	56[90]	320[90]
N,4-Dimethylcyclohexan-1-amine	166 (est.)[91]	-

To prevent the contamination effect of the amines, the addition order was changed in the last experiment. Here, the reaction mixture was added to the spots first, in order to ensure the formation of an active ester. This active species might then directly undergo the amidation after addition of the amines to the droplets. The results in the third graph in Figure 30 indicate a higher conversion rate for amide **12a**, but also in the neighboring spots with a gradient of decreasing conversion with increasing distance to the spot of origin. The results for the second amine **19** are similar with low conversion in the directly neighboring spots, but show a lower conversion rate for the original spots in row D. This might be due to handling difficulties, as all addition and collection steps were carried out manually using pipettes.

In summary, there was a significant contamination by the amines observed, which correlated on the one hand with the distance, showing decreasing signal intensities for diethylamine (**18**). On the other hand, the contamination effect decreases with the boiling point of the amine and therefore its volatility, as the N,4-dimethylcyclohexan-1-amine (**19**) only shows products in the directly neighboring spot compared to diethylamine (**18**). This offers the chance to prevent this

side reaction in neighboring droplets by using the amines as ammonium salts, which are known to have a much higher boiling point. The base DIPEA, which is used in the reaction in excess could be also used to create the free amine *in situ*, in low concentrations, which can directly react with the active ester in the droplet.

An additional point to consider was the distance factor. In the setup with 2.83 mm diameter spot, the distance between the border of two droplets is at least 1.5 mm. At the aimed 900 µm diameter DMA, the spots are very dense with distances of 225 µm. Furthermore, the ratio of the surface area of a droplet compared to its volume increases with decreasing droplet size, so the problem of volatility becomes even more important. Hence a new reaction readout for downscaled synthesis was required to test the hypothesis of ammonium salts in the final size scale.

3.1.6 MALDI-MS Measurements for Small-Scale Reaction

For direct chemical analysis on the Dendrimer-DMA slide, MALDI-MS measurements were performed. Based on previous work, where the detection of lipids was shown for low amounts down to low femtomoles on 900 µm diameter spots, the measurements were optimized for this setup of small molecules. The measurements in this work were performed in collaboration with the group of PROF. CARSTEN HOPF at the CENTER FOR MASS SPECTROMETRY AND OPTICAL SPECTROSCOPY (CEMOS), UNIVERSITY OF APPLIED SCIENCE in Mannheim. All measurements and preliminary evaluation of the acquired data were performed by DR. STEFAN SCHMIDT (CEMOS, UNIVERSITY OF APPLIED SCIENCE, Mannheim) or by students under his supervision.

In the first measurement, the limit of detection, optimal matrix molecule and its concentration was evaluated. As representative analyte, amide **12b** was dispensed in different concentrations on the DMA, the solvent was evaporated and α-cyano-4-hydroxycinnamic acid (HCCA) was added as matrix in an acetonitrile (ACN)/water mixture (1:1). Due to the omniphilic/omniphobic surface properties, the solution formed stable droplets on the DMA, despite the low surface tension of acetonitrile. Because of the high volatility of acetonitrile, the solvent evaporated immediately during the dispensing process. To ensure that the analyte was well dissolved and could co-crystallize with the matrix molecules, ACN/water mixture was dispensed to several spots again to redissolve matrix and analyte molecules. This led to less homogeneous matrix crystals and was therefore not considered in further experiments Figure 31B.

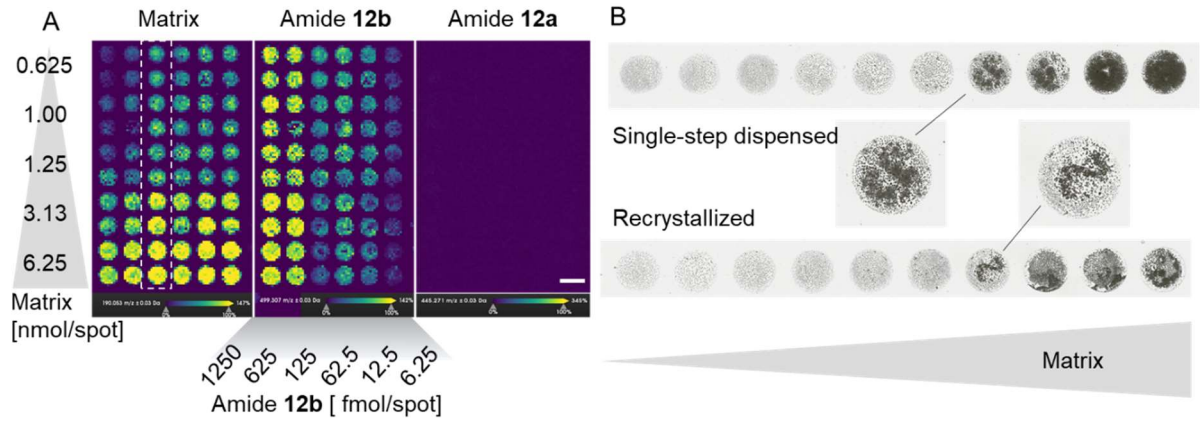

Figure 31: MALDI-MS results for matrix and analyte concentrations. A) Amide **12b** was dispensed in different concentrations from 1250 to 6.26 fmol/spot (left to right) and HCCA was added in different concentrations from 6.25 to 0.625 nmol/spot (bottom to top, 2 rows as replicates). Shown is the ion map for the same position on the DMA for following signals: matrix (left, m/z = 190.05 +/- 0.03, $[M+H]^+$), Amide **12b** (center, m/z = 499.31 +/- 0.03, $[M+H]^+$) and Amide **12a** (right, m/z = 445.27 +/- 0.03, $[M+H]^+$). +/- 0.03 represents the tolerance in the ion image. Scale bar is 1 mm. B) Scanned image of one row with different matrix concentrations (increasing left to right). The matrix was dispensed (top) and for one row, 50 nL of ACN/water mixture was added again after evaporation (bottom) to test optimal crystallization conditions. In the middle, a zoomed image of a spot is shown without (left) and with (right) addition of additional solvent. Images adapted with permission from DR. STEFAN SCHMIDT.

The DMA was analyzed with a BRUKER Rapiflex in positive ion mode. Although acids are known to be detected in negative mode with the negatively charged carboxylate group, the analytes used in this project are based on a core structure containing several amine groups, which are prone to be ionized in positive mode. 0.1% trifluoroacetic acid (TFA) was added to the matrix solution to support this process, which resulted in high signal intensities also for the acid **10a**.

Figure 31A shows the ion intensity image of the region of the DMA, where matrix and amide concentration were varied resulting in a two-dimensional matrix. The ion maps result from the MALDI-MS imaging of the whole DMA slide and represent the intensities for one m/z signal. In the left part, the signal for HCCA matrix (m/z = 190.05 +/- 0.03, $[M+H]^+$) is shown, which is increasing as expected with increasing matrix concentration, but also with decreasing concentration of amide **12b** (left to right). Latter one can be explained by quenching of matrix signal with increasing additional analyte concentration. Furthermore, the shape of the spots is clearly visible without showing any matrix signals on the omniphobic areas, indicating that there is no leakage during any dispensing step. The image in the center shows the signal for the analyte **12b** that was added (m/z = 499.31 +/- 0.03, $[M+H]^+$) with intensity increasing with its increasing concentration. Traces could be detected up to 6.25 fmol/spot, which highlights the high sensitivity of this analytical method. The matrix concentration (top-bottom) does not show

a significant impact on the signal intensity. As expected, the third ion intensity image does not show any signal for m/z = 445.37 (amide **12a**, $[M+H]^+$), which was not added to the spot, to demonstrate that there was no contamination with the different compound.

In the next step, a mixture of acid **10a** and analyte **12a** was added to the spots to mimic an artificial yield. Figure 32 shows the ion intensity images for both analytes with decreasing intensity for the signal of acid **10a** and with increasing signal for amide **12a** for higher yields. As MALDI-MS requires additional standards and exactly reproducible ionization conditions in terms of analyte and matrix crystallization,[31] it was not used to exactly calculate yields based on this curve, but this experiment showed that both analytes could be detected in mixtures without crucial quenching of their signals. The final goal was to use MALDI-MS in a semi-quantitative manner, with heatmaps indicating if the product is either the main peak, detected but in low intensity or not detected.

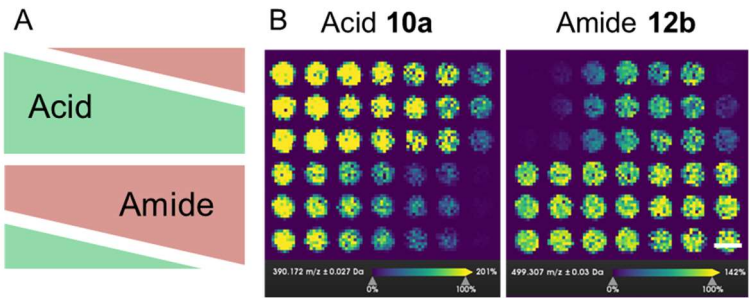

Figure 32: MALDI-MS measurements of artificial yields. A) dispensing scheme showing the different ratios of acid **10a** and Amide **12b**, every condition was dispensed in triplicates. B) Ion intensity image for acid **10a** (left, m/z = 390.17 +/- 0.027, $[M+H]^+$) and amide **12b** (right, m/z = 499.31 +/- 0.03, $[M+H]^+$) for 1.25 pmol total amount per spot. Scale bar is 1mm. Image adapted with permission from DR. STEFAN SCHMIDT.

On the same slide, at last the reaction was performed in different concentrations with acid **10a** and amine **19** as well as amine **18b** as hydrochloride salt. The reaction solution containing 1.00 equiv. acid **10a**, 1.10 equiv. HATU, 5.00 equiv. DIPEA and 0.25 equiv. 4-DMAP was dispensed in different concentrations to result in final reaction concentrations ranging from 416 µM (12.5 pmol/spot) to 0.42 µM (0.013 pmol/spot). To one part, the free amine **19** was added and with one row containing no amine in-between, amine **18b** hydrochloride was added to the rows below. The signal intensities for the starting material **10a** and both products **12a** and **12b** are presented in Figure 33. For the three highest concentrations up to 41.7 µM, the formed product was detected for the respective spots. The comparably high signal intensity for acid **10a** in the third column indicates a lower conversion with high amount of starting material left. The missing signal for the two lower concentrations can be explained with the low conversion rate for low concentrations in the reaction solution, as signals of the starting material

are visible. In addition, the pure analyte was detected up to 6.25 fmol/spot, which is still lower than 12.5 fmol/spot for the lowest reaction concentration.

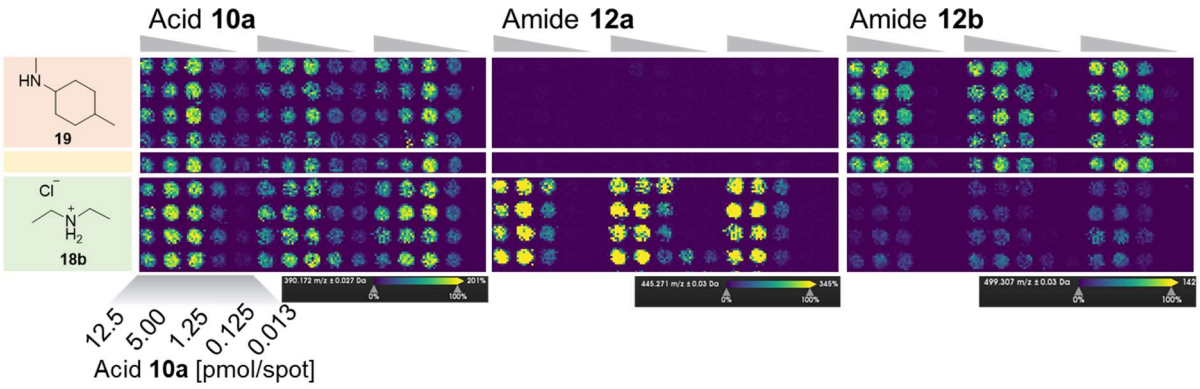

Figure 33: MALDI-MS measurements of reaction and contamination. The reaction solution was added to all columns in different concentrations, indicated by the grey arrow. To the top part (red), amine **19** was added and to the bottom part (green) amine **18b** was added in the respective concentrations, while one row was left without any amine. The ion intensity images are shown for the same region for m/z = 390.17 +/- 0.027 (left, acid **10a** $[M + H]^+$), m/z = 445.37 (center, amide **12a**, $[M+H]^+$) and m/z = 499.30 +/- 0.03 (amide **12b**, $[M+H]^+$). The four rows and three blocks of five columns are replicates. For the reaction, the same equivalents as in chapter 3.1.5 were used, based on the given amount of acid. Image adapted with permission from DR. STEFAN SCHMIDT.

Additionally, the signal distribution of both amides gave a clear information about the amine contamination caused by the volatility. The amide **12b**, resulting from the reaction with the free amine **19**, was detected in the row where no amine was added, but which was in close proximity to the spots containing amine **19**. Also, for the spots where amine **18b** was added, traces of amide **12b** are visible. In contrast, the amide **12a**, resulting from the ammonium salt **18b** was only detected in the spots where it was directly added. This indicated on the one hand, that the reaction is also working with *in situ* transformation of the ammonium salt to the active amine, but also on the other hand shows that this method can be used to avoid the contamination of the neighboring droplets even in the small scale with 225 µm distance between the droplets.

All these results were obtained from one single DMA slide within a single scan by the mass spectrometer. Furthermore, all reaction tests were prepared with two different matrix concentrations, where only the best results were used, and half of the slide was used to test 2,5-dihydroxybenzoic acid (DHB) as second matrix. Here, the matrix signals were not clearly detected due to too low concentrations and non-homogeneous matrix crystallization. Those results were not further evaluated.

The dendritic surface structure based on covalent reaction with oxygen groups on the glass surface is also possible when ITO-coated glass slides are used. However, in this case the patterned slides show slightly worse performance. Droplets formed on this surface seem to be

less stable and lower volumes must be used to avoid leaking. To investigate if the ITO-coating is strictly necessary for highly sensitive and exact measurements, their performance in MALDI-MS were compared with normal dendrimer DMAs from glass slides. Amide **12a** and HCCA were dispensed on both slides as described before and analyzed. In addition, a conductive tape was sticked to the back of the glass slide to allow discharge of the slide, which was presented by WEISSENBORN *et al.*[92] and WU *et al.*[93] as possibility to measure MALDI-MS directly from glass slides. The resulting mass spectra for the three conditions are presented in Figure 34A, with a zoom into the region of the analyte signal.

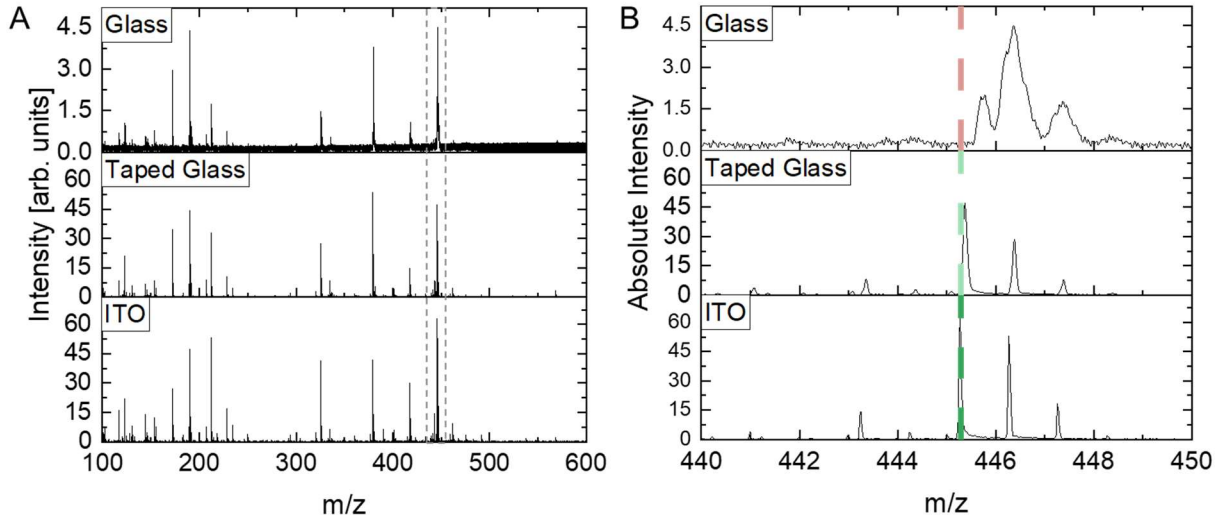

Figure 34: Comparison of different surfaces for MALDI-MS measurements. A) Mass spectra of amide **12a** with calculated m/z = 445.29 $[M+H]^+$ and HCCA matrix (m/z = 190.04 $[M+H]^+$) on a glass slide (top), glass slide with conductive tape on the back side (middle) and ITO-coated glass slide (bottom). All slides were patterned with the dendrimer modification. B) Zoomed region of the same spectra.

On all three slides, the analyte was detected, but with much lower intensity for the bare glass slide, while the ITO showed the best signal. In addition to sensitivity, the accuracy of the measurement is important to clearly identify the compounds. The mass resolution was very high for the ITO slide, resulting in sharp peaks at the predicted position, while the spectra from the taped glass slide shows slightly broader and shifted peaks. The glass slide led to very broad, overlapping peaks with a high shift to a higher mass range. This confirms that the ITO coating despite its challenge during the modification of the surface, is the best way to measure MALDI-MS from DMA slides with the Rapiflex used in this work. As alternative solution, different MALDI-MS devices like the timsTOF could be used.

3.1.7 Reaction Screening with MALDI-MS Readout

After proving that the reaction is working in small scale with the hydrochloride salt of an amine and that MALDI-MS can be used as direct readout, a first screening was performed on the DMA slide. Additional acids with a slightly varied core structure were synthesized by SANOFI, but were only available as either TFA or HCl salt due to the amine core structure. To see if the additional salt shows any impact on the reactivity of the acid, the first variation in the screening was to compare acid **10a** in free form with both salts. Furthermore, two additional acids **10b** and **10c** were chosen, where **10c** was also added as TFA and HCl salt. To make sure, that the MALDI-MS readout is comparable between the different starting materials, some compounds were added in a dilution series on a slide and analyzed by MALDI-MS Figure 35. Free acid **10a** was compared with the two salts in Figure 35A, to test if the additional salt leads to different signal intensities. The signal intensities did not vary significantly, while the salts tend to have a slightly higher signal intensity at the same concentration. Figure 35B shows that the signal intensity of the two different acids **10a** and **10c** is comparable, so that the same measurement method could be used to compare different products from different acids. In Figure 35C, the pure amide **12a** was compared with a crude reaction mixture incubated before in a reaction tube. The lower signal intensity can be explained by a conversion in the tube lower than 100%, but indicates that none of the compounds in the reaction solutions leads to significant signal quenching.

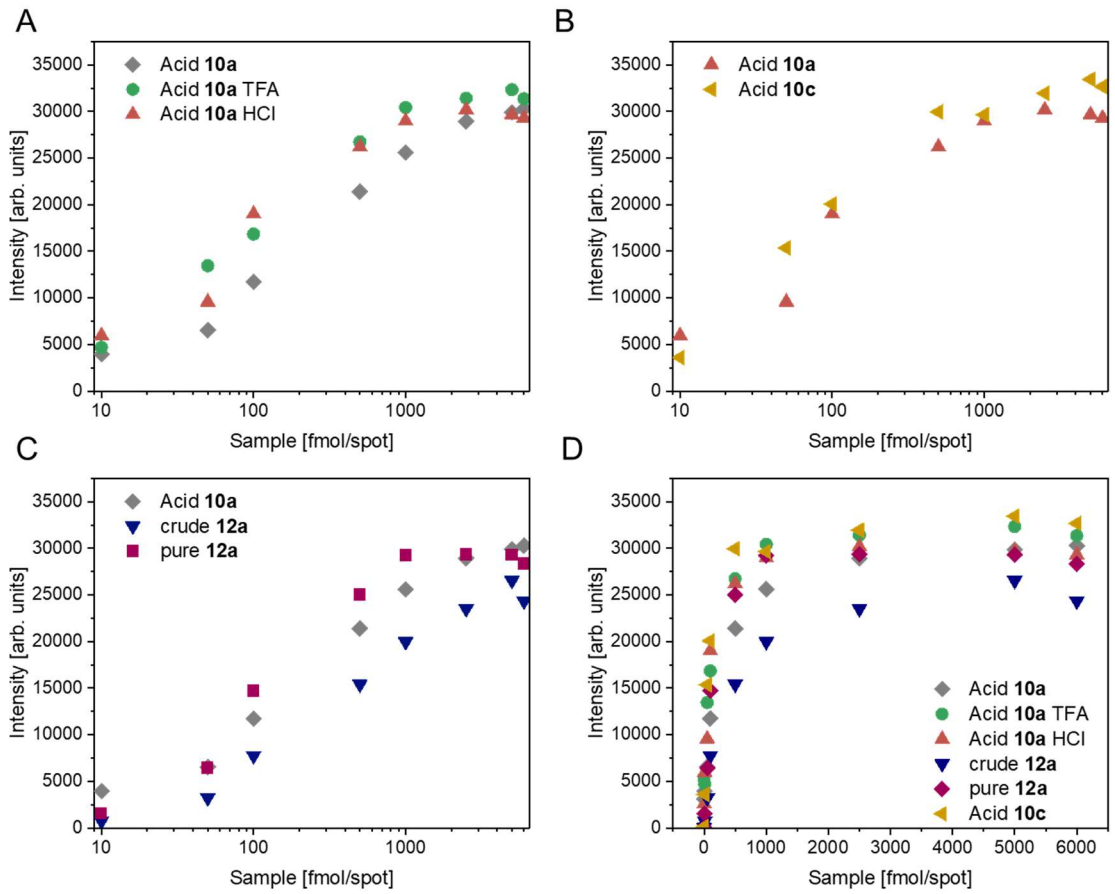

Figure 35: Signal intensity for different acids and amides. All reagents were dispensed in different concentrations on an ITO-DMA and analyzed via MALDI-MS after addition of HCCA matrix as described above. The signal intensity is plotted against the analyte concentration. A) Acid **10a** was added in its free form (grey) and as TFA (green) and HCl (red) salt. B) The signal intensity is shown for two different acids **10a** (red) and **10c** (yellow), both as HCl salt. C) Starting material acid **10a** (grey) was added and a reaction mixture after overnight reaction in a reaction tube to yield amide **12a** (blue) as well as the pure product amide **12a** (purple). D) Summary of all described samples with linear x-axis scale.

For the screening, those six acids described above were combined with five different amines, all available as ammonium hydrochloride salts. In addition, the reaction conditions were varied to use different equivalents of amine and DIPEA, and the overall reaction concentration was set to two extreme values of 20 µM and 120 µM in respect of the acid. All combinations that were tested in this multivariate screening are visualized as connection lines in Figure 36, resulting in 180 different reaction conditions. All reactions were performed in four repetitions, which were distributed over parts of the whole slide in a randomized way, which leads to 720 single reactions performed on only one DMA slide.

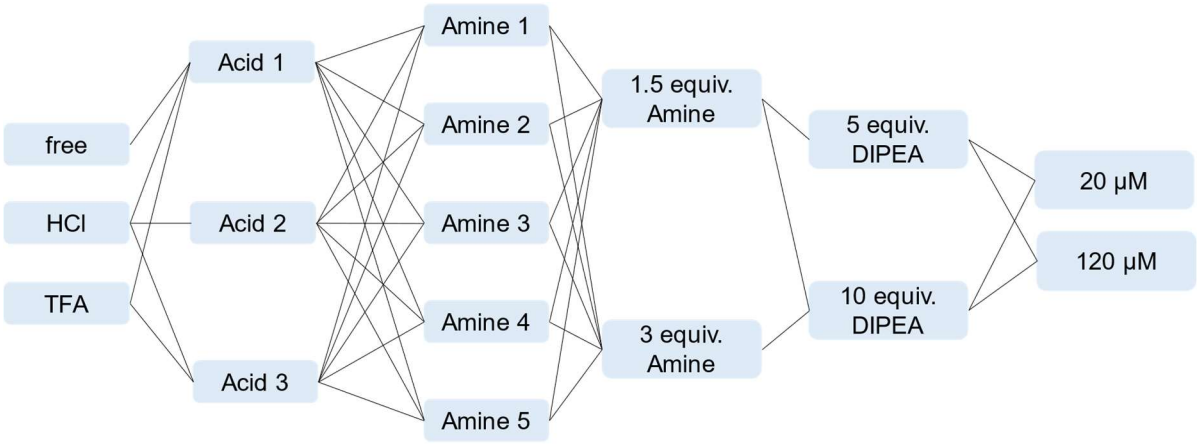

Figure 36: Variation of compounds and reaction conditions that were used for the first screening resulting in 180 different reactions on one DMA slide.

All solutions for dispensing were prepared from stock solutions in DMSO, diluted by DMF to the respective concentration. The dispensing was performed in five dispensing steps using volumes down to 10 nL resulting in 50 nL reaction volume. The whole dispensing was finished within 50 min, while single dispensing steps took around one minute using the CERTUS FLEX liquid dispenser. The slide was incubated between the dispensing steps and afterwards at room temperature in a closed glass petri dish containing a DMF reservoir to maintain a saturated environment. In addition, in the first step the two outer lines of the DMA were filled with 60 nL DMF to reduce evaporation during dispensing steps. After overnight incubation, the solvent was removed under reduced pressure to stop the reaction, resulting in the performance of 720 single reactions having two hours of active working time.

Next, the matrix was added as described before to every spot and the DMA slide was sent for MALDI-MS analysis. The six different acids resulted in three different structures, as the TFA and HCl salts were detected as the same m/z values. An overview of all possible structures is listed in Figure 37. A reaction ID was used to describe the different reaction conditions. Short, three following numbers describe the synthesis of the same compound with the three different reaction conditions (5.00 equiv. DIPEA / 1.50 equiv. amine; 10.0 equiv. DIPEA, 1.50 equiv. amine / 10.0 equiv. DIPEA, 3.00 equiv. amine), the whole list can be found in the appendix.

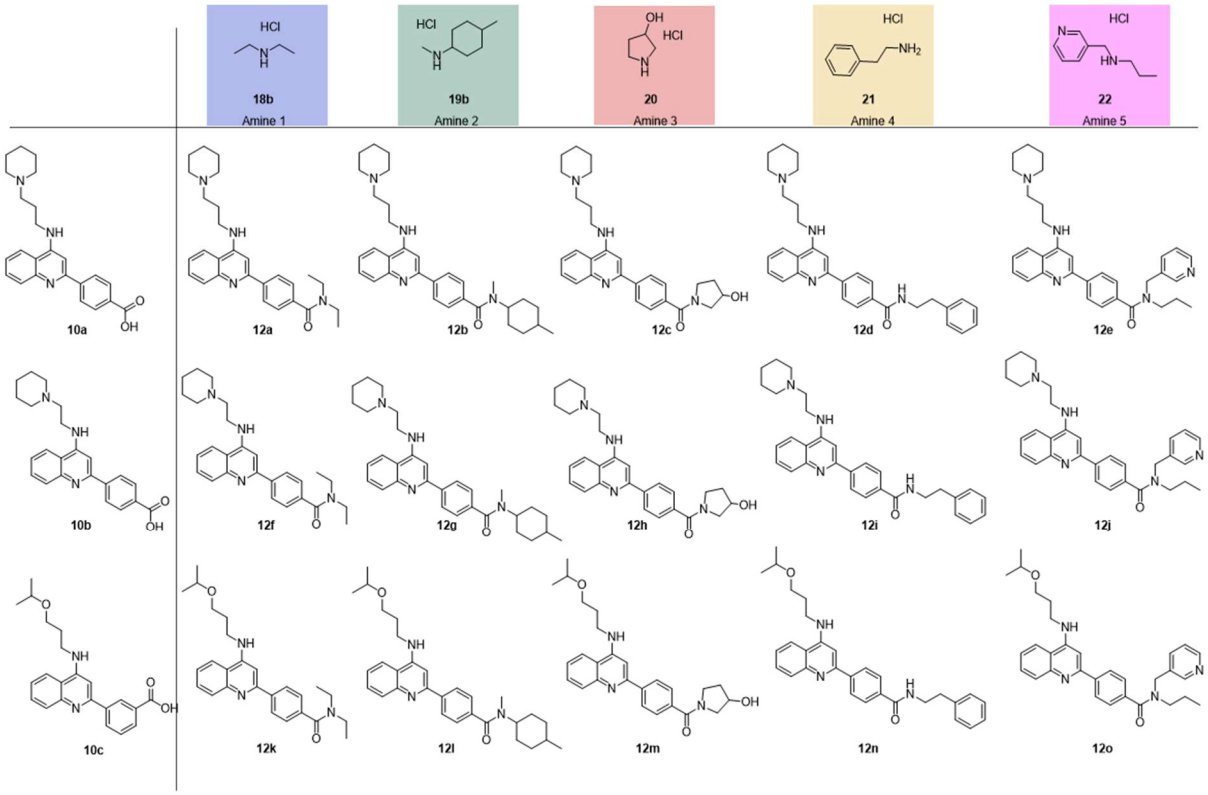

Figure 37: List of all starting materials and products used for the first screening slide. All amines were used as HCl salts, acid **10a** was used in free, HCl and TFA form, acid **10b** as HCl salt and acid **10c** as HCl and TFA salt.

For reactions with acid **10a**, the results of the MALDI-MS screening can be found in Figure 38. The ion intensity was extracted for every m/z signal that corresponds to the product or starting material and the mean value and standard deviation was calculated out of the four repetitions. For the first acid, for the HCl salt only product with m/z = 459.23 ($[M+H]^+$) corresponding to amide **12c** was detected on the expected three spots and very low signal intensities for amide **12b** (m/z = 499.20, $[M+H]^+$) and amide **12e** (m/z = 522.22 $[M+H]^+$). The results for the two other acid forms did not show any product signals and can be found in the appendix. Instead of further product signals, in most reaction spots a signal with m/z = 417.12 ($[M+H]^+$) was detected. This can be explained by a side reaction, where the acid is coupled with dimethylamine (**25**) instead. This amine is formed by hydrolysis of the solvent DMF (**23**) into dimethylamine (**25**) and formic acid (**24**, Figure 38). Especially at the low concentrations of amine in the reaction mixture, this side reaction seemed to be favored and can explain why no product was detected. The high abundance of the side product is also presented in Figure 38C, where for the free acid **10a** (1-29), the HCl (31-59) and TFA salt (61-89) the acid **10a** (grey) and amide **26** (red) signal intensities are summed up. The generally higher signal intensity for the HCl salt was already shown in the preliminary test in Figure 35.

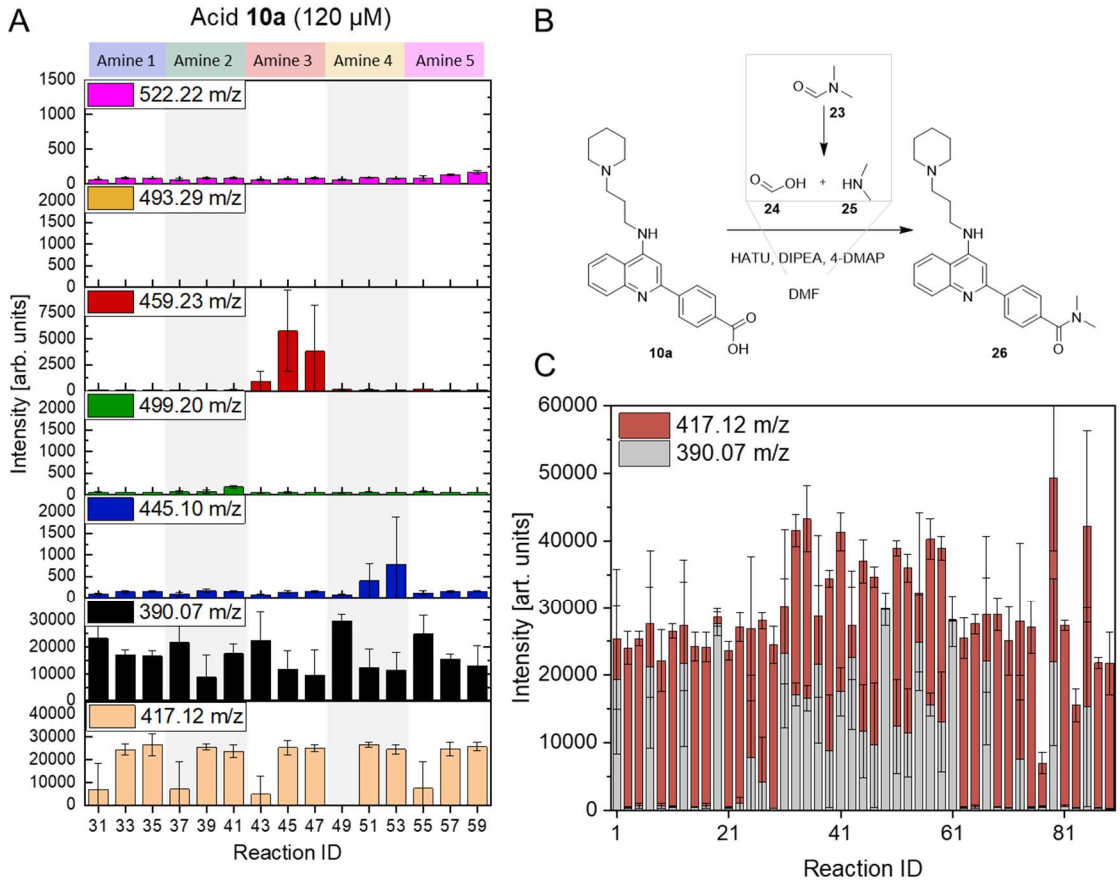

Figure 38: MALDI-MS results for acid **10a**. A) intensities for different masses $[M+H]^+$ for the different amides assigned to the respective amine by color coding as well as the signal for the starting material **10a** (black, m/z = 390.07 $[M+H]^+$) and the side product **26** with m/z = 417.12 ($[M+H]^+$). The reaction ID on the x-axis describes which amine and which reaction condition was used. B) Scheme of the side reaction to form the dimethylamide **26**. C) Graph showing the signals for the starting material **10a** and side product **26** for the different reaction spots for free (1-29), HCl (31-59) and TFA (61-89) form of **10a**.

For reactions with acid **10c**, the results are presented in the same way in Figure 39. Here, there were significant product signals for three different amides **12m**, **12n** and **12o** detected. The different signal intensities could indicate that the reaction has higher yields with higher DIPEA content, as the second spots gave the highest signal intensity in most cases. There were no significant differences for the HCl or TFA salt observed, the slightly lower signal intensity for the HCl salt could indicate a lower conversion due to a higher conversion in the side reaction. In addition, the clear signals at the expected spots could prove that the on-chip synthesis was working in principle, without any side effects by neighboring amines. However, there were some optimization steps required to solve the question if the missing product signals for amine **18b** and **19b** were caused by dispensing, evaporation or side reactions.

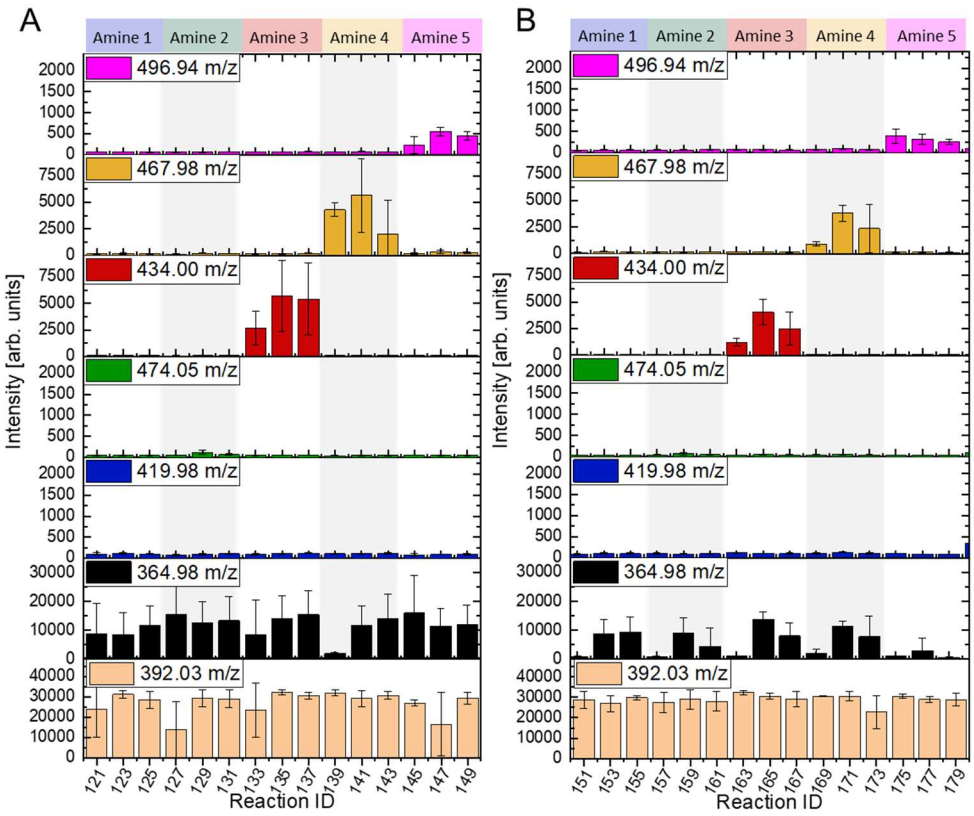

Figure 39: MALDI-MS results for Acid **10c** as HCl salt (A) and TFA salt (B). The signal intensity is given for different mass signals, assigned by color code to the respective amide and acid. The reaction ID on the x-axis describes the condition of the reaction.

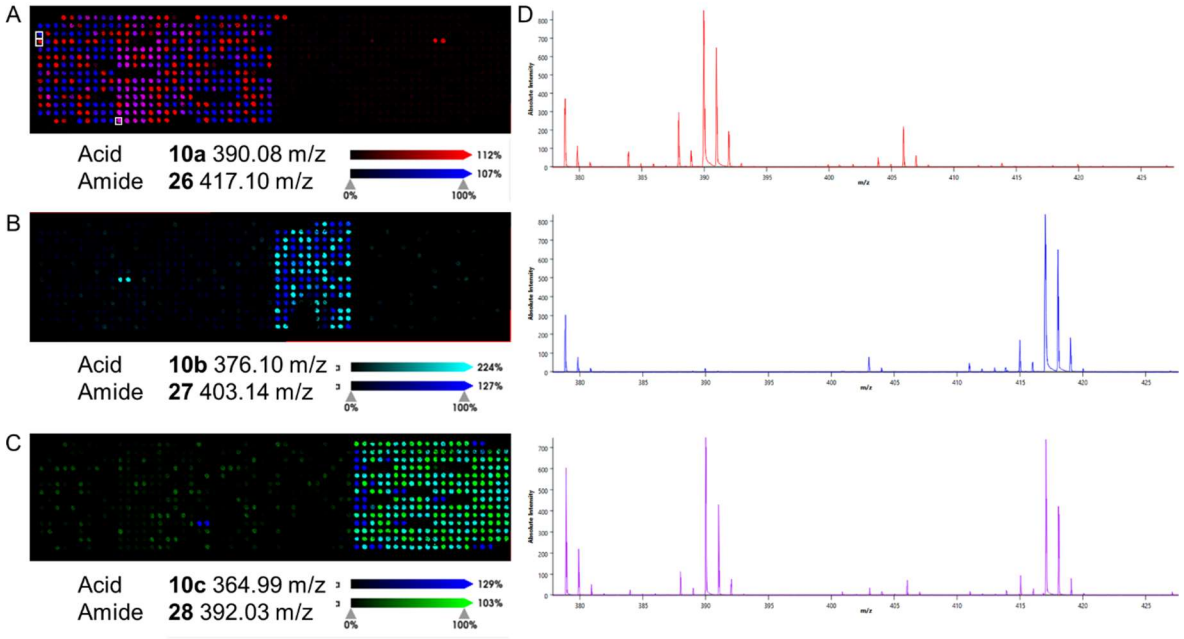

Figure 40: MALDI-MS results for dimethylamide side reaction. A-C shows an ion image of the slide for A) acid **10a** (m/z = 290.08, $[M+H]^+$, red) and the dimethylamide **26** (m/z = 417.10, blue); B) acid **10b** (m/z = 376.09, $[M+H]^+$, cyan) and the dimethylamide **27** (m/z = 403.14, $[M+H^+]^+$, blue) C) acid **10c** (m/z = 364.98, $[M+H]^+$, blue) and the dimethylamide **28** (m/z = 392.03, $[M+H]^+$, green) D) Mass spectra for different spots, indicated in A) containing only acid (red, top), amide (blue, middle) and a mixture of both (purple, center). Image adapted with permission from DR. STEFAN SCHMIDT.

To show the spatial distribution, the ion intensity maps for the three different acids and dimethylamides are presented in Figure 40, representing color coded if either only acid, amide or both signals could be detected. In addition, the mass spectra of representative spots are shown for acid **10a** and amide **26**. There is no evidence that the position of the droplet is advantageous for the side reaction. A detailed dispensing scheme and all mass signal intensities can be found in the appendix.

3.1.8 Investigations on the Side Reaction

For more detailed and quantitative reaction analysis, the reactions in low concentrations were again performed in 500 µL scale. Therefore, a dilution series of the whole reaction mixture from 100 µM to 20 µM of acid **10a** in DMF with 4.00 equiv. of HATU, 5.00 equiv. DIPEA, 0.25 equiv. 4-DMAP and 3.00 equiv. amine **18b** was prepared, with additional variation of equivalents for DIPEA and HATU at 40 µM. The reaction solution was shaken overnight and analyzed by LC-MS. For evaluation, the ratio of the peak area in the chromatogram compared to the whole absorbance spectrum at 254 nm was used.

As shown in Figure 41A, the yield for the highest concentration was very high. 86% of the summed peak area is from product **12a** and no starting material **10a** was detected. But also in this case, the side product **26** with dimethylamine (**25**) from the solvent was detected in low amounts of 14%. With decreasing reaction concentration, the yield also decreased slowly, while the conversion to the side product was increasing. While a reaction yield of 74% for 60 µM reaction concentration might be acceptable, the conversion was getting drastically lower for 40 µM concentration, where the side reaction yield was comparable with the main reaction. For 20 µM, no product **12a** could be detected anymore, while most of the acid **10a** was converted into the dimethylamide (**26**).

The impact of the coupling reagent is also high, as shown for the 40 µM reaction in Figure 41B. With lower equivalents of HATU, the side reaction was clearly favored, while the increase of DIPEA to 10.0 equiv. slightly increased the yield to 53% product formation.

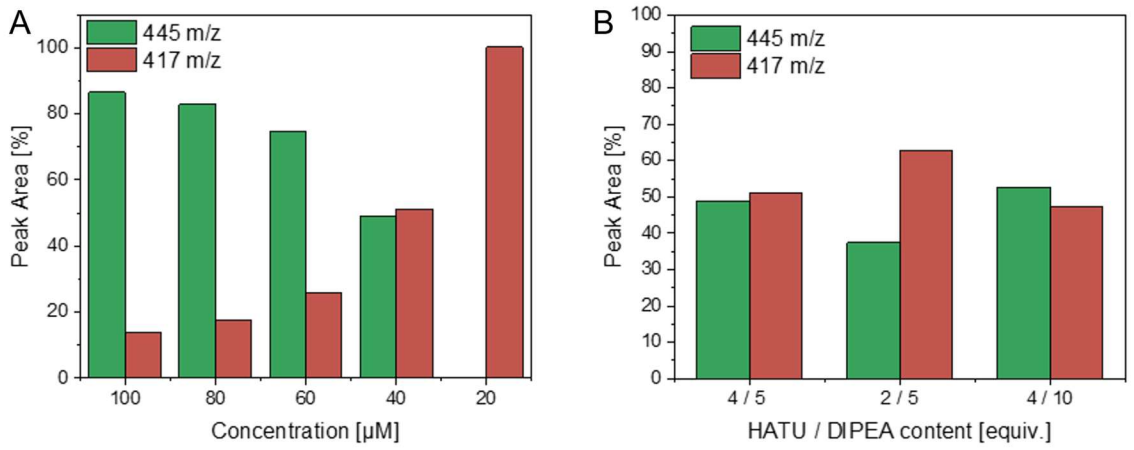

Figure 41: Impact of reagent concentration on reaction yield. A) The reaction solution with 1.00 equiv. acid **10a**, 3.00 equiv. amine **18b**, 4.00 equiv. HATU, 5.00 equiv. DIPEA and 0.25 equiv. 4-DMAP in DMF was prepared in different concentrations based on the acid in 500 µL in a 1.5 mL reaction tube. After 20 h, the reaction solution was diluted 1:1 with ACN and analyzed by LC-MS. The peak area of the two detected signals with m/z = 445 ($[M+H]^+$) at 6.91 min indicating the product **12a** and the signal with m/z = 417 ($[M+H]^+$) at 6.13 min indicating the side product **26** was determined in % in the chromatogram at 245 nm. B) At 40 µM concentration of the acid the content of HATU and DIPEA was varied as indicated on the x-axis. The LC-MS measurement was performed and analyzed as mentioned in A).

The final aim was to optimize the reaction for the enzymatic readout, where lower amounts of inhibitor are favored to distinguish between starting material and product. Furthermore, the side reaction, which most probably also leads to a potent inhibitor, falsifies the readout. Therefore, this side reaction must be suppressed. Furthermore, in this setup there is no purification step planned, so a huge excess of reaction additives like coupling reagent might also have an impact on the enzymatic readout. The easiest way to do so is to change to a different solvent. Hence, the reaction was performed again with 2.00 equiv. HATU and 5.00 equiv. DIPEA, 0.25 equiv. 4-DMAP and 3.00 equiv. amine **18b** in 120 µM and 40 µM concentration in respect of acid **10a**. This time, the solvents were varied to compare DMF with two other high boiling organic solvents DMSO and N-methyl-pyrrolidine (NMP) in 5 µL droplets on 2.83 mm spots on a DMA, after overnight incubation in separated petri dishes for different solvents, the solvent was evaporated under reduced pressure and the samples were analyzed via LC-MS.

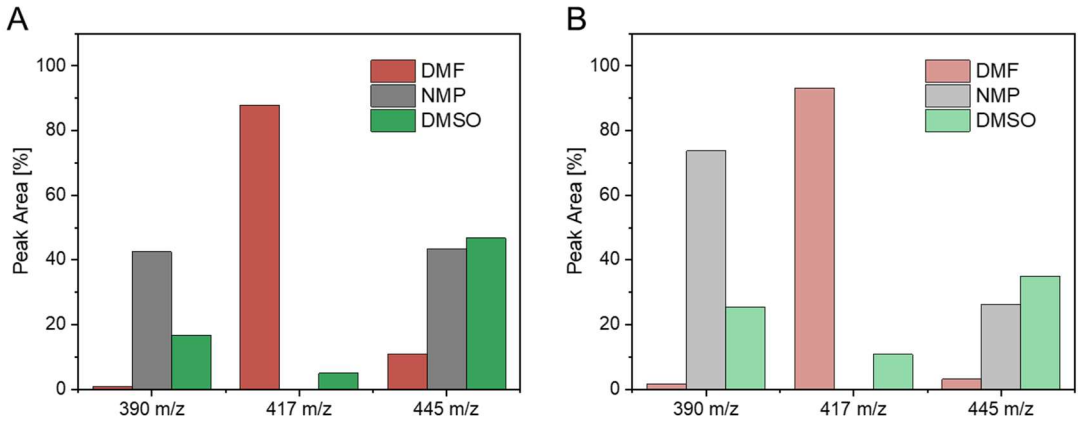

Figure 42: Variation of solvents on 2.82 mm scale. Peak areas for three different signals from the reaction solution in DMF (red), NMP (grey) and DMSO (green) were compared (acid **10a**: m/z = 390, $[M+H]^+$; dimethylamide **26**: m/z = 417, $[M+H]^+$; diethylamide **12a**: m/z = 445, $[M+H]^+$) for high reaction concentration of 120 µM (A) and low concentration of 40 µM (B).

The change of the solvent led to complete (NMP) or at least mostly (DMSO) removal of the side reaction, as there was no significant peak for that mass observed for high and low concentrations. Still, the reaction yield was not too high, resulting in a yield of 43% for high concentrations and 26% for low concentrations with NMP as solvent. The comparably large peak for the starting material **10a** with m/z = 390 ($[M+H]^+$, 73% for 40 µM, 42% for 120 µM) indicates that the reaction might be much slower with the different solvent, but there does not seem to be any competing side reaction that might lead to falsified results by the enzymatic readout. The best result in this comparison was achieved for DMSO as solvent, with 34% yield for 40 µM reaction concentration and 47% for 120 µM. Here, a small peak indicated some side reaction, but not in a significant amount. Also in this case, the remaining acid **10a** might be converted in a longer reaction time or with optimized reagent ratios.

In summary, the product formation on the DMA was confirmed by LC-MS for 5 µL reaction droplets and measured directly from the DMA surface with MALDI-MS for 50 nL reaction droplets down to 1.25 pmol/spot. The cross contamination between different spots by the volatile amines was succesfully tackled by using the respective hydrochloride salts, and a high-content library of five different amines and six different acids with six reaction conditions for each combination was screened with exact spatial distribution of the product signals detected. A second side reaction with the solvent DMF was furthermore detected, and the use of different solvents showed promising results in the first tests. This shows that the miniaturized chemical synthesis in solution on the DMA can be performed in highly dense arrays with an exact and fast analytical readout directly from the DMA.

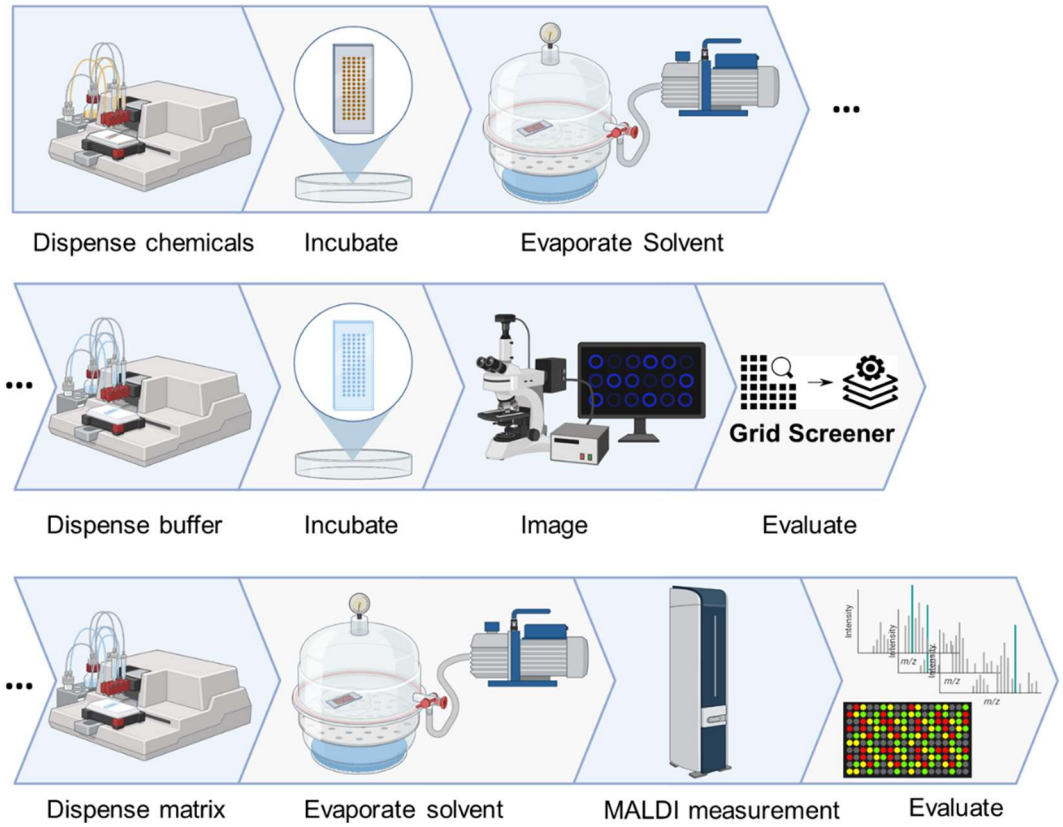

Figure 43: Summary of the workflow of combined synthesis and biochemical screening with additional mass analysis on the DMA.

In this project, all stages of the life-cycle in the early drug discovery stage were investigated and applied to the DMA platform. The high potential of this highly miniaturized platform, suitable for uniting different areas of synthesis, screening and analytics could be shown, as well as the challenges that arise. During the process development, a new readout method for the enzymatic assay needed to be developed, as the miniaturized format did not allow the use of commercially available plate readers. The evaporation rate in droplets of 100 nL or less could be controlled by building a suitable environment. This could be used for fast reaction termination after the synthesis step. Furthermore, the missing purification step set the challenge of interfering starting material, which could be overcome by adjustment of the enzyme concentration and the use of a reference. In addition, the direct application of MALDI-MS measurement on the same platform allowed to proof that the problem of amine contamination was solved by using the respective salts and allowed the fast structural analysis of 720 parallel reactions. With a final combination of the synthesis, screening and analytic step, which were all optimized in this work, this platform could be used to create and screen large libraries with low personal effort and amount of costly material for a cheap and fast hit identification.

3.2 Nanoliter Scale Liquid-Liquid Extraction

After showing an example of solution phase synthesis, combined with an on-chip analytical method as well as an enzymatic screening to analyze the combination of reaction yield and biological activity, the last missing link in the toolbox of miniaturized chemistry is a possibility to purify a crude mixture on the DMA in a HT manner. Purification steps are necessary for most chemical reaction, and require in most cases the highest workload with manual handling steps.

3.2.1 Introduction of the Extraction Concept

Purification describes the separation of a mixture of compounds, where a desired product of interest is supposed to be separated from leftover starting materials, some additional reagents or side products after a reaction. For this, several possibilities have been developed in large scale. However, few examples have been demonstrated to work in miniaturized scales so far.

LLE uses the principle of the different affinity of compounds towards aqueous and organic liquids. Two immiscible solvents are combined to create an interface, which can be than used for mass transfer. In bulk scale, the extraction is usually performed in a separation funnel in milliliter to liter scale. After addition of solvents, the mixture has to be shaken manually to increase the interface by creating an emulsion to accelerate the mass transfer.[94] The two liquids are separated afterwards due to their different densities by leaving them exposed to gravity. After this step, which can take a few minutes, the solutions can be collected separately. In most cases, the aqueous phase is extracted several times with fresh solvent to increase the extraction efficiency. To obtain pure product in the end, the organic solvent needs to be removed by evaporation, which can be time consuming for higher boiling point solvents. This iterative procedure with high solvent consumption is therefore very time consuming. Additionally, it would require complex setups to perform it in an automated or even parallelized way.

To implement this separation technique in a miniaturized experimental setup, the basic working principle needs to be adjusted, as separation by gravity requires complex 3D setups as well as manipulation techniques. One first step in the miniaturized extraction techniques using the DMA was presented by FENG *et al.*[72] and BENZ *et al.*[71] The setup described in their work consisted of two DMA slides, one high surface tension liquid slide containing aqueous droplets, one low surface tension liquid slide with droplets of 1-octanol. These slides were aligned in a special sandwiching adapter so that the droplets could be brought in contact. This setup with the DMAs allows the parallel workup of several droplets at once, but it is not mentioned in detail how many extractions could be performed in one step and how large much solvent has

been used. The sandwich adaptor used in this work is based on two parts which can be assembled with a variable distance determined by four single screws. The use of the two slides requires a very precise aligning tool, and bears the risk of contamination by neighboring droplets when the spots are too close or the two slides are not perfectly aligned, especially when thinking about further miniaturization.

One new possible on-chip extraction method was initially developed in previous works in our group by YELDA NUR DEMIRDÖGEN[1] which resulted in a joint publication based on the master thesis project and this work. In the following, the work of the master student is summarized as an introduction to the method.

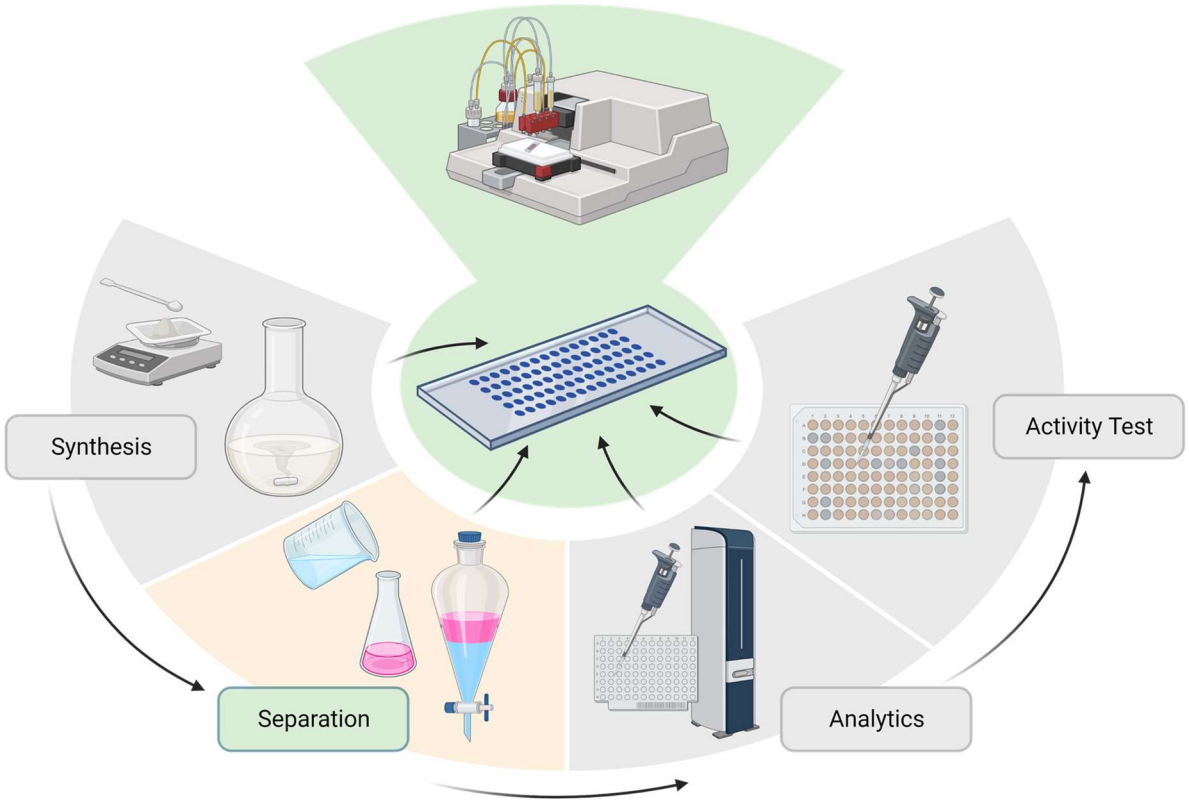

Figure 44: Goal of this project was to develop a liquid-liquid extraction step as missing link for miniaturized synthesis and screening on the DMA.

The method is based on the merging and separation of two neighboring droplets on the DMA. The procedure is schematically shown in Figure 45 and described shortly in the following. The aqueous droplets need to be dispensed first in the center of an omniphilic spot of a Dendrimer DMA slide. By dispensing the organic droplets in a second step with a slightly shifted dispensing pattern, the organic droplets are deposited between the spot containing the aqueous droplet and the next, free spot. The droplets are getting in contact with the aqueous droplets and form an interface where analytes can be exchanged according to their affinity. At the same time,

the organic droplet is spreading on the free omniphilic spot. With time, the spot with higher vapor pressure is evaporating and thereby shrinking, which reduces the connecting interface, until the repelling force is stronger and the droplets are separated on their respective spots. To achieve best extraction results from the aqueous to the organic phase an organic solvent with a lower vapor pressure than water was chosen, so that the aqueous droplet evaporates at first.

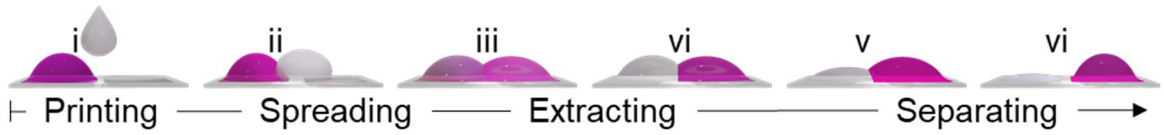

Figure 45: Extraction procedure on the DMA developed by YELDA DEMIRDÖGEN.[1] The aqueous droplet (left) containing an analyte (pink) is merging with the shifted printed organic droplet (right). Over the interface, the analyte is transferred to the organic droplet and the evaporation of the aqueous droplet induces the separation. The image is adapted from the joint publication.[2]

In the previous works, the extraction of the pink dye Rhodamine B from an aqueous solution to 1-octanol was analyzed. Furthermore, the extraction efficiency dependent on the volume ratios of the solvents were tested and investigations on multiple extractions at once by merging several organic droplets with one aqueous droplet in the center were done. The results are presented in the first part of the joint paper[2] and summarized in Figure 46.

1-Octanol was chosen as organic solvent because it evaporates much slower than water. This is advantageous if the extraction from water into the organic solvent is investigated, as reduced volume due to evaporation increases the concentration in the remaining water droplet. The Dendrimer DMA was patterned with omniphilic square spots with a side length of 900 µm, separated by 225 µm omniphobic borders. This close distance and spot geometry enabled the planned merging of the droplets when printing with a 875 µm shifted printing frame.

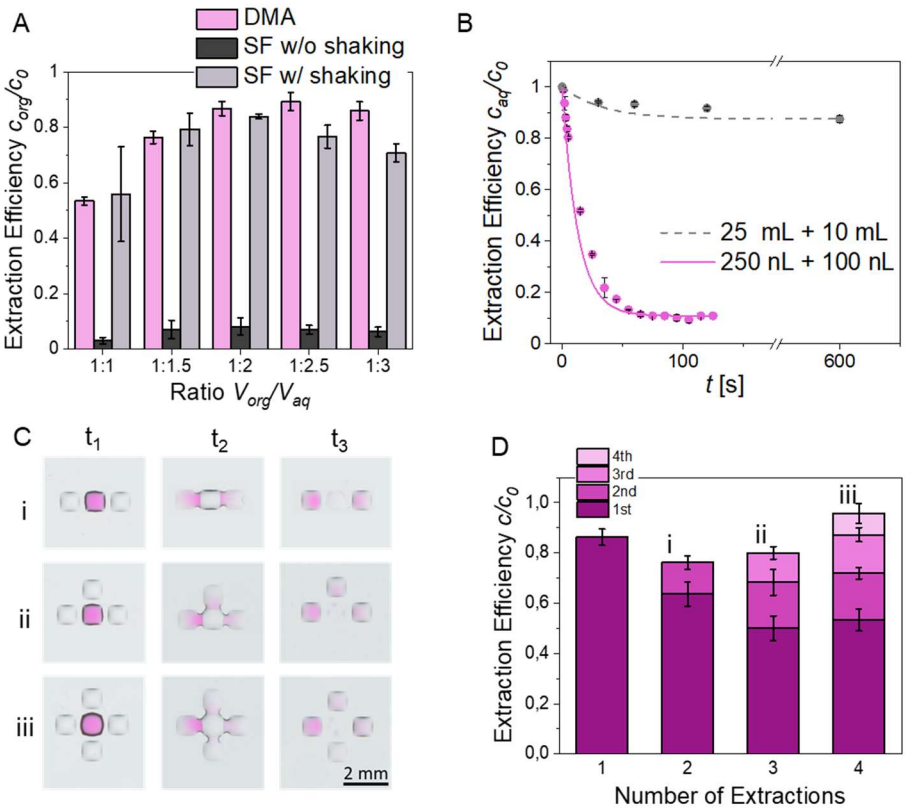

Figure 46: Results of the previous project about the extraction efficiency of rhodamine B to 1-octanol. A) The extraction efficiency of the extraction of 0.2 M Rhodamine B solution on the DMA is compared with the separation funnel using 10^5 times more solvent. B) Kinetics of the extraction between two static phases in 35 mL (grey) and 350 nL (pink). The lines are drawn to guide the view. C) Multiple extractions imaged before (t_1), during (t_2) and after (t_3) extraction. D) Extraction efficiency for different numbers of extracting spots. The extraction efficiency was calculated for every extracting droplet and summed up to the total extraction efficiency. Images are modified from WIEDMANN *et al.* [2]

First, the extraction efficiency was compared to the bulk separation funnel. By analyzing the color intensity of the 1-octanol spots after extraction with the image analysis software IMAGEJ, the extracted amount was calculated by a calibration curve of different concentrations of Rhodamine B in 1-octanol. It was shown that the miniaturized extraction method showed high extraction efficiencies between 53 and 89%, which is in the same range as the commonly used extraction method in the separation funnel with manual agitation. On the DMA, no shaking was required, while the static bulk extraction in the separation funnel resulted in very slow kinetics (Figure 46B) and low extraction efficiencies (Figure 46A). In analogy to iterative extraction steps in bulk procedures, the extraction efficiency could be further improved by merging several organic droplets with one aqueous droplet in the center at once. The images in Figure 46C show the transfer of the dye to all two (i), three (ii) or four (ii) spots depending on the order of mixing. Figure 46D presents the increased overall extraction efficiency by summing up the extracted amount in every spot, resulting in extraction efficiencies of 95%.

All results presented in the following were obtained in this PhD work. Contributions by other people are clearly indicated.

3.2.2 Impact of Environmental Conditions

As described before, the separation of the two phases is based on evaporation. Therefore, the two solvents need to show high differences in evaporation time, which can be defined by the vapor pressure. In contrast to the boiling point, the vapor pressure gives the information about the evaporation tendencies at room temperature. The vapor pressure was used to estimate the volatility and evaporation speed in the miniaturized format, as it gives information about the pressure required to evaporate at room temperature. Higher pressures indicate that the solvent evaporates already at atmospheric pressures, while solvents with extremely low vapor pressure often require reduced pressure by a vacuum pump for evaporation at room temperature. The two solvents used in the model extraction were deionized (dI) water with a vapor pressure of 3.17 kPa and a boiling point of 100°C[95] and 1-octanol with a vapor pressure of 8.7 Pa and a boiling point of 195°C[96] The evaporation kinetics are presented in Figure 47 where 1-octanol droplets did not show significant reduction in droplet size, even for small volumes, while water droplets were completely evaporated after four minutes. 1-Octanol droplets could be evaporated under reduced pressure (Figure 47C).

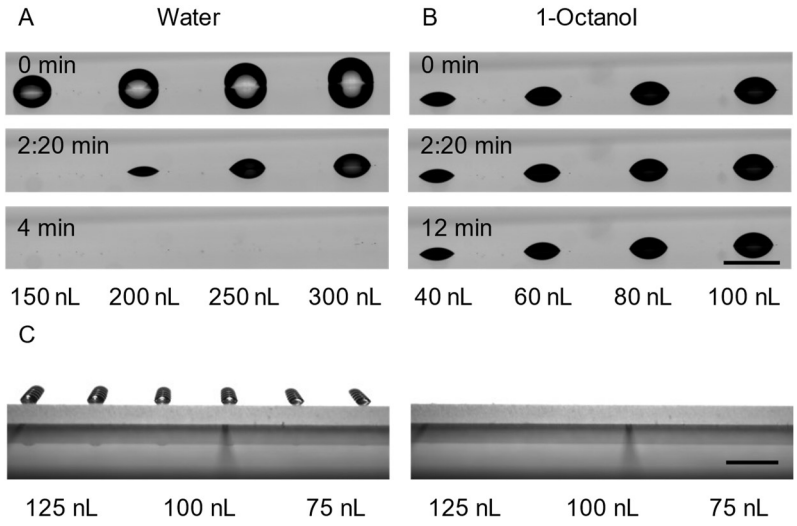

Figure 47: Evaporation of water and 1-octanol. A) Evaporation of 150 – 300 nL water droplets within 4 min. B) 1-octanol droplets between 40-100 nL with only minor evaporation after 12 min. C) 1-octanol droplets of 75-125 nL before (left) and after (right) 1 h evaporation under reduced pressure. The figure was adapted from WIEDMANN *et al.*[2]

In most cases, the slide was placed in an opened petri dish in a fume hood for ten minutes. This resulted in a slightly different extraction time for spots on the outer borders, which separated first after five minutes compared to the ones in the center with much higher surrounding

humidity. To make sure that this aspect can be controlled, several different environmental setups and their impact on the extraction efficiency and time were investigated. 186 extractions were performed in parallel in 6 × 31 rows with 250 nL aqueous Rhodamine B solution and 75 nL of 1-octanol. The first slide was placed in the fume hood on a well-ventilated place, while a second slide was placed in a so-called humidity chamber, consisting of a petri dish with a water-soaked tissue sticking to the lid. This increases the surrounding humidity and was used to prevent unwanted evaporation. After 15 min, the droplets were still all merged and the slide was placed in the fume hood for separation. Here, the droplets took again 10 min to separate completely. The third slide was placed in a desiccator connected to a vacuum pump to accelerate the evaporation, which resulted in separated droplets after 3 min. This shows that the extraction time can be easily adapted and controlled by the environment. In the next step, the extraction efficiency was evaluated to see if the manipulation of the extraction time also has an impact on the extraction efficiency. For that, the slides were imaged by the document scanner and the images were evaluated with IMAGEJ. The images were transferred to HSV-stacks, which means that the colors of the slide were described by three independent images with values for the Hue, Saturation and Value (Figure 48B).

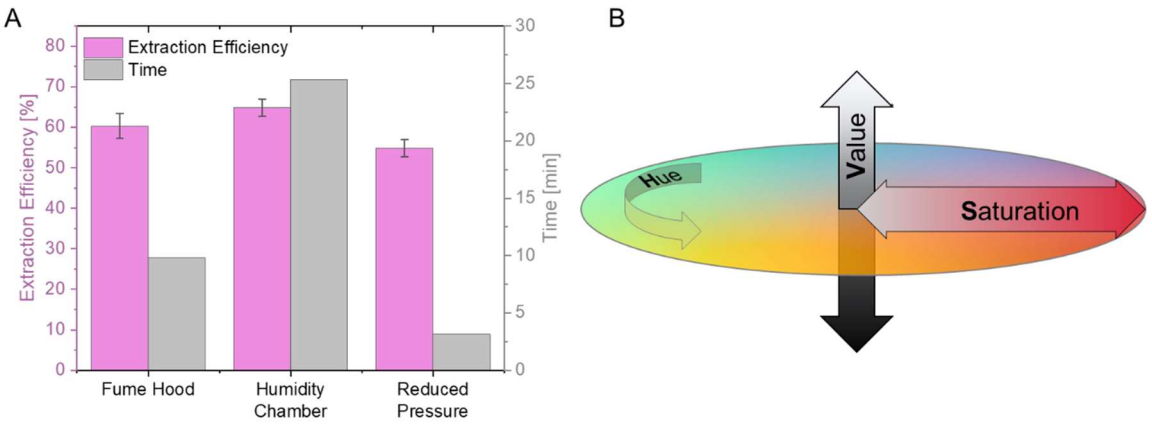

Figure 48: Extraction Efficiency depending on the environmental conditions. A) The extraction efficiency was calculated for a slide placed in a fume hood, in a petri dish with a soaked tissue in the lid containing dI water and for a slide in a desiccator connected to a vacuum pump (pink), as well as the time until the last spot on the slide was separated (grey). B) HSV color space which can be used to describe a color by its Hue (H), Brightness (Value, V) and Saturation (S). The saturation value was used to measure the color intensity and thereby concentration of Rhodamine B.

The extraction was observed by the color change from the colorless 1-octanol to the intense pink droplet, which can be exactly described by the saturation value *S*. The *S*-value was determined for a certain area inside one droplet and 25 randomly distributed droplets from each slide were used to calculate a mean saturation value with a standard deviation. To determine

the concentration, a dilution series of Rhodamine B was dispensed, dried and redissolved in 75 nL Rhodamine B and analyzed in the same way to give a calibration curve which can be found in the appendix. The calculated extraction efficiency was divided by the calculated concentration of 100% transfer of Rhodamine B to the 75 nL droplet and is presented in Figure 48A in pink. As expected, the extraction efficiency was slightly increased by 4% after prolonged extraction time, while it was reduced by 6% when the evaporation took place earlier. The comparably small error bars of +/- 2-3% indicate that despite the different extraction times between outer borders and spots in the centers, the extraction efficiency is not changed significantly. This shows that the extraction efficiency and duration could be adjusted by the environmental humidity and can therefore be adapted to the requirements of any applications.

To be able to understand the high extraction efficiency of this static system compared to the separation funnel, where the system needs to be vigorously shaken to achieve sufficient extraction efficiency, the ratio of interfacial area to the volume of the solvents needed to be considered. Therefore, the dimensions of the miniaturized system needed to be analyzed further. With the help of a computational model of droplets on the DMA, the interfacial area of the merged droplets was calculated in collaboration with YANCHEN WU and FEI WANG in the group of BRITTA NESTLER. The behavior of aqueous droplets was already studied before in this system[97] and was applied to the organic droplet based on the different contact angles of 1-octanol in Table 4.

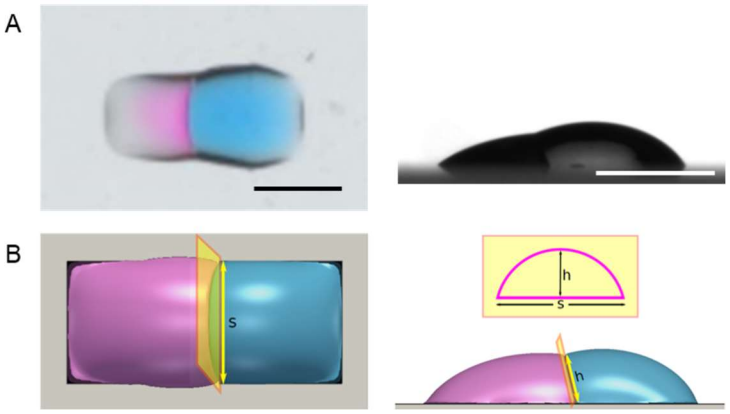

Figure 49: Phase-field modeling of the merged droplets.Real image of an organic (pink) and aqueous (blue) droplet from top (left) and side view (right). B) Image of the modelled system from top (left) and side (right) to estimate the yellow interfacial area. The figure was adapted from WIEDMANN *et al.*[2]

Table 4: Contact angles for water and 1-octanol on the dendrimer DMA

	Omniphilic surface	Omniphobic surface
Water	34° +/- 0.1	111° +/- 0.7
1-octanol	22° +/- 0.3	73° +/- 0.7

Based on this phase-field model, the contact area was 0.25 mm^2 for droplets of 200 nL. Comparing that to a normal separation funnel with a diameter of 7 cm and 200 mL volume, the ratio between surface and volume is 100 times higher for the droplets. This results in a fast mass exchange without the necessity to further increase the size of the interface.

3.2.3 MALDI-MS for Low Concentrated Extractions

The final goal of biological application requires the handling of quite low concentrations in lower micromolar to nanomolar range.[59] To investigate the extraction efficiency for lower concentrations, a new readout method with higher sensitivity was needed. MALDI-MSI was therefore used to detect the extraction of 20 nM – 4 µM Rhodamine B samples.

As mentioned before, MALDI-MS measurements are supposed to be performed on ITO-DMAs. Even though the dendrimer modification can be applied to ITO-coated surfaces, the hydrophobicity of the border was not sufficient to separate the droplets by pushing the 1-octanol droplet back to its original spot after the extraction. Therefore, a normal glass slide was used to perform the extraction experiment. For charge transfer of the system, a conductive tape was placed on the back side of the slide before the measurement and directly connected to the adaptor (Figure 50B). This method was described by WU *et al*. as efficient method to measure MALDI-MS on a non-conductive glass surface.[93] After performing the extraction, 1-octanol was evaporated as well under reduced pressure over night and 50 nL of 0.1 M HCCA matrix was dispensed on every spot. The slide after crystallization of matrix is shown in Figure 50A, which shows clearly separated spots with quite homogeneous matrix crystals. Application of the tape and MALDI-MS measurement was done by DR. STEFAN SCHMIDT in the working group of PROF. CARSTEN HOPF (CEMOS). A BRUKER rapiflex was used for measuring to image the whole slide with a step-size of 100 µm with a mass resolving power of 10 000. This resulted in several measurement points for one spot. A script designed by DR. STEFAN SCHMIDT was used to extract the mean value for every spot, which was used for further evaluation.

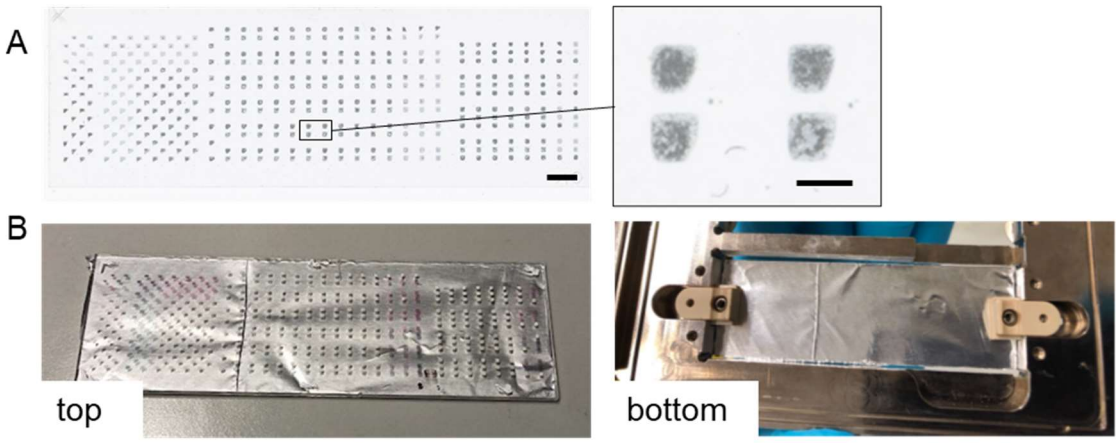

Figure 50: Setup for MALDI-MS measurements on a glass slide. A) Scanned image after dispensing of matrix to the respective spots. B) Glass DMA in the MALDI-MS adaptor from BRUKER with conductive tape on the back from top (left) and bottom (right). The figure was adapted from WIEDMANN *et al.*[2]

The $[M\text{-}Cl^-]^+$ signal of Rhodamine B (m/z = 443.24 +/- 0.04) was detected on the control spots as well as the 1-octanol spots after extraction up to 50 fmol/spot of initially added analyte. This corresponds to 0.2 µM, concentration in 250 nL. Furthermore, for all different concentrations, there is no significant Rhodamine B signal detected in the spots, where the aqueous droplet was placed. This results in a high extraction efficiency also for very low concentrations. This shows that in addition to the low volumes, also very low concentrations can be handled and extracted with this method.

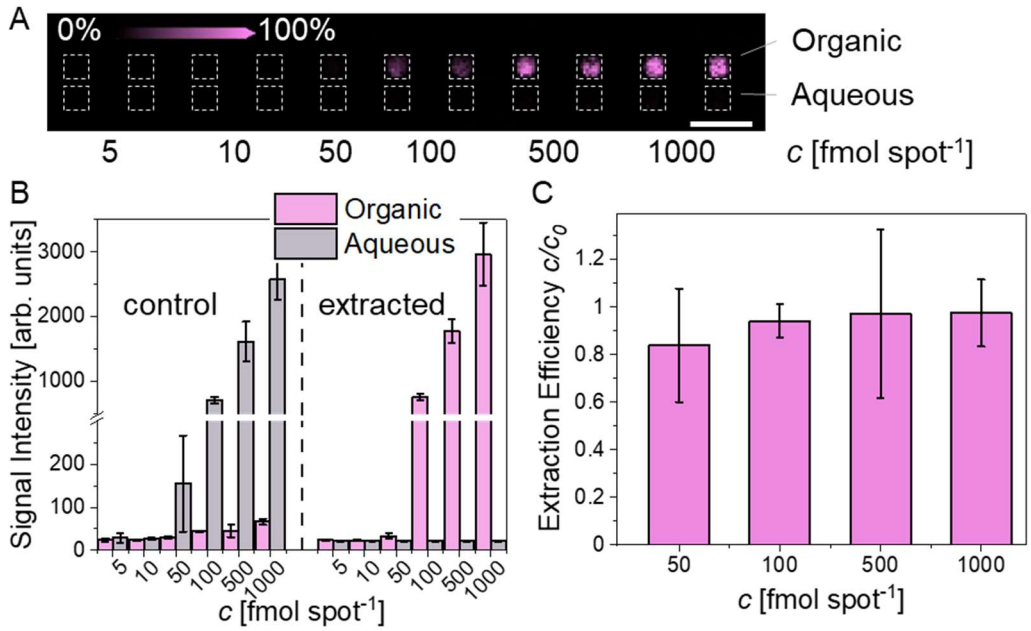

Figure 51: MALDI-MS results for Rhodamine B extraction. A) Ion intensity plot for the Rhodamine B signal after extraction of different low concentrations between 5 and 1000 fmol/spot from the aqueous droplet (bottom) to 1-octanol (top). The signal intensity is represented by the color intensity. Scale bar is 2mm. B) Signal intensity on the organic (pink) and aqueous spots (grey). The values are mean values of three repetitions with their standard deviation. The left half represents the spots without extraction, the left part after extraction process. C) Extraction efficiency calculated by the ratio of signal intensity on the organic spot to the sum of signal intensity on both spots. The figure was adapted from WIEDMANN *et al.*[2]

3.2.4 Separating and Detecting a Mixture of Dyes

So far, the description of the extraction process was based on the single transfer of one dye. To support the hypothesis of selective extraction through different affinity to the two phases, a second analyte, Methylene Blue was introduced. This blue dye showed a better solubility in water than 1-octanol and was therefore not extracted to the organic phase. Both dyes were first printed separately and the extraction method was performed with 1-octanol. For better visualization, in Figure 52A and D 1-octanol was printed next to the aqueous droplet without merging in the "before" mode, and water was added to the evaporated aqueous spot after extraction. The top part in Figure 52A-C reproduces the extraction of the pink dye Rhodamine B. The part below proved the selectivity aspect, as the blue dye was not transferred to the neighboring droplet, but stayed in the initial aqueous spot. This proves the assumption that the mass transfer is based only on affinity, despite the completely evaporated aqueous droplet.

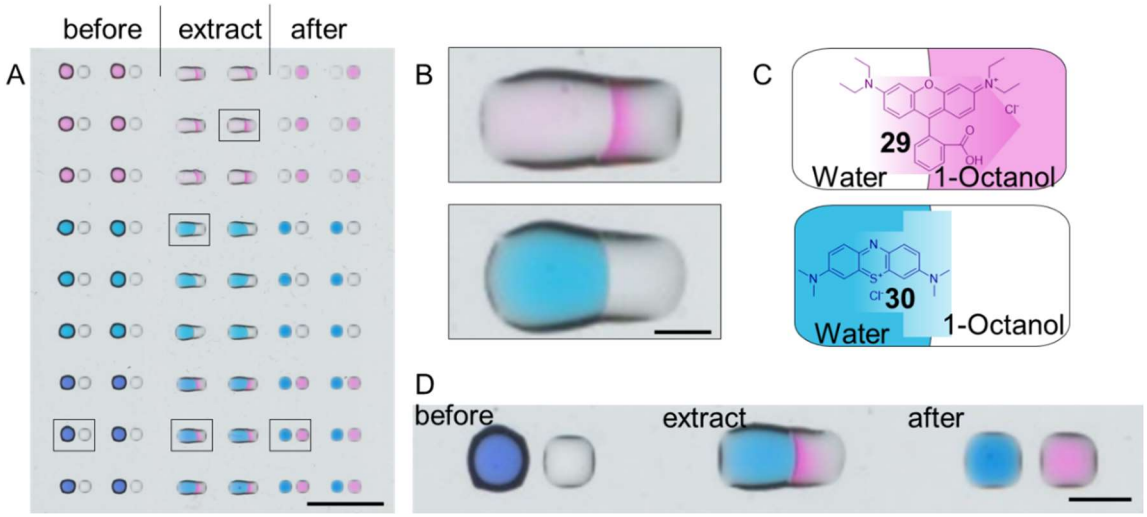

Figure 52: Extraction of Rhodamine B and Methylene Blue. A) Overview of parts of a slide containing 250 nL aqueous solution (left spot) with Rhodamine B (top), Methylene Blue (center) or a mixture of both dyes before (left), during (middle) and after (right) extraction with 100 nL 1-octanol (right spot) in six repetitions each. B) Zoomed images for a spot containing Rhodamine B (top) or Methylene Blue (bottom). C) Scheme of the extraction containing the chemical structures of Rhodamine B (top) and Methylene Blue (bottom). D) Zoomed images of an extraction of a mixture of both dyes. The separation of the mixture (purple spot) to Methylene Blue in the aqueous droplet (left, blue) and Rhodamine B in the organic phase (pink, right) can be observed by the color shift. All images are obtained by a document scanner. Images was adapted with modifications from WIEDMANN *et al.*[2]

In the next step, a mixture of both dyes was extracted with the same method, represented in Figure 52A in the bottom part and Figure 52D. Here, it could be observed how the purple mixture of both dyes in the beginning was separated into a blue part on the left, indicating the aqueous droplet containing Methylene Blue and the pink droplet on the right containing

1-octanol with Rhodamine B. This is the first example of a separation of a mixture directly on this DMA platform in nanoliter scale without any additional slide or manual handling needed.

After observing this separation clearly by eye, the next challenge was finding a method to measure this separation in nanoliter format. One quite sensitive technique commonly used in organic synthesis is the Thin Layer Chromatography (TLC).[98] The method can be used to analyze a mixture and to identify a reagent, if its specific Rf value is known for the solvent system or if it is directly compared to the pure compound as reference. For sampling, a thin capillary was used to directly pick up the sample from the DMA, which was redissolved by acetonitrile as it is shown in Figure 53 A. The TLC is shown in Figure 53B, where the mixture was added to the first spot, followed by the organic droplet (2) and aqueous droplet (3). As comparison, an aqueous Rhodamine B solution was added to position 4 and aqueous Methylene Blue solution to position 5. The mixture of dyes is clearly separated after running the TLC in DCM with 10 vol% methanol. Furthermore, the control spots show the same height and therefore Rf value as the two spots in the first lane. The successful separation can be proved by the fact, that there is only one spot visible for each droplet from the DMA, only Rhodamine B from the organic spot and Methylene Blue from the aqueous spot.

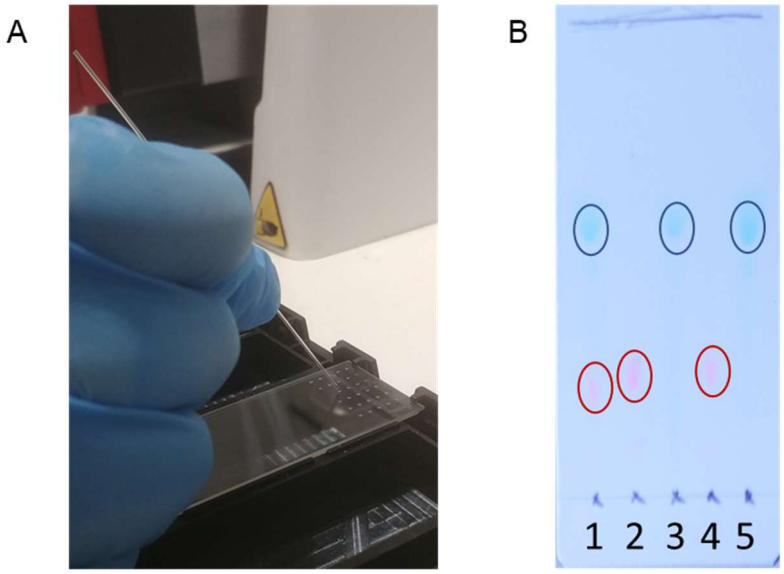

Figure 53: TLC analysis of the separation of the dyes. A) Sampling with a thin glass capillary directly from the DMA. B) TLC with (1) mixture of Rhodamine B and Methylene Blue, (2) Organic droplet collected from the DMA, (3) aqueous droplet collected from the DMA, (4) pure Rhodamine B solution and (5) pure Methylene Blue. The TLC plate was developed in DCM containing 10% methanol. The TLC was imaged by a camera and the spots surrounded with the respective color. Modified from WIEDMANN *et al.*[2]

A second detection method was again based on the scanned image and an image analysis method. In this case, the CIELAB color space was used to determine the color on the droplets.

In this color space, the color intensity is given by the L value, the *a* vector is describing the color range between blue and yellow and the *b* vector the color shift between red and green. Analyzing the images, it turned out that the *a* value can be used to clearly differentiate the color shift between blue, purple and pink (Figure 54A).

A

CIELAB	L	**a**	b
Rhodamine B	70	**35**	-22
Methylene Blue	69	**-25**	-27
mix	53	**17**	-52

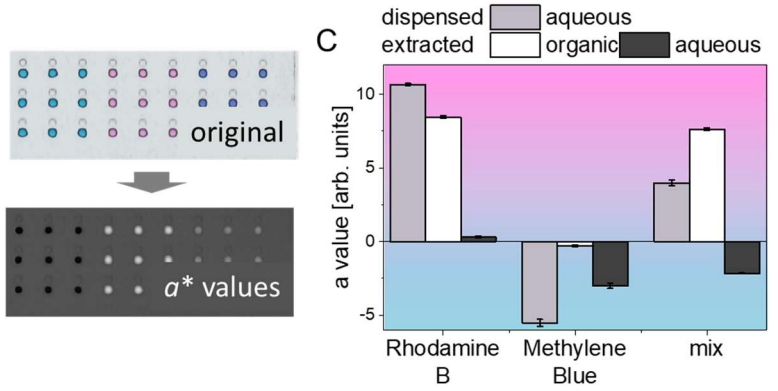

Figure 54: Color analysis in the L*a*b color space. A) The color space is described with the vector a (yellow/blue) and b (red/green). The L, a, and b values were determined for the different colors. B) Image of the original image obtained after scanning with 3 × 3 samples of Methylene Blue, Rhodamine B and a mixture of both (from left to right) on top and the layer describing the *a* values after the image was transformed to a L*a*b stack. C) *a* values for three different extraction experiments (y-axis) for the aqueous spot before extracting (grey) and the 1-octanol droplet (white) and water droplet (black) after extraction was performed. C) was adapted from WIEDMANN *et al.*[2]

Therefore, the scanned image from Figure 52A was converted into a lab stack in Image J (Figure 54B) and the *a* value was measured for every spot within a small square in the center. The *a* value ranges from -5 for Methylene Blue containing spots to +10 for Rhodamine B spots, while the colorless phase after extraction shows a value around zero and the phases where the dye is expected shows slightly less extreme values. For the purple mixed phase directly after dispensing the aqueous phase only, a value of 4 was measured representing a color between the two extremes. After extraction, the organic phase showed an increased a value of 7.6 in the same range as the extracted Rhodamine B spot and the aqueous phase showed a negative value of -2.1, which is close to the value of 3.0 obtained from the pure Methylene Blue control experiment.

This unfamiliar approach is an example for using image analysis to confirm and transform our optical readout into clear values, which describe the shift of a color. This highlights the possibility of developing new readouts if the volumes are getting too low to be analyzed via commonly used uv/vis spectrometers or plate readers. Even though the color intensity was high enough to detect some absorbance, their default setting based on the microtiter plate format did not allow to use this highly miniaturized and dense format.

While MALDI-MS could be easily adapted to the 18 × 64 DMA format, the possibility of ion suppression must be considered when two different compounds should be detected in a mixture. Therefore, a two-dimensional concentration gradient of both compounds was dispensed on different spots in duplicates. The different ratios of both dyes were analyzed by MALDI-MSI and the signal intensity for both signals of 284.06 m/z for Methylene Blue and 443.09 m/z for Rhodamine B were plotted. In both graphs in Figure 55, the signal intensity for the respective m/z signal was plotted against the concentration of Rhodamine B on the x-axis for all concentrations of Methylene Blue in the color code. The signal intensity in Figure 55A clearly depended on the concentration of both dyes, as the signal intensity for higher concentrations of Rhodamine B is decreasing with a higher concentration of Methylene Blue. This indicates a strong ion suppression effect of Methylene Blue on Rhodamine B, which means that the concentration of Rhodamine B in a mixture with Methylene Blue cannot be determined quantitatively by MALDI-MS. In Figure 55B, the signal intensity of Methylene Blue is plotted. Here, the signal intensity was as expected increasing with increasing concentration of Methylene Blue. At the same time, the signal intensity is nearly constant for all concentrations of Rhodamine B, indicating that there is negligible impact on the ionization of Methylene Blue by Rhodamine B. Only for the two highest concentrations of Rhodamine B the signal intensity was slightly decreasing for all concentrations of Methylene Blue. This indicates that MALDI-MS measurements in this format can be only used to qualitatively detect if Rhodamine B is transferred while Methylene Blue is retained in the initial spot, but not for a quantitative description of the amount of Rhodamine B that is remaining in the initial spot.

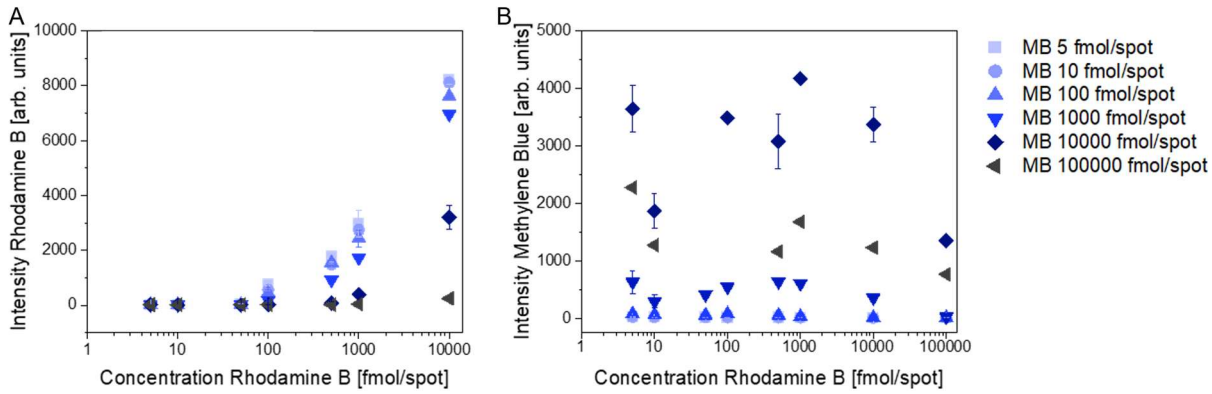

Figure 55: MALDI-MS measurements for mixtures of Rhodamine B and Methylene Blue. The two dyes were dispensed in a two-dimensional gradient matrix to analyze the ion signal intensity for both components in different ratios. A) The intensity of Rhodamine B (m/z = 443 $[M\text{-}Cl^-]^+$) is shown for different concentrations from 5 to 10000 fmol/spot. The different colors indicate different concentrations of Methylene Blue added to the same spot. B) The intensity of Methylene Blue (m/z = 284.058 $[M\text{-}Cl^-]^+$ is presented for the same concentrations of Rhodamine B dispensed on the same spot. The different colors of the symbols indicate the dispensed amount of Methylene Blue.

3.2.5 Variation of Solvents

So far, the organic solvent used for extraction was 1-octanol. In the next step, the scope of solvents with different properties and their impact on the extraction was investigated. In bulk extractions, the separation is based on gravity, which means that the phase with higher density is accumulating on the bottom of a separation funnel. The phases are separated by pouring out the different phases from the bottom of the separation funnel. By changing the organic solvent, the order of the two phases can change depending if the density of the organic solvent is higher or lower than 0.997 g/mL, which is the density of water. This can lead to confusion especially for unexperienced chemists and might cause problems in automatization of processes when solvents need to be changed.

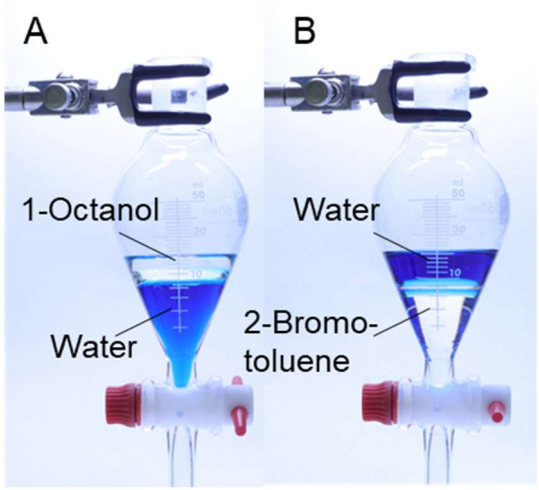

Figure 56: Behavior of organic solvents with different densities. A) Separation of 1-octanol (colorless) and water (blue). B) Separation of 2-bromotoluene (colorless) and water (blue). The aqueous phase is stained with Methylene Blue for better visualization. The figure was adapted from WIEDMANN *et al.*[2]

Having the small volumes of 100 nL on this open platform, most commonly used solvents like dichloromethane or ethyl acetate can't be used in this miniaturized extraction, as the droplets immediately evaporate. Nevertheless, this does not need to be a drawback, as completely new solvents suddenly become suitable if they can be evaporated under reduced pressure in small droplets with high surface areas. The two organic solvents 1-octanol (0.83 g/mL) and 2-bromotoluene (1.42 g/mL) were used as examples with higher and lower density than water (Table 5). Both have a lower vapor pressure than water to make sure that the established working principle of the aqueous phase evaporating first is the same. Again, a mixture of Methylene Blue and Rhodamine B was used to demonstrate the separation. In the case of 2-bromotoluene, it needs to be mentioned that the intense pink color of Rhodamine B was quenched if dissolved in an aprotic solvent in lower concentrations.[99] In Figure 57, scanned images before, during and after the extraction process are presented. After the respective

organic solvent was merged with the aqueous droplet, the aqueous phase turned light blue as before, while the transfer of the pink color was only observed for 2-bromotoluene. To compare the extraction result, the solvent was evaporated for all spots and 100 nL of water was added to all spots, resulting in a pink color for the extraction with 1-octanol as well as 2-bromotoluene. Even though the aqueous spot shows a slightly darker color, indicating only partial extraction, a visible color change proves that the extraction works in the same way for solvents with higher densities.

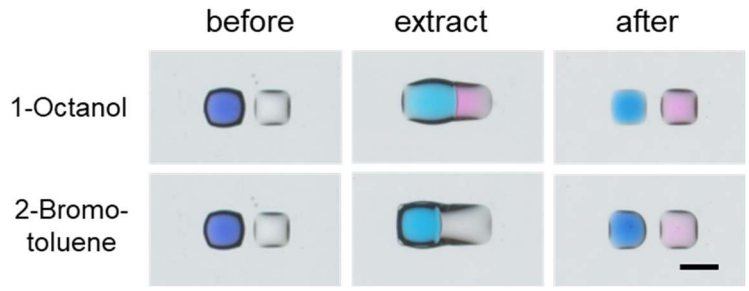

Figure 57: Extraction with 1-octanol and 2-bromotoluene. In every image, the aqueous droplet is placed on the left side and the organic on the right side. The figure was adapted from WIEDMANN *et al.*[2]

The last result seems to be obvious, as the separation in the array format is not based on gravity, but on evaporation. Therefore, toluene was chosen as third solvent, having a lower density, but higher vapor pressure than water, resulting in a faster evaporation. Due to bad solubility of Rhodamine B in toluene, a different dye was used to observe the extraction procedure. In this case, Bromothymol Blue was used, showing a bright yellow color at neutral pH. This dye showed a higher affinity to water than toluene, resulting in a setup where the toluene droplet containing the yellow dye was added to a colorless aqueous spot. As shown in Figure 58, the dye is transferred from the toluene containing spot on the right to the aqueous droplet on the left.

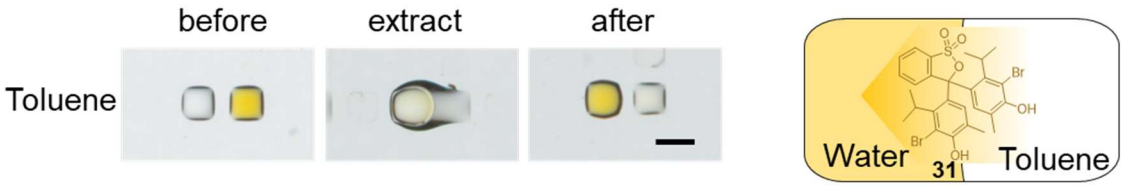

Figure 58: Extraction of Bromothymol Blue from toluene (right) to water (left). The scheme on the right shows the chemical structure of the dye (**31**) and the extraction behavior. The figure was adapted from WIEDMANN *et al.*[2]

Showing the possibility of using organic solvents with different densities and boiling points, with the same setup of two dispensing steps in the same order, resulting in the same array of separated phases as it was dispensed, the huge impact of the two-dimensionality of the

extraction in array format was highlighted. In case of applications in a fully automated system, the choice of solvents for extraction does not have any impact on the procedure and the following steps, as the organic phase can be always collected form the same spot where it was initially printed.

Table 5: Solvents and their physical properties (data obtained from[90])

	Density [g/mL]	Vapor pressure [kPa]
Water	0.99	3.16
1-Octanol	0.83	0.0087
2-Bromotoluene	1.43	0.133
Toluene	0.87	3.79

3.2.6 Acid-Base Extraction

After presenting and characterizing the extraction system with dyes for better visualization, the next approach was motivated by the idea of performing a reaction workup directly after synthesis on the spot. For separation of more complex mixtures, the variation of the pH value in the aqueous phase can be used to change the affinity of different compounds to the two phases based on their pKa value. Exemplarily, this was investigated with two model compounds, a carboxylic acid 2,5-dihydrobenzoic acid (DHB) and an aromatic structure with an amine group, *p*-anisidine. In their neutral state, both molecules are extracted to the organic phase because of their positive logP value (DHB 1.74,[100] *p*-anisidine 0.95[101]). But by changing the pH value, they can be transformed into their protonated or deprotonated and thereby charged form. This was used to manipulate the mixture of both compounds to selectively pull one of them into the 1-octanol droplet.

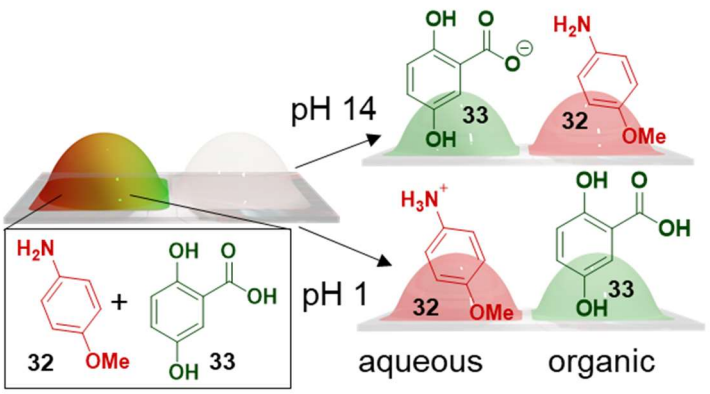

Figure 59: Acid-Base Extraction of DHB and p-anisidine. The scheme shows the structure of the amine (red) and carboxylic acid (green) and their expected separation between the aqueous and organic phase for basic (top) or acidic (bottom) pH values. The figure was adapted from WIEDMANN *et al.*[2]

Figure 59 shows schematically the pH dependent separation, where the carboxylate is retained in the aqueous phase at high pH values and the ammonium salt stays in the aqueous phase at low pH. In the first experiment, the aqueous mixture was dispensed on the DMA with different pH values and extracted with 1-octanol. The compounds don't show any intense color and therefore an indirect detection method was required. As described above, single spots of the extraction phase could be collected by a glass capillary and spotted on a TLC plate. After developing the TLC in a mixture of DCM/MeOH/acetic acid (89/10/1) and staining with iodine vapor, the plates were imaged by a camera. The TLC in Figure 60A shows the compounds in the organic spots after extraction. The top spot with an Rf value of 0.83 and a smaller spot below at Rf = 0.55 can be assigned to p-anisidine. The lower one can be explained by some o-anisidine contamination in the stock. The lower band with Rf = 0.33 can be clearly identified as DHB. Therefore, the hypothesis was confirmed. A comparison of the aqueous and the organic spots of both extractions in Figure 60 C indicate that the selective extraction did not have 100% efficiency, as in both cases a weak signal of the second compound can be observed. This means that the setup can be used to extract a pure compound to a new spot.

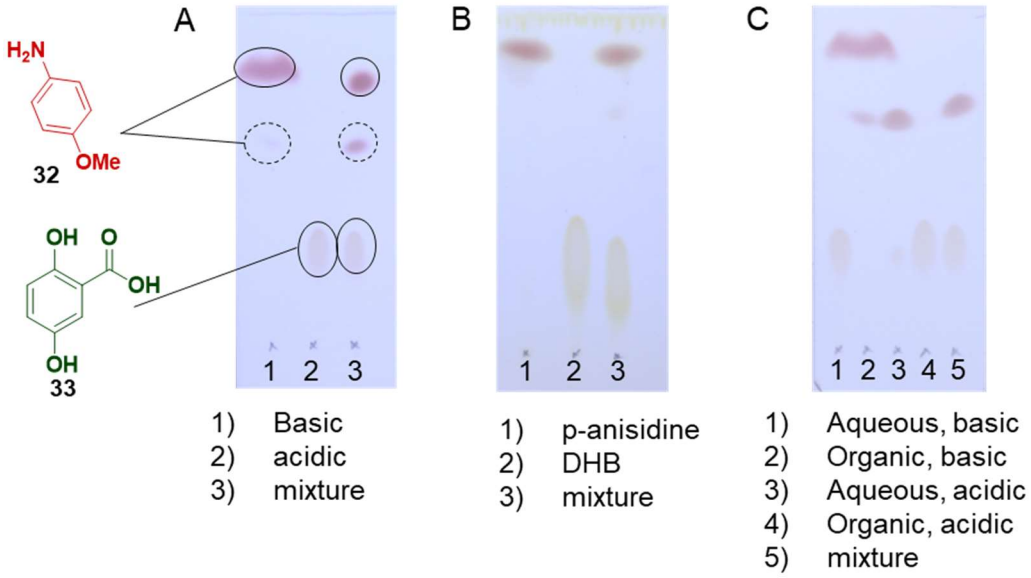

Figure 60: TLC results of aicd-base extraction. A) organic spots were collected after extracting from a basic (1) or acidic (2) solution. As reference, a neutral mixture of the compounds was added in the 3rd lane. B) controls of the single compounds p-anisidine (1), DHB (2) and a mixture of them (3) to identify the spots in A). C) aqueous and organic spots collected after extraction at basic or acidic pH. The figure was adapted from WIEDMANN *et al.*[2]

Thinking further about workup workflows, both compounds might be isolated if the pH value is changed between two extraction steps. To do so, a basic mixture of DHB and p-anisidine was dispensed on a spot, extracted with 1-octanol and evaporated. After that, 0.1 M HCl solution was dispensed to the same spot to change the pH value to acidic before the next extraction

procedure from the same spot to the opposite direction was started. This resulted in the selective deposition of the two compounds from a mixture to two different spots. Also in this case, the transfer was confirmed by TLC.

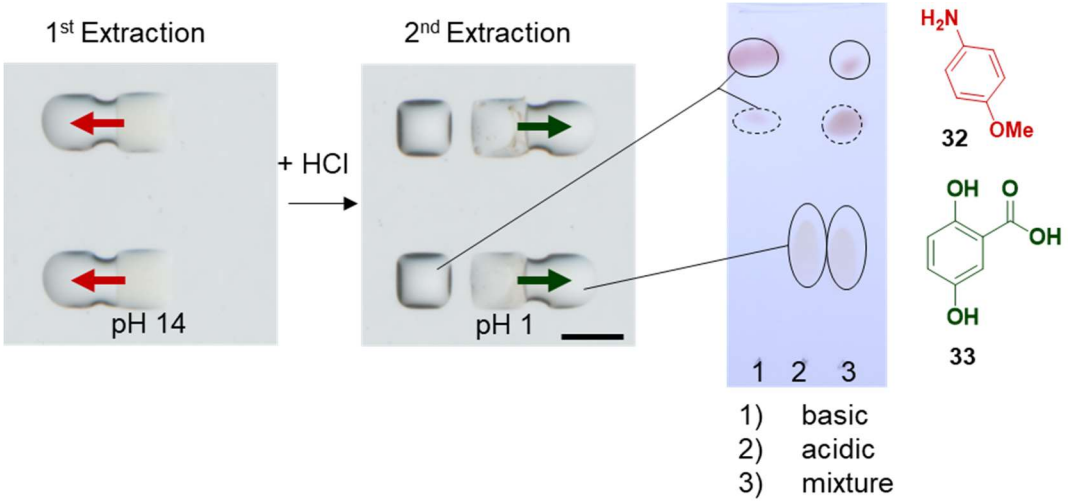

Figure 61: Separating a mixture in two steps with acid/base extraction. For the first extraction at basic pH, 1-octanol is dispensed on the left side next to the aqueous droplet. After addition of hydrochloric acid, the second extraction is performed by dispensing 1-octanol on the right side next to the aqueous spot. The TLC sample was collected from the left spots (1), right spots (2) and a mixture as control. The figure was adapted from WIEDMANN *et al.*[2]

In summary, the presented method was further characterized with a mathematical model to explain the high extraction efficiencies, and new characterization methods were investigated to describe and evaluate the extraction process on a size scale which is beyond most commonly used analytical methods. The model system was furthermore extended with additional analytes and solvents, resulting in a controlling mechanism to pull selectively compounds out of a mixture and transfer them on separate spots.

3.2.7 Dip-Extraction: A New Ultra-High-Throughput Extraction Method

The extraction in the array format enables a whole new handling tool for nanoliter volumes on the DMA. Still, the two dispensing steps require high precision of the liquid dispenser. The next idea was to develop a Dip-Extraction by immersing a whole DMA slide containing droplets into a second phase to bring all droplets at the same time in contact to this phase for simultaneous extraction. The dendrimer modification shows affinity of the omniphilic spots for both, aqueous and organic solvents, and was therefore not suitable for this method development. Furthermore, the idea of dipping an organic droplet in aqueous solution was not possible due to the very high surface tension of water in combination with Dendrimer DMAs.

Based on the extremely high affinity of aqueous droplets to the Z-DMA surface, this was the modification used for this approach. Due to the surface tension and affinity to the slide, the droplets were stable when moved or turned upside down. To further use this property, a whole slide containing aqueous droplets was carefully immersed into DCM, a volatile, low surface tension solvent. While the droplets remained sticking on the modified glass slide, an interface was formed between the aqueous droplet and the organic phase, which could be then used for extraction. Exemplarily, the pink dye Rhodamine B was used in 0.4 mM concentration in the aqueous solution to observe this process.

In Figure 62, a slide with 2.82 mm diameter spots containing 80 spots with 5 µL aqueous 0.4 mM Rhodamine B solution was immersed in 40 mL DCM in a glass petri dish. The image in Figure 62B shows the stability of the droplets during the immersion of the slide in DCM. All spots were still intact and the dye was extracted to the organic solvent. The fast extraction of the dye directly on the surface of the droplet can be already seen in Figure 62 E, directly after immersion. The disappearing color on the outer layer of the droplets has the effect that the image seems blurry. The removal of the pink dye took 15 min due to diffusion of the dye in the comparably large droplet to the interface. After pulling the slide out of DCM, there was a thin layer of DCM observed on the slide, which evaporated within seconds. The aqueous droplets were stable and remained on the DMA slide.

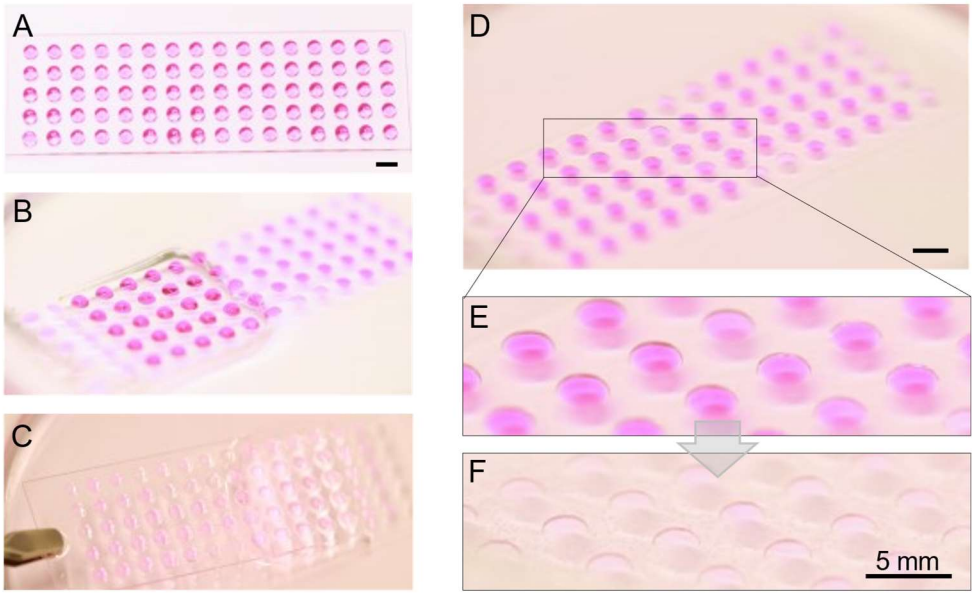

Figure 62: Dip extraction of 3 mm spots. A) The whole slide with 80 spots containing 5 µL each of 0.4 mM aqueous Rhodamine B solution. B) Immersion of the slide in DCM in a petri dish. C) The slide is taken out of DCM after 10 min extraction. D) Slide during extraction in DCM. E) Zoomed region showing the spots shortly after immersion. C) Zoomed region showing the spots after 15 min immersion. Scale bar is 5 mm.

After this first proof-of principle, a DMA with smaller spots was used to increase the throughput from 80 parallel extractions to 672 extractions on one DMA slide with square spots with a side length of 1mm and a volume of 250 nL per spot.

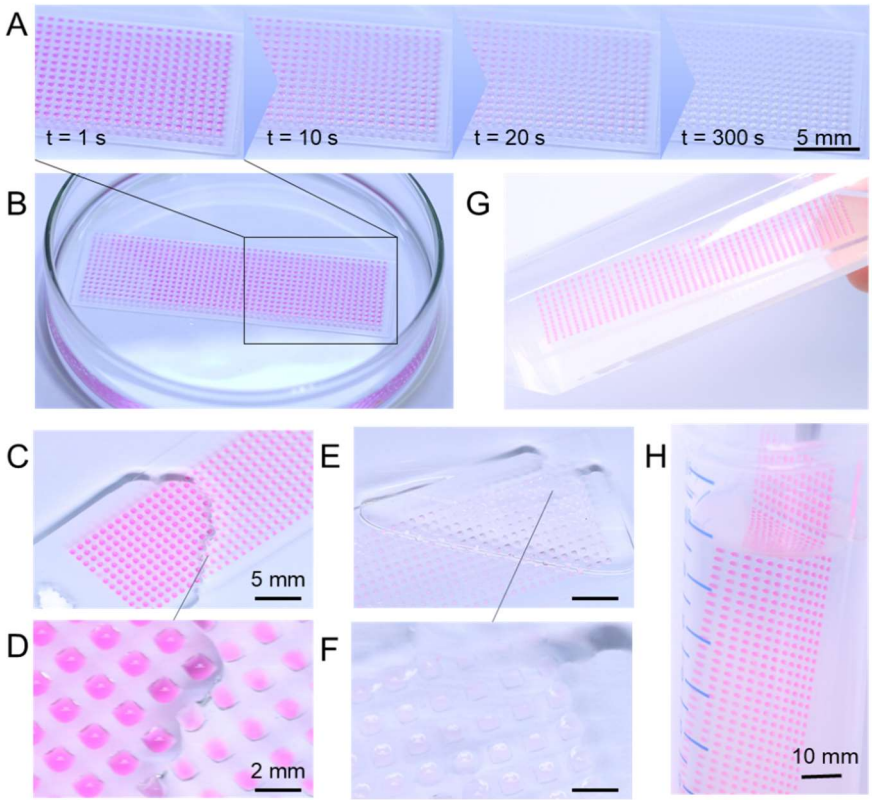

Figure 63: Dip-extraction of 672 spots. A) The immersed slide with 250 nL aqueous droplets is imaged during the extraction process in DCM. Scale bar is 5mm. B) Image of the whole slide in the petri dish containing DCM. C) DMA slide during immersion in DCM, scale bar is 5mm. D) Zoomed region of C), scale bar is 2mm. E) DMA slide when taken out of the organic solvent after extraction. Scale bar is 5 mm. F) Zoomed region of E). scale bar is 2 mm. G) DMA slide immersed in 45 mL DCM in a centrifuge tube, tilted. H) DMA slide during immersion in a 50 mL centrifuge tube for extraction in a vertical state.

Shown in Figure 63A, the extraction was much faster for the smaller spots, resulting in colorless droplets after five minutes. The droplets were stable when immersed and removed from the organic phase, as it can be seen in Figure 63C-F. For a quantitative characterization, the DMA slide containing 250 nL droplets with 40 mM Rhodamine B was scanned with the document scanner for different immersion times. The amount of dye present in the droplet was measured by the saturation of the pink color of Rhodamine B. A linear dependency of the concentration of Rhodamine B to the color saturation was confirmed by a calibration curve presented in Figure 64B. After ten seconds immersion, the amount of analyte present in the droplets was already reduced to 50% and after one minute, 83% of the dye was extracted. This fast kinetics can be explained by the high surface area of the small droplets, where the mass transfer is taking place. In addition, the low volume leads to short diffusion ways from the center of the droplet to the

interface. A prolonged extraction time of five minutes resulted in 90% extraction efficiency, which is a very high efficiency for a single extraction step without exchange of the organic phase.

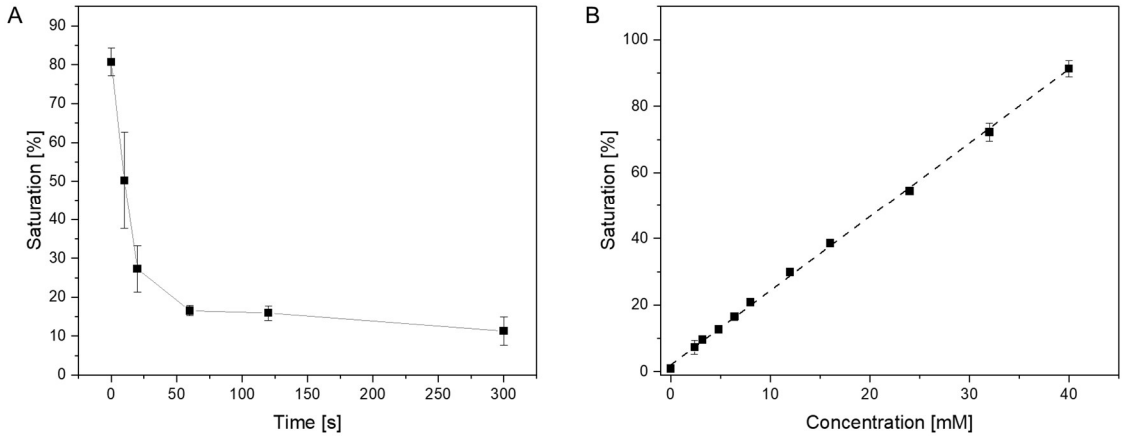

Figure 64: Kinetics of the extraction in 1 mm spots. A) The reduction in color saturation represents the removal of the pink analyte upon different immersion times in DCM. B) A calibration curve was created using different concentrations of Rhodamine B without extraction. The saturation of the pink color was estimated with the GRID SCREENER.

Furthermore, in addition to the flat, horizontal petri dish, a 50 mL centrifuge tube was used as DCM reservoir. The droplets sticked stable to the DMA slide also when immersed vertically into the organic phase (Figure 63H), but also when the reservoir was tilted (Figure 63G). This shows the high stability of the aqueous droplets, their independence from gravity and might allow new possible applications, like the usage of a continuous flow system for high extraction efficiencies for the static droplets.

In the following step, the selectivity of the extraction mechanism was investigated. Therefore, 0.4 mM Rhodamine B solution, 4.9 mM Methylene Blue solution and a mixture of both were added to different spots on the DMA. As the blue dye shows higher affinity to water, the blue droplets were expected to stay blue, while the pink dye was supposed to be removed as shown before. The slide is shown in Figure 65 before (top), during (right) and after (bottom) the dip-extraction step. The pink color nearly disappeared from the pink spots, while the blue surrounding spots remained blue. In addition, the mixture of both dyes, which showed a darker purple color in the beginning, turned blue as well. This proofs that the color-removal is based on the selective extraction step by the affinity of the analytes to the aqueous and organic phase.

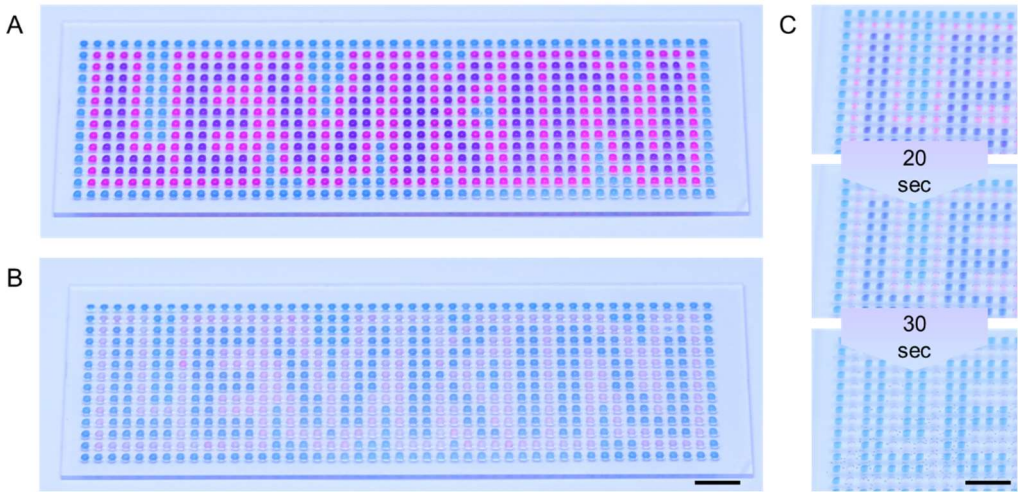

Figure 65: Selective Extraction. A) A DMA slide with 1.00 mm square spots containing 250 nL aqueous solution containing either 0.4 mM Rhodamine B (pink), 4.9 mM Methylene Blue (blue) or a mixture of both (purple). B) Same slide as A), but after 10 min extraction in DCM after removed from the organic reservoir. C) Part of the slide immersed in DCM during the extraction at different time steps. Scale bar is 5 mm for all samples.

Next, the long-term stability of droplets immersed in DCM was analyzed. When handling DMAs with 250 nL droplet or less, evaporation happens fast under atmospheric pressure at room temperature. This leads to challenges for long-term incubation. To test the behavior of small droplets for long incubation times in DCM, a slide containing 672 droplets of 250 nL 0.4 mM aqueous Rhodamine B solution was immersed in DCM in a closed petri dish for one hour (Figure 66). Due to the extraction, the droplets turned colorless and were hard to see. However, after taking out the droplets were still present on the DMA slide. This effect impressed even more when the extracted droplets were compared to a slide containing the same solution, which was left at room temperature for 15 min, where all spots evaporated and only the dye remained in dry state on the spots (Figure 66D).

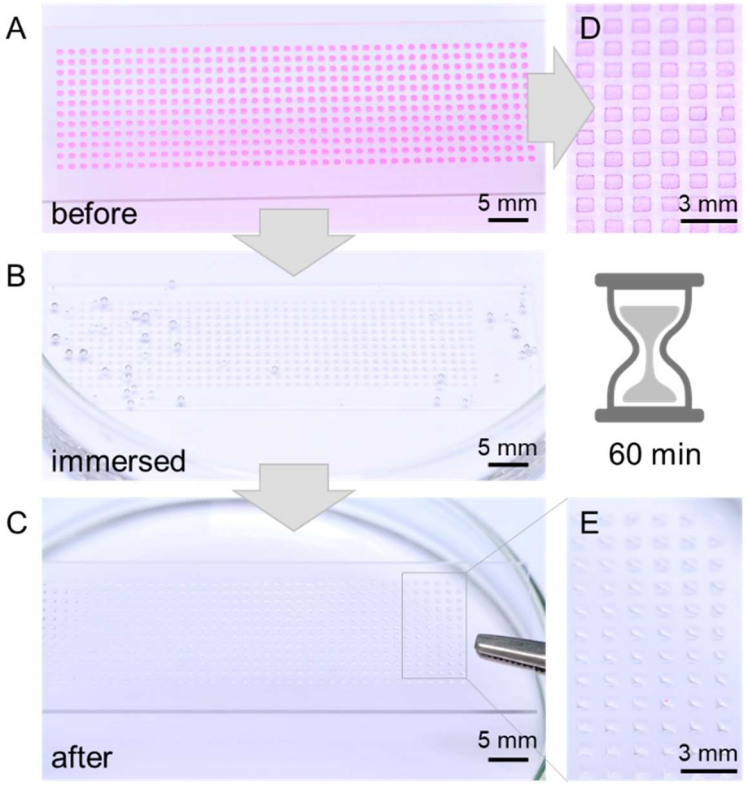

Figure 66: Long-term stability of immersed slides. A) DMA containing 672 spots with 1.00 mm side length, containing 250 nL 0.4 mM aqueous Rhodamine B solution before extraction. B) Same DMA slide in 40 mL DCM after 1h incubation. C) DMA slide after taken out of the solution. Scale bars are 6.00 mm. D) DMA slide after 15 min incubation at room temperature. E) Zoomed region of C). Scale bar is 3 or 5 mm.

To increase the possible throughput, the spot size was further decreased to 0.25 mm^2 square spots with a side length of 500 µm. With this setup, 28 × 96 droplets could be created on one single glass slide. The decrease in spot size and thereby the decrease in volumes caused challenges with the liquid dispenser. For that, the discontinuous dewetting method described by UEDA *et al.*[49] was used in a slightly adapted way. The patterned glass slide was shortly immersed in an aqueous solution containing 1.55 mg/mL Methylene Blue. After taking out, small droplets were formed on the hydrophilic areas, separated by the hydrophobic borders. This slide was directly immersed in DCM and imaged. The dye was chosen due to its high affinity to water, so that it was not extracted. This enabled the visualization of the droplets after immersion in DCM in Figure 67B,D and when the slide was removed from the organic phase (Figure 67C). With that step, it was shown that also highly miniaturized droplets are stable when immersed in the organic phase and that this could be used for parallel extraction of 2688 samples at one single step.

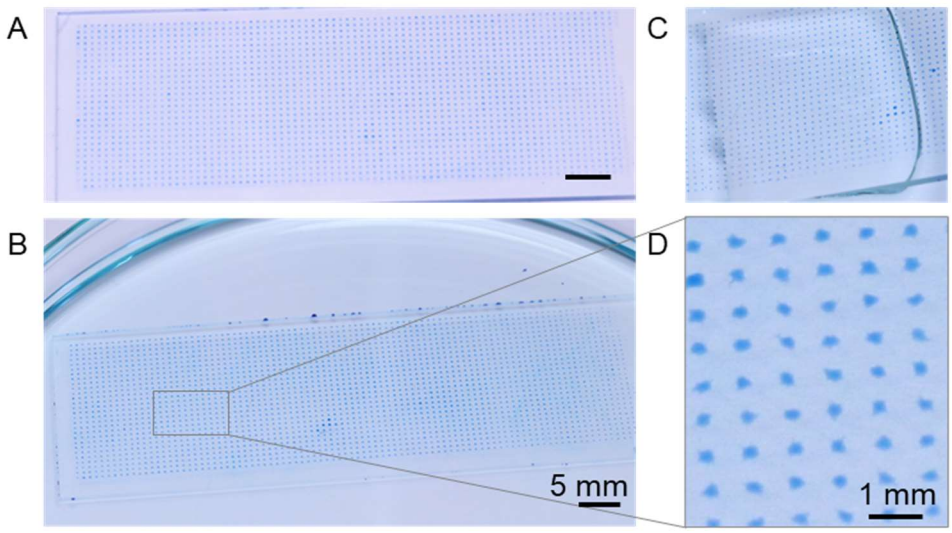

Figure 67: Extraction of 2688 spots. A) DMA slide with 2688 spots with a side length of 500 µm, containing Methylene Blue containing aqueous droplets. B) DMA slide from A) immersed in 45 mL DCM. C) Slide containing droplets when taken out of the solution. D) Zoomed region from B) Scale bar is 5mm for A and B and 1mm for D.

After showing the application for spots in different sizes and high-throughput, the versatility of the system was tested by using various geometries (Figure 68). In addition to different shapes, the size range was increased resulting in flat reservoirs with a high surface area for fast extraction, containing up to 60 µL aqueous solution. All different structures were stable upon full immersion in the organic phase and showed intact shape after the slide was taken out. For imaging reasons, the slide was not left in DCM until complete extraction of the dye, but in analogy to the results shown before, the dye could be completely extracted at longer incubation times.

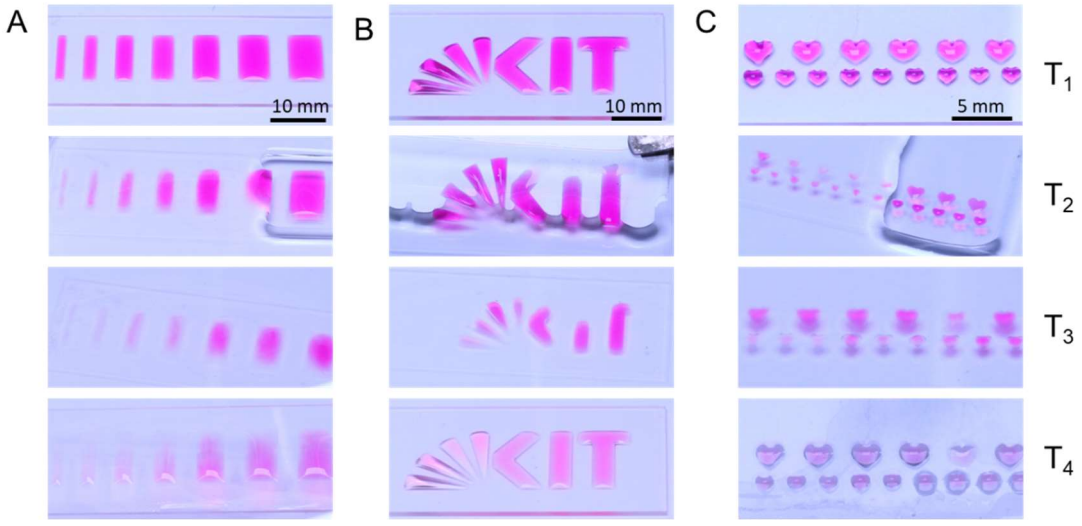

Figure 68: Dip-Extraction of spots with various geometries. Different patterns on DMA slides (A-C) filled with 0.4 mM Rhodamine B solution and imaged before (T_1) and during (T_2) the dipping, immersed (T_3) and after taking out (T_4) from 40 mL DCM in a petri dish. For imaging, the samples were taken out before the dye was completely extracted.

In a next step, the extraction was reversed to stain aqueous solutions of different pH values by immersing a DMA slide in DCM containing Bromothymol Blue. This pH sensitive indicator shows a dark blue color at high pH values, slightly green color at neutral pH value and a yellowish color in acidic solutions. The yellowish powder showed poor solubility in DCM, but was nevertheless quickly absorbed by aqueous droplets upon contact with the organic layer. The pH of deionized water was adjusted with NaOH solution to pH = 5, 7 and 12.5 and the colorless solution was added to a DMA with either 2.83 mm diameter spots (3 µL) or 1.00 mm side length (150 nL). The DMA was immersed in the organic phase containing 60 mg of the indicator and the change from colorless (Figure 69A) to the pH-dependent color (Figure 69B) was observed. The fast transfer can be seen in Figure 69C and D, where the slide was imaged during the immersion step, showing the instant color development on the basic droplets after getting in contact with the organic phase and the fast gradient of increased color intensity. The slides with both spot sizes and geometries were imaged by the document scanner after staining for 30 sec.

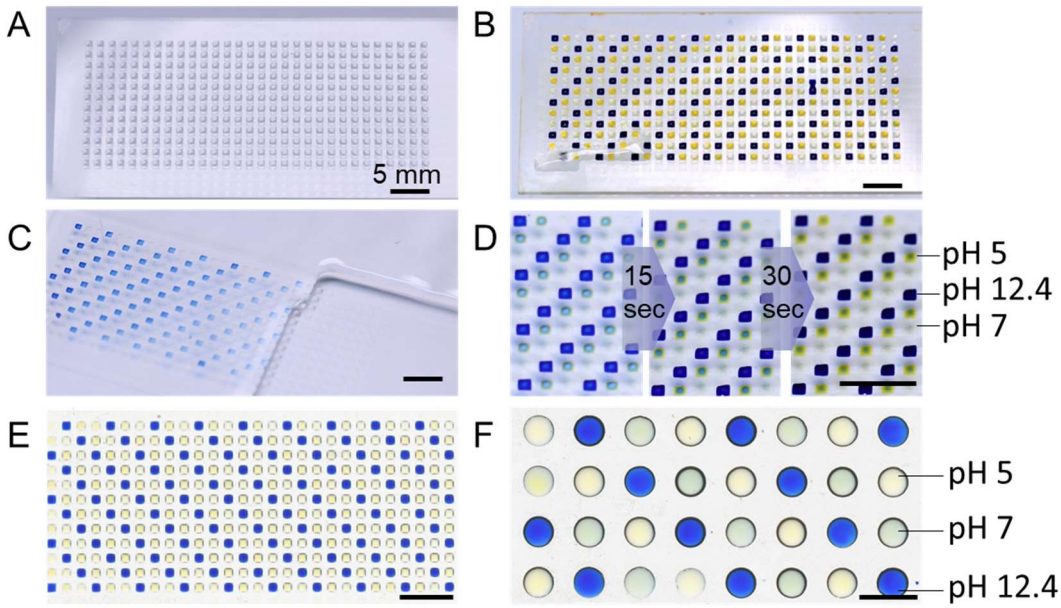

Figure 69: Staining by dip-extraction. A) 150 nL of aqueous solutions with three different pH values (5, 7, 12.4) were pipetted as colorless solution on a DMA with 1.00 mm diameter square spots. B) The same slide after immersion in DCM containing Bromothymol Blue for 120 sec. C) Slide from A) during immersion. D) Zoomed region of the slide during staining. E) Scanned image of a slide after 30 sec staining. F) Scanned image of a slide containing 3 µL aqueous droplets on 2.83 diameter spots with different pH values after staining in Bromothymol Blue containing DCM. Scale bar in all images is 5 mm.

The different colors of neighboring spots with different pH values show that the aqueous solutions remained separated without contamination by neighboring droplets when immersed in the organic solvent, during the extraction and when they are taken out. This fast staining

allows the pH determination of 672 or more solutions within 30 seconds by a simple dipping step, which could easily be automated and could be used to establish a readout for pH determination of aqueous samples on the DMA.

In summary, the described new dipping method offers a very fast way for parallel treatment of an array of aqueous droplets. Consisting of one simple dipping step, the extraction can be performed without the need of special equipment. This setup allows the extraction from a broad variety of geometries, but also the possibility of downscaling in terms of volumes and upscaling in terms of number of extractions starting from 80 × 50 µL droplets to 2688 single extraction with volumes below 40 nL. Further possible applications could be the removal of contaminants from aqueous samples, or as shown in the last experiment the addition of reagents, for example for pH determination. Beyond that, it is an impressive demonstration of the stability of aqueous droplets on the DMA slide, introducing a new HT manipulation step.

Conclusion and Outlook

In this work, different aspects of miniaturization and parallelization for high-throughput drug development, such as synthesis, purification, characterization, screening and handling have been investigated. In a field, where high risks of failure are combined with high costs, the challenge is to save compounds, materials, solvents and time as valuable resources. This leads to the motivation to incorporate all important steps in early-stages of drug discovery on one small but versatile platform. The droplet microarray offers a fitting platform, as it has demonstrated value for high-throughput biological screenings with both eukaryotic and prokaryotic cells as well as for compound library synthesis *via* solid-phase chemistry. The idea of solution phase synthesis with reaction control by uv/vis spectroscopy, liquid-liquid extraction of dyes, MALDI-MS measurements of compounds and cell culture have been already presented before in early stages of miniaturization and integration. Nevertheless, in most cases an array of 5 × 16 droplets with a diameter of 2.8 mm – was used, comparable to a 384-well microtiter plate, still using microliters of reagents for one experiment. To exploit the whole benefit of an open platform with dimensions solely limited by photomasks, the aim in this work was to further miniaturize to a size range and throughput beyond microtiter plates. Therefore, spots with a side length or diameter of 900 µm were used, resulting in an array of 18 × 64 spots on a single microscope glass slide, with volumes between 50 and 300 nL.

In the first part of the work, a library synthesis with subsequent biochemical assay was adapted to the Droplet Microarray. The library synthesis and screening had been performed before by the pharmaceutical company SANOFI with single bulk reactions, purification and characterization in bulk. The compounds were tested in a biochemical assay in a 384-well plate to identify potential new compounds for treatment of diabetes type II. The biochemical readout was based on the inhibition of the enzyme Low-molecular weight protein tyrosine phosphatase. The proof of principle could be successfully performed in an array with the same alignment as a 384-microtiter plate with slightly reduced volumes from 4 µL to 3 µL and readout with a commonly available plate reader. Due to the limitation of plate readers to 384 and 1536 well plates in ANSI standard format, the plate reader could not be used for the characterization of further miniaturized platforms of 900 µm diameter spots with 225 µm borders. Here, a document scanner was used for an optical readout with image analysis performed in collaboration with MARCEL SCHILLING and PROF. MARKUS REISCHL, but the sensitivity was not sufficient for the small droplets of 100 nL. Therefore, a fluorescence-based assay and readout based on a fluorescence microscope were used. The array detection and image analysis were

developed in collaboration with MARCEL SCHILLING and PROF. MARKUS REISCHL. With optimized environmental conditions, the Z' value indicated an 'excellent assay'. The assay showed good compatibility with all reagents used in the planned amide coupling reaction, so that the direct screening of the crude mixture after removal of the organic solvent was possible. As one complication, the acid used as starting material showed already some inhibitory activity, leading to only a small difference of signal intensity for analysis and rendering differentiation between effects of starting material and product difficult. This could be improved by increased enzyme and substrate concentrations, which finally allowed to detect if product was formed and if the yield was low, intermediate or high.

In detailed reaction analyses in larger scale with LC-MS, the product formation was observed, but also a significant cross-contamination with the volatile amine of the neighboring spots. This could be solved by using a hydrochloride salt instead of the free amine, as confirmed via MALDI-MS analysis in the small 900 µm diameter spots and reaction volumes of 50 nL. MALDI-MS analysis allowed the fast screening of one DMA of 1152 spots within 20 min. Therefore, one single DMA was enough to test the sensitivity of a model product in different concentrations of the analyte and matrix, as well as for two different matrices and two different matrix application methods. Furthermore, different mixtures of a starting material and product allowed the detection of both compounds on one spot and therefore the estimation of a possible yield of crude reaction mixtures. In addition, a first amide coupling reaction was performed in five different concentrations and with two different amines, where the product was successfully detected up to a reaction concentration of 42 µM. All those experiments could be combined on one single DMA, which highlights the high density of information gained in this miniaturized format. In addition, the reaction reagents and other samples were directly dispensed on the DMA, the solvent was evaporated after the reaction incubation and matrix could be dispensed in a second dispensing step. After this proof of principle, a screening with six different acids, five different amines and three different reaction conditions in two concentrations were performed on one slide, resulting in 180 different reactions. All reactions were performed in four repetitions, so in total 720 reactions were performed together with some additional control spots. Every reaction was performed in 50 nL droplets, so in total 36 µL reagents were used for the whole slide. Not all potential products could be detected, but for the successful reactions, the product signal was clearly identified only within the predicted spots. This indicates that the high-density reactions with the dispensing protocol were working without any crosstalk, after free amines had shown contamination of neighboring spots before. As explanation for missing

product signals, a side reaction was identified, resulting from a reaction of the acid with dimethylamine, which is present in the used solvent DMF. The high amount of the side product was likely caused by the addition order of the reagents, but predominantly by the low concentration of the reagents required by the following assay. The impact of the concentration of the reagents on the side reaction was confirmed by LC-MS analytics in 500 µL scale. As possible solution to this challenge, alternative solvents were chosen, which were compatible with reactions on the Droplet Microarray and did not lead to side reactions in 5 µL reactions with following LC-MS characterization.

The results described here show the possible implementation of a miniaturized synthesis, analytics and screening of a library on the Droplet Microarray. Several challenges were identified during the work, which could be solved with adapted procedures. Here, the fundamental work has been done to optimize and adapt all needed handling steps to the Droplet Microarray platform. A larger screening of the envisioned library for hit identification with following confirmation in bulk will finally show the impact of this miniaturized platform. Furthermore, the screening setup could be easily adapted to different biological targets, if different enzymes and starting materials were used. For the application in industry, an automated high-throughput sample handling setup as well as powerful evaluation software would be required to allow a drastic increase of target-compound couples tested with much lower effort and costs. This reduction of required time and costs with increasing number of experiments at the same time could accelerate hit identification in a drug discovery pipeline and thereby incentivize the investigation of possible drug candidates for less abundant diseases.

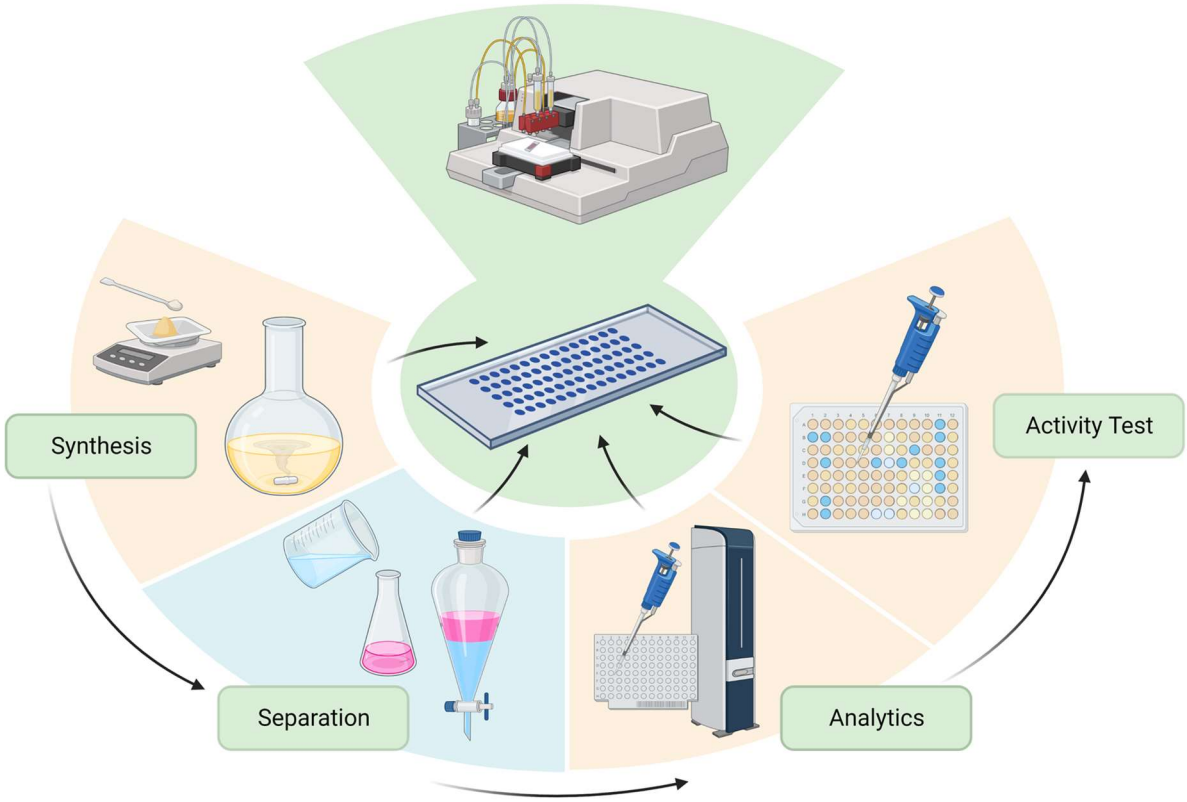

Figure 70: Summary of the work of miniaturization, parallelization and integration. Synthesis, analytics and activity tests were integrated in one workflow on 900 µm round spots in the first part of the work, while the separation aspect in small scale was investigated in the second part. All steps were performed by dispensing reagents with the CERTUS FLEX liquid dispenser.

In the second part of the work, the focus was set to the aspect of droplet manipulation for a possible workup procedure on the Droplet Microarray. In previous work, a method for merging an aqueous and an organic droplet was presented to perform liquid-liquid extraction of a pink dye Rhodamine B from the aqueous to the organic droplet. The simple setup of merging during dispensing and separating by evaporating allowed up to 186 parallel extractions on one glass slide with 300 nL of solvent per extraction step. In this work, the environmental conditions were further investigated to manipulate the extraction time and therefore change the resulting efficiency. For the first time the separation of a mixture in a planar setup on the Droplet Microarray was presented. By introducing a second dye, which was not extracted, the mixture of both dyes was separated into two differently stained droplets. This was seen as final proof, that the transfer is based on the affinity to a different solvent and not by simple evaporation effects. Due to the small scale, less convenient methods like image analysis and thin layer chromatography were evaluated as readout for the extraction efficiency and the selectivity. Furthermore, the independence of the extraction procedure from the density or volatility of the solvent system was shown, which is a promising factor for future automatization techniques. In

addition, the separation of a carboxylic acid and amine was demonstrated with a thin layer chromatography readout. In analogy to bulk experiments, the acid/base extraction could be used to selectively pull one compound to the neighboring spot. In addition, the pH of the aqueous droplet could be changed by addition of acidic or basic solution and a multi-step extraction could be performed to extract two different compounds to two different neighboring spots. This was shown in this work with two basic chemicals, but could be applied in future screenings of synthesized libraries with possibly interfering starting materials, side products or catalysts, if they can be separated. Another possible application can be found in mass spectrometric analytics of biological samples, where buffer component present in the biological sample can cause problems during measurements. Removing lipophilic compounds from a crude cell mixture could therefore increase the sensitivity in the analysis of cell membranes or metabolic compounds. In comparison to manual handling in bulk extraction in separation funnel, this method relies solely on the dispensing of solutions to the Droplet Microarray slide without any additional manual transferring steps.

Last, a second principle of liquid-liquid extraction was developed on superhydrophilic Droplet Microarray slides, where aqueous droplets could be immersed in a second, organic phase of dichloromethane, while maintaining their shape. The interface created in this way could be used for extraction, again exemplarily shown by a dye. After extraction, which could take up to 60 minutes without an impact on the droplets, the Droplet Microarray slide could be pulled out carefully, still containing all droplets. The extraction could be also performed in the opposite way, by staining the aqueous droplets with a pH indicator dissolved in the organic solvent. The droplet size was varied from 5 × 16 round droplets with volumes of 5 µL over 14 × 48 square spots with 250 nL on 1 mm^2 to 2688 spots with a side length of 500 µm, holding approximately 40 nL in an array of 28 × 96. In addition to that, the geometries could be varied to immerse flat squares with up to 60 µL or heart-shaped droplets. This approach highlights impressively the performance of the Droplet Microarray with aqueous droplets stably sticking to the surfaces. Especially the ultra-high-throughput approach with 2688 extractions performed upon one simple dipping step demonstrates the huge effect and possibilities of miniaturization and parallelization. Also in this case, the extraction step can be performed without requiring special devices and could be easily implemented in an automated workflow.

Besides all the challenges arising when the samples are further miniaturized beyond the limit of manual handling, this work could introduce several different aspects of miniaturized and parallel droplet manipulation. The combination of organic synthesis in 50 nL with a

biochemical assay in 100 nL or MALDI-MS measurements on the same slide as well as the extraction procedure by merging droplets are all based on the addition of the required reagents with a liquid dispenser. Despite the high density of 1152 droplets on a microscope glass slide, each spot can be addresses individually to create large libraries with different compounds spatially encoded. For further applications, additional automated analytics are required to handle the high load of data obtained from a single Droplet Microarray, as the image analysis tools developed recently by SCHILLING *et al.*[102] but also in an integrated way for structural characterizations of the synthesized compounds. While reaction planning and evaluation was performed in this work mainly working with EXCEL, the next generation of screenings requires a next generation of software solutions. Besides high-throughput experimentation to find the most promising hits, the load of created data could further be used to train algorithms for the computational prediction of optimized structures and reactions. This would act as a second booster to the development of new materials, in particular of potential drugs. If the Droplet Microarray finds its application in large pharmaceutical companies to accelerate and integrate miniaturized drug development, not only large amounts of chemicals can be saved regarding costs and sustainability, but also a larger number of targets could be tested for hits and enable the development of affordable treatments that are urgently required.

5 Experimental Part

5.1 Materials

For the SANOFI project (Chapter 3.1), the starting materials **10a-10c** were synthesized at SANOFI in Frankfurt and provided as 10.0 mg powder. Amines **18 - 22** were purchased by SANOFI and provided in 20.0 mg batches. All chemicals were dissolved in DMSO to prepare 10 mM (acid) and 50 mM (amine) stock solutions for the screening. The samples were stored at room temperature.

For the enzymatic assay, the enzyme hmLMPTP and substrate DiFMUP was provided by SANOFI.

Acetone, ethanol, and 2-propanol at technical grade and 1,4-dithiothreitol were purchased from MERCK KGaA (Darmstadt, Germany). For MALDI-MS measurements, UHPLC grade acetonitrile and water from Sigma-Aldrich (Darmstadt, Germany) were used.

Triethoxyvinylsilane, DMPAP, 4-pentenoic acid, 1-thioglycerol, Rhodamine B, PFDT, *p*-anisidine, 2,5-dihydroxybenzoic acid, HCCA, DIPEA and 1-octanol were purchased from SIGMA-ALDRICH (Darmstadt, Germany).

DIC was purchased from ALFA AESAR–THERMO FISHER GMBH (Kandel, Germany). Bromothymol blue and HATU was purchased from VWR INTERNATIONAL GMBH (Darmstadt, Germany). 4-DMAP was bought from NOVABIOCHEM (Darmstadt, Germany). Methylene blue hydrate was purchased from FLUKA. TRIS-HCL was purchased from CARL ROTH (Karlsruhe, Germany). All chemicals were used without further purification.

NEXTERION Glass B microscopic glass slides were bought from SCHOTT TECHNICAL GLASS SOLUTIONS GMBH (Jena, Germany). Photomasks were bought from ROSE FOTOMASKEN (Bergisch Gladbach, Germany)

UV Cuvettes were bought from BRAND GMBH AND CO. KG (Wertheim, Germany). Capillary tubes were purchased from MARIENFELD (Lauda Königshofen, Germany). ALUGRAM Xtra SIL G/UV254 plates for TLC were purchased from MACHERY–NAGEL (Düren, Germany)

5.2 Methods

5.2.1 Fabrication of Droplet Microarray Slides

Dendrimer DMA

Dendrimer DMA slides were prepared according to the protocol based on BENZ *et al.*[47] Microscope glass slides were activated by 10 min UV treatment using an UVO-cleaner 42-220 from JELIGHT COMPANY INC. (California, USA). Then, two glass slides were silanized with 400 µL triethoxyvinylsilane in a 50 mL tube for 16 h at 80°C. Next, an UV induced tiol-ene click reaction using 10% (v/v) thioglycerol with 1% DMPAP in ethanol/water (1:1) was performed on the surface with 2 min irradiation at 260 nm twice. Two slides were placed in a 50 mL tube containing 50 mL acetone with 4-DMAP (56 mg, 458 µmol), 4-pentenoic acid (125 µL, 127 mg, 1.27 mmol) and 180 µL DIC (180 µL, 220 mg, 1.75 mmol) for 4h. The two steps of thiol-ene and esterification reaction were repeated three times to build the dendritic structure. In the last step, a 10% (v/v) PFDT solution in isopropanol was used and a photomask was applied during irradiation to create the omniphobic border. Last, the remaining spots were modified with the thioglycerol solution as described before. With this procedure, 1152 round omniphobic spots were created with a diameter of 900 µm and a pitch of 1125 µm between the centers of the spots in an array of 18 × 64.

Z-Pattern DMA

The nanoparticle solution for coating the slides was prepared by mixing 0.25 g Silica nanoparticles (AEROSIL 200, Evonik) with 30 mL ethanol followed by 30 min sonication at room temperature with an ELMASONIC S 30 H sonicator. 340 µL vinyltrimethoxysilane and 200 µL conc. HCl were added and sonicated for 60 min. The solution was aged at room temperature overnight.

The glass slides were activated by 10 min UC treatment using an UVO-cleaner 42-220 from JELIGHT COMPANY INC. (California, USA). The slides were spin-coated with five times 500 µL of the nanoparticle solution and spinning at 1000 rpm for 15 sec with a SPIN150i spin coater (SPS EUROPE, Ingolstadt, Germany). After that the slides were cured for 1 h at 150°C with a heating plate PRÄZITHERM PZ60 (HARRY GESTIGHEIM GMBH, Düsseldorf, Germany).

The slides were washed with acetone and patterned by using 300 µL of a 10% (v/v) PFDT solution in isopropanol and a photomask covering the required spots. The slide was irradiated for 60 s with UV light in the UVA CUBE (DR. HÖNLE AG, Gilching, Germany) and washed with acetone. In the last step, 300 µL of a solution containing 10% (v/v) thioglycerol with

1% DMPAP in ethanol/water (1:1) was added, the slide was covered with a quarz glass and irradiated again for 60s.

Depending on the photomask, the spot size could range from 2.82 mm diameter (5 × 16 spots) to 350 µm side length (144 × 42 spots).

5.2.2 Dispensing on Droplet Microarray Slides

For all dispensing steps, CERTUS FLEX from FRITZ GYGER AG (Gwatt, Switzerland) was used. The DMA slides were placed in a slide holder purchased from AQUARRAY (Eggenstein-Leopoldshafen, Germany). The solutions were dispensed with the respective calibration at 0.3 bar. For the enzymatic assay, the estimated density of the buffer by weighing respective volumes was used for calibration. For 1-octanol the pressure was set at 0.6 bar to ensure proper printing of the solvent with higher viscosity.

5.2.3 Enzymatic Assay

The assay was modified on the base of Stanford et al. 1M BIS-TRIS solution was prepared in HPLC grade water and the pH was adjusted to 6.1 with conc. HCl. The solution was stored at 4°C. Base buffer for the assay containing 50 mM BIS-TRIS, 0.01% Triton X-100 and 1.0 mM DTT was prepared freshly before each experiment. *hm*LMPTP enzyme was stored in aliquots at -20°C at 1.148 mg/mL and diluted to a concentration of 0.29 µg/mL in base buffer to give the enzyme buffer. For fluorescence readout, DiFMUP was used as substrate and stored as 200 mM stock solution in DMSO at -20°C. For substrate buffer, the stock was diluted to a concentration of 20 mM in Base buffer. For the colorimetric assay, the substrate buffer contained 6 mM *p*-NPP and enzyme buffer contained 0.3 µg/mL *hm*LMPTP. Enzyme and substrate buffer were prepared freshly every time.

Before performing the biochemical assay on a DMA slide, a humidity chamber was prepared by placing tissues soaked with 15 mL of base buffer in the lid and on the bottom of a darkened petri dish. Prior to dispensing, the channel for enzyme buffer was filled with 1.0 mL of 5% BSA in base buffer and incubated for 10 min. After that, the channel was emptied and flushed with 1.0 mL base buffer before Enzyme buffer was filled in. The DMA slide containing the preprinted and evaporated samples was placed in an adaptor and 50 nL of enzyme (high control, samples) or base buffer (low control) were dispensed on each 900 µm spot, with the exception of a frame of the two outer rows containing 120 nL base buffer to prevent evaporation. The slide was placed in the humidity chamber and incubated at room temperature for 30 min. Then, 50 nL of substrate buffer were dispensed on each spot and the slide was incubated in the

humidity chamber at room temperature for 60 min. For the colorimetric assay with *p*-NPP, 100 nL 1 M NaOH solution was added.

For larger 3 mm spots, 1.5 µL of enzyme buffer and 1.5 µL substrate buffer were dispensed. After 60 min incubation, 3 µL of 1 M NaOH solution was added before imaging for the *p*-NPP assay.

To evaluate the results, a excel table was created to automatically calculate the mean values for all repetitions of a sample and the standard deviation. Based on Equation I and II, the % Inhibition and Z' value was calculated.

5.2.4 Synthesis on the Droplet Microarray Slide

Stock solutions of the starting materials in DMSO were stored at room temperature and diluted with the respective organic solvent to the final concentration prior to dispensing. The reaction mixture consisting of 4-DMAP, HATU and DIPEA were mixed directly before the dispensing step by diluting stock freshly prepared stock solutions to achieve the final ratios (0.25 equiv. 4-DMAP, 1-5 equiv. HATU, 5-10 equiv. DIPEA). 14 nL of the acid and reaction solutions were dispensed on the spots surrounded by a frame of two rows 80 nL of the organic solvent. The slide was placed in a glass petri dish containing a tissue in the lid and on the bottom, soaked with the organic solvent. The petri dish was sealed with parafilm and incubated for 20 min at room temperature in a fume hood. After that, 22 nL of the amine solutions were added and the slide was incubated in the sealed petri dish for 18 h. To stop the reaction, the slide was placed in a desiccator and vacuum was applied using a VACUUBRAND (Wertheim, Germany) pump until the solvent was removed. Control solutions of known inhibitors and starting material were dispensed in the same way.

5.2.5 Extraction Procedure

For on-chip extraction, Dendrimer DMAs were used with square spots with a side length of 900 µm. 100 – 300 nL of the aqueous solution was dispensed with 0.3 bar in the center of the respective spots first. The organic solvents were dispensed with a printing scheme that was shifted by −875 µm with a volume of 75–100 nL. 1-octanol was printed with 0.6 bar, for 2-bromotoluene, toluene, and cyclohexanone, a pressure of 0.3 bar was used. If nothing else is mentioned in the description, the slide was placed in an opened hood until the separation of the droplets was completed.

In the Dip-Extraction experiments, Z DMAs were used with different patterns. If not stated otherwise, the pattern was filled with 0.4 mM aqueous Rhodamine B solution (900 µm: 100 nL,

1 mm square: 250 nL, 2.83 mm round: 5 µL) and then carefully immersed in 45 mL DCM either in a 50 mL centrifuge tubes or 15 cm diameter glass petri dish. After the extraction was done or at a certain time point, the slide was slowly taken out using tweezers. Remaining DCM was dropping of or evaporated within 20 sec. Then the slide was imaged either with a camera, microscope or scanner for further analysis.

5.2.6 Analytical Methods

MALDI-MS measurements

MALDI- MSI measurements were performed by the group of PROF. CARSTEN HOPF (CEMOS) under the supervision of DR. STEFAN SCHMIDT (CEMOS) on a rapifleX MALDI Tissuetyper (BRUKER DALTONICS GmbH, Bremen) in reflector positive operation mode with a raster size of 100 µm. For each data point, ion intensities emerging from 200 laser shots were accumulated at a repetition rate of 10 000 Hz. The laser fluency was optimized for every slide. Spectra were recorded in a mass range from 100 to 600 Da. Calibration of the mass spectra was done by clusters of red phosphorus[47] in cubic enhanced mode.

Data analysis was initially performed in SCiLS Lab MVS (BRUKER DALTONICS GmbH, Version 2022b Pro). Mass features were selected, and the corresponding ion images were exported as imzML format using the reduced feature list, total ion count normalization and peak area. Exported ion images were analyzed in a Python3.8 script using the pyimzml parser (Fay D. pyimzML parser for the imzML format. https://github.com/alexandrovteam/pyimzML) for data import. For each DMA spot, the sum intensity for a given spot was calculated and used for further analysis.

TLC

For TLC, plates with silica gel coated with fluorescent indicator F254 from MERCK were used. The compounds were collected with a capillary from the DMA and added on the plate. This was placed in a TLC chamber with the respective solvent mixture. Some compounds were stained with iodine vapor and the plates were imaged with a digital camera.

LC-MS

Samples were either diluted to a max. concentration of 50% DMF in either pure acetonitrile or in an ACN/water mixture (1:1) or directly dissolved in the mentioned solvent. For evaluation, the peak area of either the TIC or absorbance chromatogram at 254 nm was compared. For this work, two different LC-MS devices have been used.

I: LC-MS measurements were performed with a gradient of ACN:water 10:90 – 99:1 over 20 min at a flow rate of 1.0 mL/min with a KINETEX 2.6µ Xb-C18 100A column on a device from Agilent. The signals were detected by a dynamic array detector in a range of 230 – 400 nm. A HP 1100 MSD Mass detector was used for the detection and AIP-ES was used for the ionization. The mass was detected in the positive mode, if not mentioned otherwise.

II: LC-MS measurements were performed on an AGILENT 1260 Infinity II system consisting of a quaternary pump (GB7111B;), autosampler (G7129A, 100 µL sample loop), a temperature-controlled column oven (G7114A) and a variable UV-VIS detector (G7114 A, VWD, flow cell G7114A 018, d = 10 mm, V = 14 µL). Separation was performed on a C18 HPLC-column (AGILENT Poroshell 120 EC-C18 4,6x100mm, 2,7µm) operating at 40 °C. A gradient of ACN:water 10:90 – 80:20 *v/v* (additive 10 mmol L^{-1} $NH_4CH_3CO_2$) at a flow rate of 1 $mL \cdot min^{-1}$ during 15 min was used as the eluting solvent. The flow was directed into an AGILENT MSD (G6136BA, AP-ESI ion source). The instrument was calibrated in the m/z range 118-2121 in the positive mode and 113-2233 in the negative using a premixed calibration solution (AGILENT). The following parameters were used: spray chamber flow: 12 L min^{-1}; drying gas temperature: 350 K, Capillary Voltage: 3000 V, Fragmentor Voltage: 100 V

Contact Angle Measurement

For determination of Contact Angles, the Drop Shape Analyzer DSA25 from KRÜSS (Hamburg, Germany) in the sessile droplet mode. 5 µL of the respective solvent were dispensed on the modified glass slide and the static contact angle was measured. Three measurements were taken at three different positions and a mean value with standard deviation was calculated.

UV-Vis spectroscopy

A DMA with spots with a diameter of 2.82 mm containing the solutions to be analyzed was placed in a 3D printed holder. A second slide was placed in the top part of the holder and both parts were stacked together so that the slides were sandwiched and the droplets were caught between both slides. In this adapter, the slides could be analyzed with a BIOTEK Synergy H1 plate reader.

Fluorescence Microscopy

To analyze the enzymatic assay, the DMA slide was covered with a sticky chamber consisting of a second quartz glass slide and a rubber band a spacer and placed in a fresh petri dish. Using a KEYENCE fluorescence microscope BZ-X800 (Neu-Isenburg, Germany), images were taken in brightfield and blue fluorescence mode.

Digital Microscope

Digital microscope images of the droplets were taken with a KEYENCE VHX 7000 from top or with different angles. For fluorescence images, an additional UV light source (360 nm) was placed next to the sample and a barrier filter (415 nm) from NIGHTSEA (Hatfield, USA)was placed in the analyzer head.

Document Scanner

Images of the Droplet Microarray were taken with a document scanner CanoScan 8800F from CANON Deutschland GmbH (Krefeld, Germany) at 70% exposure. The images are shown in the figures without any color modification.

Image Analysis

ImageJ

Before the GRID SCREENER Tool[103] was developed, the color intensity was analyzed using the software IMAGEJ. The image was converted to a HSV-stack for color intensity or LAB-stack for color identification. A square within the spots was analyzed to give the mean intensity value. This was done manually, keeping the frame always in the same size for the measurements.

Grid Screener

For most color and fluorescence intensity evaluations, the GRID SCREENER from SCHILLING *et al*.[103] was used. The array was detected in the semi-automated mode by marking the right and left border of a randomly chosen spot and in addition the top left, top right and bottom right spot in the center. After identification of the grid, the evaluation method was chosen. The mean value of the fluorescence per spots was evaluated with *mean_intensity_fluorescence* after loading the respective image of the fluorescence channel. For color determination, the *color_evalutaion* was used, where the exact values of the color to be analyzed was added. The intensities were given as value per spot in a text file and were evaluated further according to the protocol. The GRID SCREENER was developed in the same time as this work, so the initial measurements were performed by MARCEL SCHILLING with a prototype version, until the user interface was developed.

Graphics were created with BioRender.com

6 List of Abbreviations

°C	degrees Celsius
µ	micro (10^{-6})
4-DMAP	4-dimethylaminopyridine
ACN	acetonitrile
ASMS	affinity selection mass spectrometry
BIS-TRIS	bis(2-hydroxyethyl)amino-tris(hydroxymethyl)methane
BSA	bovine serum albumin
conc.	concentrated
DAPI	4'-6-diamidino-2-phenylindole dihydrochloride
DCM	dichloromethane
DHB	2,5-dihydroxybenzoic acid
dI	deionized
DIC	*N,N'*-diisopropylcarbodiimide
DiFMUP	8,6-difluoro-4-methylumbelliferyl phosphate
DIPEA	diisopropylethylamine
DMA	Droplet Microarray
DMF	dimethyl formamide
DMPAP	2,2-dimethoxy-2-phenylacetophenone
DMSO	dimethyl sulfoxide
EDMA	ethylene dimethacrylate
ELRIG	european laboratory research and innovation group
EMA	european medicines agency
FDA	food and drug administration
HATU	[O-(7-Azabenzotriazol-1-yl)-N,N,N',N'-tetramethyluronium-hexafluoro phosphate
HEMA	2-hydroxyethyl methacrylate
HPLC	high performance/pressure liquid chromatography
HCCA	*alpha*-hydroxycinnamic acid
HCl	hydrochloric acid
hmLMPTP	human low molecular weight phosphotyrosine protein phosphatase
HT	high-throughput
ITO	indium tin oxide

LC-MS	liquid chromatography mass spectrometry
LLE	liquid-liquid extraction
MALDI	matrix-assisted laser desorption/ionization
MeOH	methanol
Mrd.	*Milliarden* (billion)
MS	mass spectrometry
NaOH	sodium hydroxide
n	nano (10^{-9})
NMP	N-methyl-2-pyrrolidone
NMR	nuclear magnetic resonance
Pa	pascal
PCR	polymerase chain reaction
p-NPP	para-nitrophenyl phosphate
SAMDI	self-assembled monolayer desorption ionization
SLAS	society for laboratory automation and screening
SPS	solid-phase synthesis
t	time
TFA	trifluoroacetic acid
TLC	thin layer chromatography
TOF	time of flight
UPLC	ultra performance liquid chromatography
UV	ultraviolet
Vis	visible

7 List of Figures

8 List of Tables

9 Literature

[1] Y. N. Demirdögen, *Master Thesis*, Karlsruhe Institute of Technology, Karlsruhe, **2020**.

[2] J. J. Wiedmann, Y. N. Demirdögen, S. Schmidt, M. A. Kuzina, Y. Wu, F. Wang, B. Nestler, C. Hopf, P. A. Levkin, *Small* **2023**, *19*, e2204512.

[3] A. S. Anderson, *Nature medicine* **2022**, *28*, 1538.

[4] J. A. DiMasi, H. G. Grabowski, R. W. Hansen, *J. Health Econ.* **2016**, *47*, 20.

[5] R. C. Mohs, N. H. Greig, *TRCI* **2017**, *3*, 651.

[6] a) H. C. S. Chan, H. Shan, T. Dahoun, H. Vogel, S. Yuan, *Trends Pharmacol. Sci.* **2019**, *40*, 592; b) S. Sun, N. T. Hartono, Z. D. Ren, F. Oviedo, A. M. Buscemi, M. Layurova, D. X. Chen, T. Ogunfunmi, J. Thapa, S. Ramasamy et al., *Joule* **2019**, *3*, 1437; c) J. Lyu, S. Wang, T. E. Balius, I. Singh, A. Levit, Y. S. Moroz, M. J. O'Meara, T. Che, E. Algaa, K. Tolmachova et al., *Nature* **2019**, *566*, 224.

[7] G. Xing, L. Liang, C. Deng, Y. Hua, X. Chen, Y. Yang, H. Liu, T. Lu, Y. Chen, Y. Zhang, *ACS Comb. Sci* **2020**, *22*, 873.

[8] A. Whitty, L. Zhou, *Future Med. Chem.* **2015**, *7*, 1093.

[9] A. Buitrago Santanilla, E. L. Regalado, T. Pereira, M. Shevlin, K. Bateman, L.-C. Campeau, J. Schneeweis, S. Berritt, Z.-C. Shi, P. Nantermet et al., *Science* **2015**, *347*, 49.

[10] G. Takátsy, *Acta Microbiol. Immunol. Hung.* **2003**, *50*, 369-82; discussion 382-3.

[11] K. S. Lam, S. E. Salmon, E. M. Hersh, V. J. Hruby, W. M. Kazmierski, R. J. Knapp, *Nature* **1991**, *354*, 82.

[12] Todd M. Doran, Paige Dickson, John Maina Ndungu, Peng Ge, Irena Suponitsky-Kroyter, Hongchan An, Thomas Kodadek in *Methods in Enzymology* (Ed.: Arun K. Shukla), Academic Press, **2019**, pp. 91–127.

[13] R. Fleeman, T. M. LaVoi, R. G. Santos, A. Morales, A. Nefzi, G. S. Welmaker, J. L. Medina-Franco, M. A. Giulianotti, R. A. Houghten, L. N. Shaw, *J. Med. Chem.* **2015**, *58*, 3340.

[14] R. Frank, *Tetrahedron* **1992**, *48*, 9217.

[15] B. Mahjour, Y. Shen, T. Cernak, *Acc. Chem. Res.* **2021**, *54*, 2337.

[16] a) S. Shaabani, R. Xu, M. Ahmadianmoghaddam, L. Gao, M. Stahorsky, J. Olechno, R. Ellson, M. Kossenjans, V. Helan, A. Dömling, *Green Chem.* **2019**, *21*, 225; b) F. Sutanto, S. Shaabani, C. G. Neochoritis, T. Zarganes-Tzitzikas, P. Patil, E. Ghonchepour, A. Dömling, *Sci. Adv.* **2021**, *7*, eabd9307.

[17] F. Sutanto, S. Shaabani, R. Oerlemans, D. Eris, P. Patil, M. Hadian, M. Wang, M. E. Sharpe, M. R. Groves, A. Dömling, *Angew. Chem. Int. Ed.* **2021**, *60*, 18231.

[18] K. Gao, S. Shaabani, R. Xu, T. Zarganes-Tzitzikas, L. Gao, M. Ahmadianmoghaddam, M. R. Groves, A. Dömling, *RSC Med. Chem.* **2021**, *12*, 809.

[19] F. A. Hansen, S. Pedersen-Bjergaard, *Anal. Chem.* **2020**, *92*, 2.

[20] S. X. Peng, C. Henson, M. J. Strojnowski, A. Golebiowski, S. R. Klopfenstein, *Anal. Chem.* **2000**, *72*, 261.

[21] a) A. Sarafraz-Yazdi, A. Amiri, *TrAC, Trends Anal. Chem.* **2010**, *29*, 1; b) G. Mafra, A. A. Vieira, J. Merib, J. L. Anderson, E. Carasek, *Anal. Chim. Acta* **2019**, *1063*, 159.

[22] P. Mary, V. Studer, P. Tabeling, *Anal. Chem.* **2008**, *80*, 2680.

[23] W. McDonald, R. Ohi, D. T. Miyamoto, T. J. Mitchison, J. R. Yates, *International Journal of Mass Spectrometry* **2002**, *219*, 245.

[24] P. Kiefer, N. Delmotte, J. A. Vorholt, *Analytical Chemistry* **2011**, *83*, 850.

[25] C. L. Barhate, A. F. Donnell, M. Davies, L. Li, Y. Zhang, F. Yang, R. Black, G. Zipp, Y. Zhang, C. L. Cavallaro et al., *Chem. Commun.* **2021**, *57*, 11037.

[26] C. J. Welch, X. Gong, W. Schafer, E. C. Pratt, T. Brkovic, Z. Pirzada, J. F. Cuff, B. Kosjek, *Tetrahedron: Asymmetry* **2010**, *21*, 1674.

[27] a) L. Gao, S. Shaabani, A. Reyes Romero, R. Xu, M. Ahmadianmoghaddam, A. Dömling, *Green Chem.* **2023**, *25*, 1380; b) A. Osipyan, S. Shaabani, R. Warmerdam, S. V. Shishkina, H. Boltz, A. Dömling, *Angew. Chem.* **2020**, *132*, 12523.

[28] A. de Villiers, F. Lestremau, R. Szucs, S. Gélébart, F. David, P. Sandra, *Journal of Chromatography A* **2006**, *1127*, 60.

[29] C. Haslam, J. Hellicar, A. Dunn, A. Fuetterer, N. Hardy, P. Marshall, R. Paape, M. Pemberton, A. Resemannand, M. Leveridge, *SLAS Discovery* **2016**, *21*, 176.

[30] K. Teuber, J. Schiller, B. Fuchs, M. Karas, T. W. Jaskolla, *Chemistry and Physics of Lipids* **2010**, *163*, 552.

[31] S. Lin, S. Dikler, W. D. Blincoe, R. D. Ferguson, R. P. Sheridan, Z. Peng, D. V. Conway, K. Zawatzky, H. Wang, T. Cernak et al., *Science* **2018**, *361*.

[32] SAMDI Tech, Inc., "SAMDI Tech inf. a charles river company", can be found under https://www.samditech.com/, **2023**.

[33] M. D. Scholle, D. McLaughlin, Z. A. Gurard-Levin, *SLAS Discov.* **2021**, *26*, 974.

[34] S. Habeshian, M. L. Merz, G. Sangouard, G. K. Mothukuri, M. Schüttel, Z. Bognár, C. Díaz-Perlas, J. Vesin, J. Bortoli Chapalay, G. Turcatti et al., *Nat. Commun.* **2022**, *13*, 3823.

[35] P. Gehrtz, S. Marom, M. Bührmann, J. Hardick, S. Kleinbölting, A. Shraga, C. Dubiella, R. Gabizon, J. N. Wiese, M. P. Müller et al., *J. Med. Chem.* **2022**, *65*, 10341.

[36] H. D. Agnew, R. D. Rohde, S. W. Millward, A. Nag, W.-S. Yeo, J. E. Hein, S. M. Pitram, A. A. Tariq, V. M. Burns, R. J. Krom et al., *Angew. Chem. Int. Ed.* **2009**, *48*, 4944.

[37] auroramicroplates, "Aurora Microplates", can be found under https://auroramicroplates.com/product/3456-round-well-white-high-base-evap-barrier-mako-solid-bottom/, **2023**.

[38] A. B. Theberge, E. Mayot, A. El Harrak, F. Kleinschmidt, W. T. S. Huck, A. D. Griffiths, *Lab on a chip* **2012**, *12*, 1320.

[39] K. Matuła, F. Rivello, W. T. S. Huck, *Adv. Biosys.* **2020**, *4*, e1900188.

[40] L. K. Weber, A. Palermo, J. Kügler, O. Armant, A. Isse, S. Rentschler, T. Jaenisch, A. Nesterov-Mueller, F. Breitling, F. F. Loeffler, *J. Immunol. Methods* **2017**, *443*, 45.

[41] V. Jokinen, L. Sainiemi, S. Franssila, *Adv. Mater.* **2008**, *20*, 3453.

[42] F. L. Geyer, E. Ueda, U. Liebel, N. Grau, P. A. Levkin, *Angew. Chem. Int. Ed.* **2011**, *50*, 8424.

[43] Y. Liu, T. Tronser, R. Peravali, M. Reischl, P. A. Levkin, *Adv. Biosys.* **2020**, *4*, e1900257.

[44] W. Feng, L. Li, E. Ueda, J. Li, S. Heißler, A. Welle, O. Trapp, P. A. Levkin, *Adv. Mater. Interfaces* **2014**, *1*, 1400269.

[45] A. Rosenfeld, M. Brehm, A. Welle, V. Trouillet, S. Heissler, M. Benz, P. A. Levkin, *Mater. Today Bio* **2019**, *3*, 100022.

[46] H. Cui, X. Wang, J. Wesslowski, T. Tronser, J. Rosenbauer, A. Schug, G. Davidson, A. A. Popova, P. A. Levkin, *Adv. Mater.* **2021**, *33*, 2006434.

[47] M. Benz, A. Asperger, M. Hamester, A. Welle, S. Heissler, P. A. Levkin, *Nat. Commun.* **2020**, *11*, 5391.

[48] Efremov A. N., Stanganello E., A. Welle, S. Scholpp, P. A. Levkin, *Biomater* **2013**, *34*, 1757.

[49] E. Ueda, F. L. Geyer, V. Nedashkivska, P. A. Levkin, *Lab Chip* **2012**, *12*, 5218.

[50] A. A. Popova, S. M. Schillo, K. Demir, E. Ueda, A. Nesterov-Mueller, P. A. Levkin, *Adv. Mater.* **2015**, *27*, 5217.

[51] A. A. Popova, K. Demir, T. G. Hartanto, E. Schmitt, P. A. Levkin, *RSC Adv.* **2016**, *6*, 38263.

[52] G. E. Jogia, T. Tronser, A. A. Popova, P. A. Levkin, *Microarrays* **2016**, *5*.

[53] T. Tronser, A. A. Popova, P. A. Levkin, *Curr. Opin. Biotechnol.* **2017**, *46*, 141.

[54] A. A. Popova, C. Depew, K. M. Permana, A. Trubitsyn, R. Peravali, J. Á. G. Ordiano, M. Reischl, P. A. Levkin, *SLAS Technol.* **2017**, *22*, 163.

[55] A. A. Popova, T. Tronser, K. Demir, P. Haitz, K. Kuodyte, V. Starkuviene, P. Wajda, P. A. Levkin, *Small* **2019**, *15*, e1901299.

[56] A. A. Popova, D. Marcato, R. Peravali, I. Wehl, U. Schepers, P. A. Levkin, *Adv. Funct. Mater.* **2018**, *28*, 1703486.

[57] Y. Liu, S. Chakraborty, C. Direksilp, J. M. Scheiger, A. A. Popova, P. A. Levkin, *Mater. Today Bio* **2021**, *12*, 100153.

[58] Y. Liu, S. Bertels, M. Reischl, R. Peravali, M. Bastmeyer, A. A. Popova, P. A. Levkin, *Adv. Healthc. Mater.* **2022**, *11*, e2200718.

[59] A. A. Popova, S. Dietrich, W. Huber, M. Reischl, R. Peravali, P. A. Levkin, *SLAS Technol.* **2020**, *26*, 274.

[60] A. A. Popova, M. Reischl, D. Kazenmaier, H. Cui, T. Amberger, P. A. Levkin, *SLAS Technol.* **2022**, *27*, 44.

[61] W. Lei, A. Deckers, C. Luchena, A. Popova, M. Reischl, N. Jung, S. Bräse, T. Schwartz, I. K. Krimmelbein, L. F. Tietze et al., *Adv. Biol.* **2022**, *6*, e2200166.

[62] S. Chakraborty, V. Gourain, M. Benz, J. M. Scheiger, P. A. Levkin, A. A. Popova, *Mater. Today Bio* **2021**, *11*, 100112.

[63] S. Chakraborty, C. Luchena, J. J. Elton, M. P. Schilling, M. Reischl, M. Roux, P. A. Levkin, A. A. Popova, *Adv. Healthc. Mater.* **2022**, *11*, e2102493.

[64] M. Noun, R. Akoumeh, I. Abbas, *Microanal* **2022**, *28*, 1.

[65] M. S. Unger, M. Blank, T. Enzlein, C. Hopf, *Nat. Protoc* **2021**, *16*, 5533.

[66] W. D. Blincoe, S. Lin, S. D. Dreher, H. Sheng, *Tetrahedron* **2020**, *76*, 131434.

[67] C. RamalloGuevara, D. Paulssen, A. A. Popova, C. Hopf, P. A. Levkin, *Adv. Biol.* **2021**, *5*, 2000279.

[68] H. Zhang, T. Oellers, W. Feng, T. Abdulazim, E. N. Saw, A. Ludwig, P. A. Levkin, N. Plumeré, *Anal. Chem.* **2017**, *89*, 5832.

[69] A. Rosenfeld, C. Oelschlaeger, R. Thelen, S. Heissler, P. A. Levkin, *Mater. Today Bio* **2020**, *6*, 100053.

[70] M. Brehm, S. Heissler, S. Afonin, P. A. Levkin, *Small* **2020**, *16*, 1905971.

[71] M. Benz, M. R. Molla, A. Böser, A. Rosenfeld, P. A. Levkin, *Nat. Commun.* **2019**, *10*, 2879.

[72] W. Feng, L. Li, X. Du, A. Welle, P. A. Levkin, *Adv. Mater.* **2016**, *28*, 3202.

[73] Levkin, P. A., Grunze, M., Dong, Z., Demir, K., Widmaier, S., Brehm, M., Popova, A., EP3733277A1, **2019**.

[74] W. Lei, K. Demir, J. Overhage, M. Grunze, T. Schwartz, P. A. Levkin, *Adv. Biosys.* **2020**, *4*, 2000073.

[75] J. Höpfner. *Unpublished Results*, **2023**.

[76] C. V. Sapan, R. L. Lundblad, N. C. Price, *Biotechnology and Applied Biochemistry* **1999**, *29*, 99.

[77] K. R. Gee, W.-C. Sun, M. K. Bhalgat, R. H. Upson, D. H. Klaubert, K. A. Latham, R. P. Haugland, *Analytical Biochemistry* **1999**, *273*, 41.

[78] K. H. Lau, J. R. Farley, D. J. Baylink, *Biochem.* **1989**, *257*, 23.

[79] E. Speckmeier, A. Pommereau, K.-C. Grosser, H. Mors, T. C. Maier, T. Licher, F. Bärenz, *SLAS Discov.* **2022**, *27*, 298.

[80] D. J. Withers, M. White, *Endocrinology* **2000**, *141*, 1917.

[81] A. R. Saltiel, C. R. Kahn, *Nature* **2001**, *414*, 799.

[82] J. Boucher, A. Kleinridders, C. R. Kahn, *Cold Spring Harb. perspec. biol.* **2014**, *6*.

[83] B. J. Goldstein, *J. Clin. Endocr.* **2002**, *87*, 2474.

[84] S. M. Stanford, A. E. Aleshin, V. Zhang, R. J. Ardecky, M. P. Hedrick, J. Zou, S. R. Ganji, M. R. Bliss, F. Yamamoto, A. A. Bobkov et al., *Nature Chem. Biol.* **2017**, *13*, 624.

[85] S. M. Stanford, M. A. Diaz, R. J. Ardecky, J. Zou, T. Roosild, Z. J. Holmes, T. P. Nguyen, M. P. Hedrick, S. Rodiles, A. Guan et al., *J. Med. Chem.* **2021**, *64*, 5645.

[86] L. Bourebaba, J. Łyczko, M. Alicka, N. Bourebaba, A. Szumny, A. M. Fal, K. Marycz, *J. Clin. Med.* **2020**, *9*.

[87] M. A. Tabatabai, J. M. Bremner, *Soil Biol. Biochem.* **1969**, *1*, 301.

[88] J. H. Zhang, T. D. Chung, K. R. Oldenburg, *J. Biomol. screen.* **1999**, *4*, 67.

[89] J. Montalibet, K. I. Skorey, B. P. Kennedy, *Methods* **2005**, *35*, 2.

[90] "PubChem", can be found under https://pubchem.ncbi.nlm.nih.gov/.

[91] ChemicalBook Inc., "Chemical Book", can be found under https://www.chemicalbook.com/ProductChemicalPropertiesCB71828149_EN.htm, **2016**.

[92] M. J. Weissenborn, J. W. Wehner, C. J. Gray, R. Šardzík, C. E. Eyers, T. K. Lindhorst, S. L. Flitsch, *J. Org. Chem.* **2012**, *8*, 753.

[93] R. Wu, L. Qin, L. Chen, R. Ma, D. Chen, H. Liu, H. Xu, H. Guo, Y. Zhou, X. Wang, *Chem. Commun.* **2021**, *57*, 10707.

[94] J. E. Leonard, *J. Chem. Educ.* **1981**, *58*, 1022.

[95] W. M Haynes, D. R. Lide (Ed.) *CRC Handbook of Chemistry and Physics*, CRC Press, Boca Raton, **2014**.

[96] T. E. Daubert, R. P. Danner (Eds.) *Physical and thermodynamic properties of pure chemicals: data compilation*, Taylor & Francis, Washington DC, **1989**.

[97] Y. Wu, M. Kuzina, F. Wang, M. Reischl, M. Selzer, B. Nestler, P. A. Levkin, *J. Colloid Interface Sci.* **2022**, *606*, 1077.

[98] *An overview on thin layer chromatography*, **2011**.

[99] H. N. Kim, M. H. Lee, H. J. Kim, J. S. Kim, J. Yoon, *Chem. Soc. Rev.* **2008**, *37*, 1465.

[100] Y. He, H. K. Lee, *Anal. Chem.* **1997**, *69*, 4634.

[101] C. Hansch, A. Leo, D. Hoekman, *Exploring QSAR*, American Chemical Soc, Washington, DC, **1995**.

[102] M. P. Schilling, El Khaled El Faraj, Razan, J. E. Urrutia Gómez, S. J. Sonnentag, F. Wang, B. Nestler, V. Orian-Rousseau, A. A. Popova, P. A. Levkin, M. Reischl, *Sci Rep* **2023**, *13*, 5107.

[103] M. P. Schilling, S. Schmelzer, J. E. U. Gomez, A. A. Popova, P. A. Levkin, M. Reischl, *IEEE Access* **2021**, *9*, 166027.

10 Appendix

LC-MS Spectra

Chapter 3.1.5

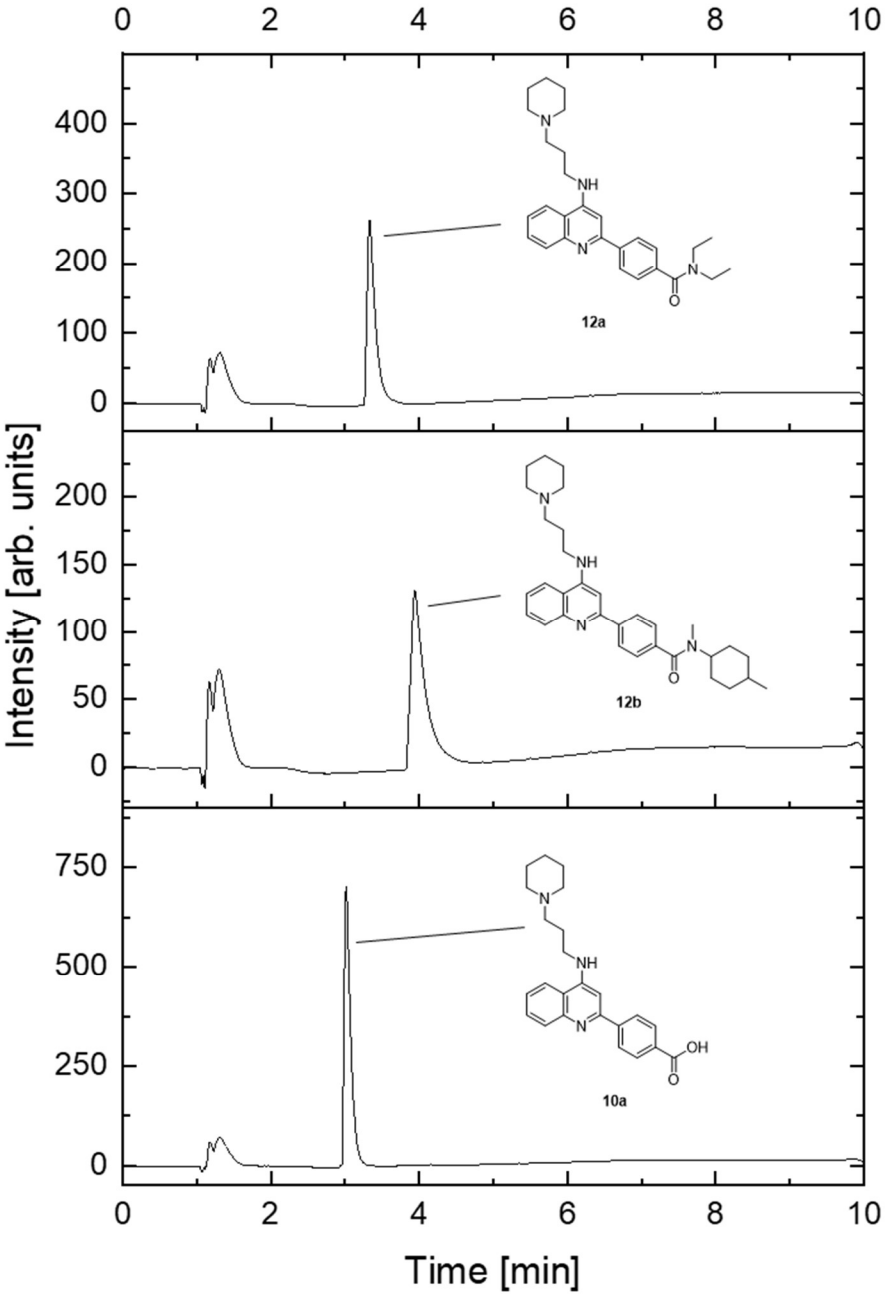

Figure 71: Control LC-MS measurements for the pure compounds **12a**, **12b** and **10a**. LC-MS method I was used.

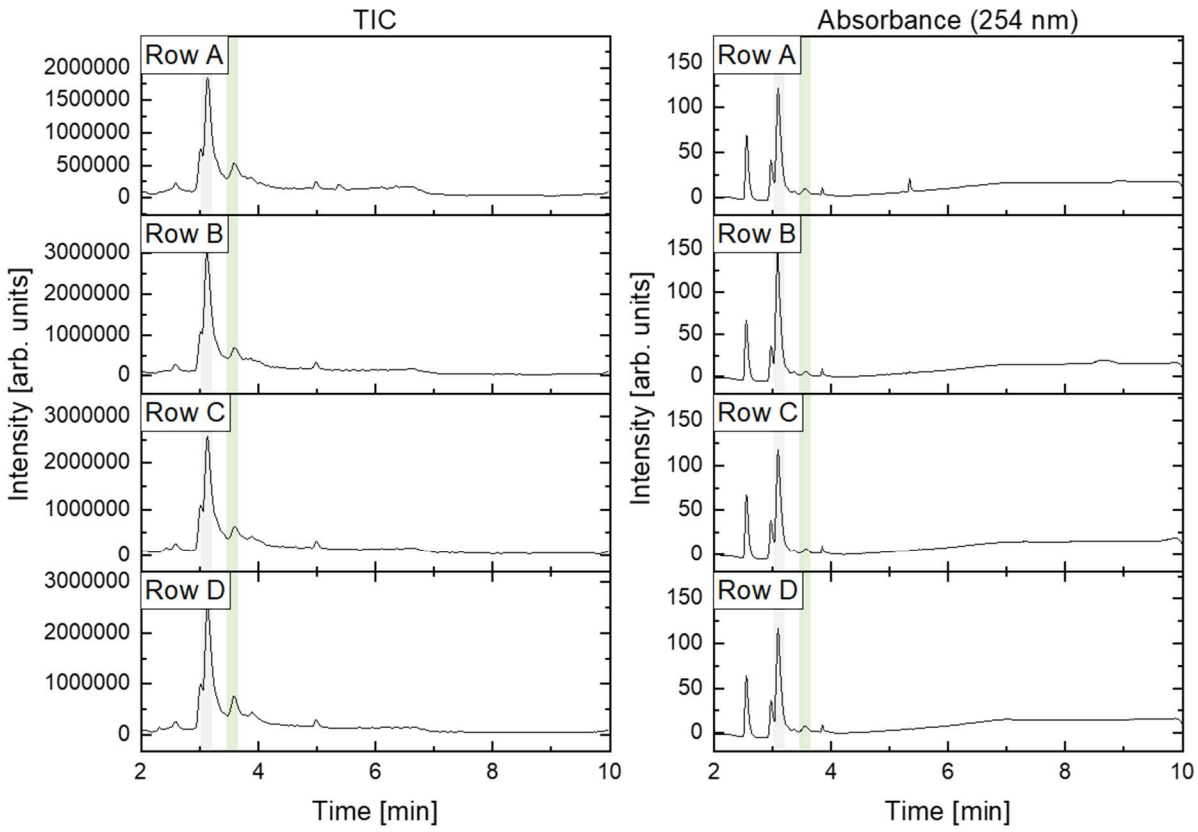

Figure 72: LC-MS chromatograms for the first experiment from Figure 30. Signals for **10a** (grey) and **12a** (green) are highlighted. LC-MS method I was used.

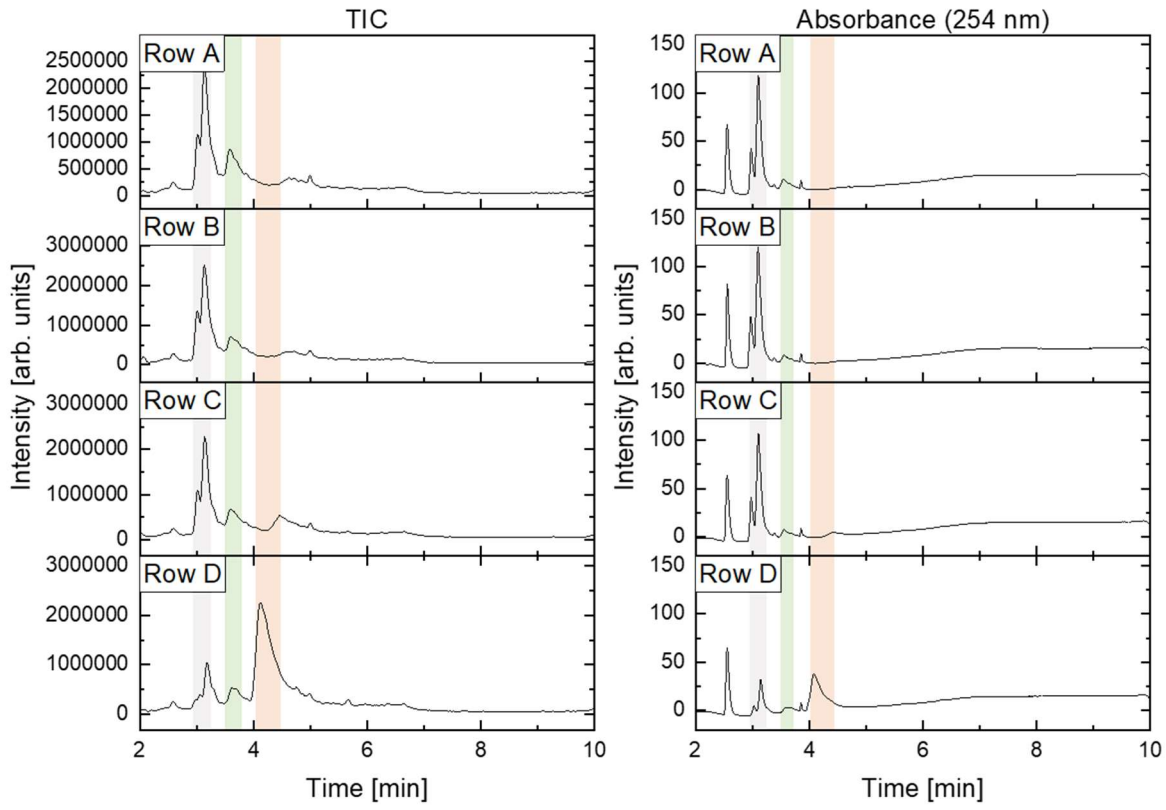

Figure 73: LC-MS chromatograms for the second experiment from Figure 30. Signals for **10a** (grey), **12a** (green) and **12b** (red) are highlighted. LC-MS method I was used.

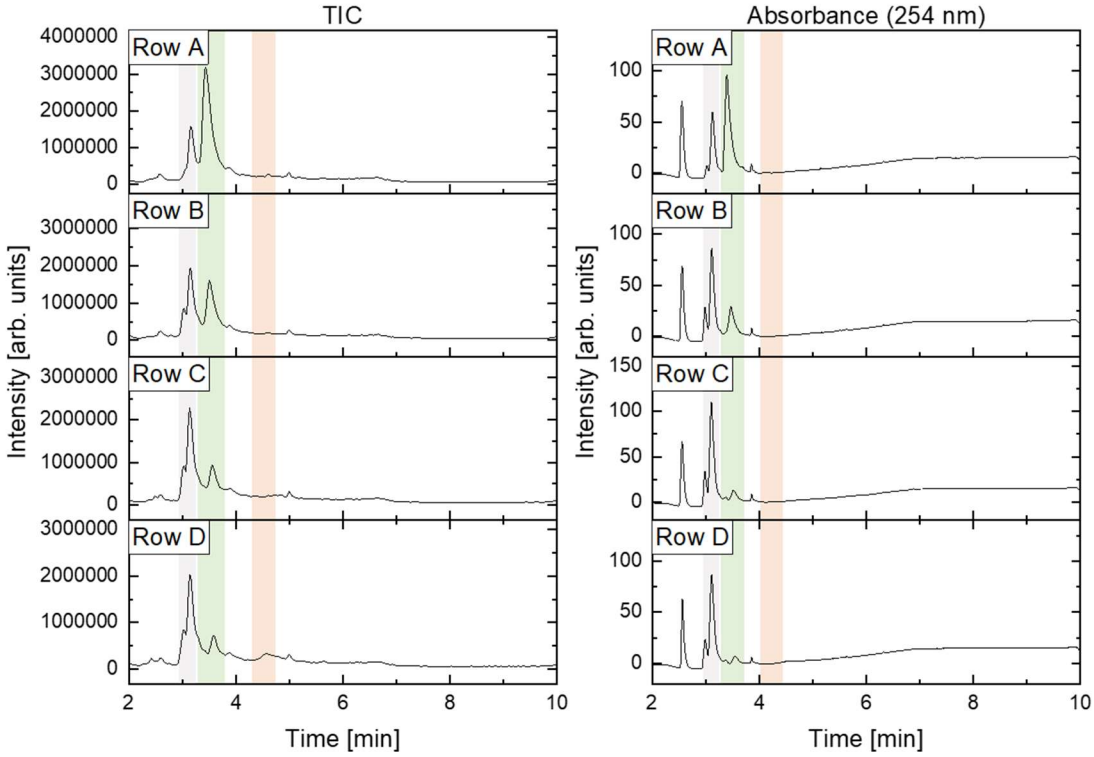

Figure 74: LC-MS chromatograms for the third experiment from Figure 30. Signals for **10a** (grey), **12a** (green) and **12b** (red) are highlighted. LC-MS method I was used.

Chapter 3.1.8

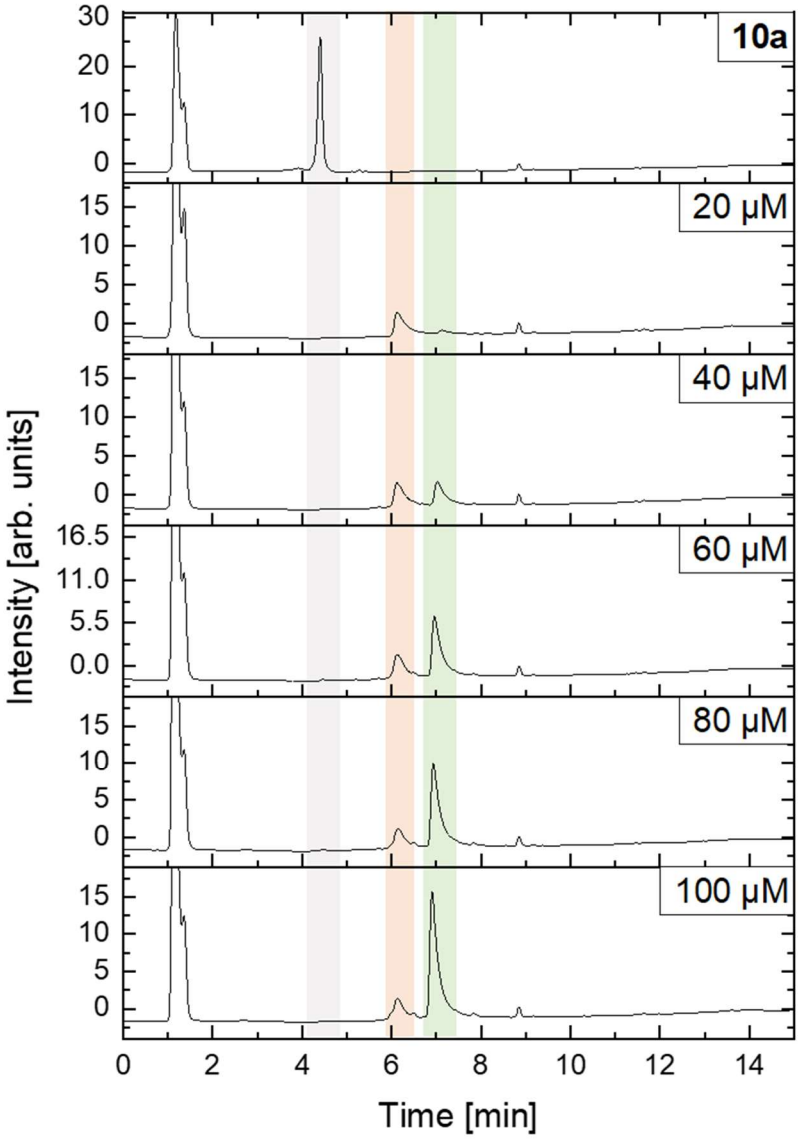

Figure 75: LC-MS measurements for the dilution series of a reaction from Figure 41 with the measurement of the starting material **10a** as control for the new device and setup. The colored bars indicate the retention time of **10a** (grey), **26** (red) and **12a** (green). LC-MS method II was used.

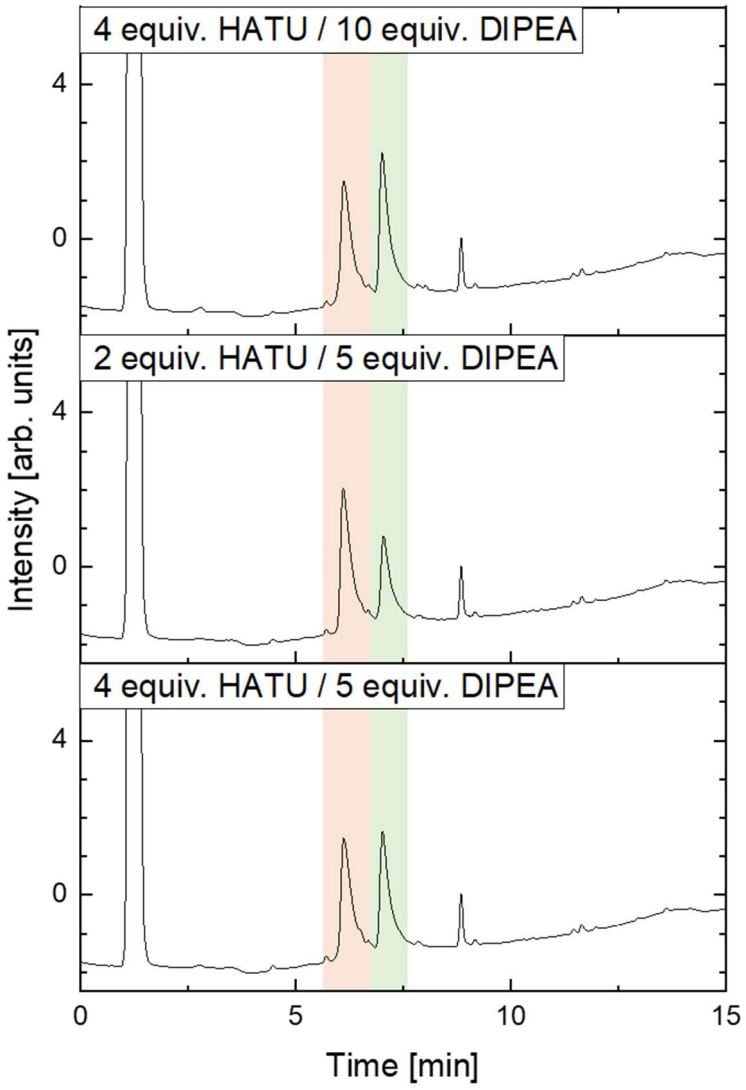

Figure 76: LC-MS measurements for the variation of the equivalents of HATU and DIPEA in the reaction from Figure 41. The colored bars indicate the retention time of **26** (red) and **12a** (green). LC-MS method II was used.

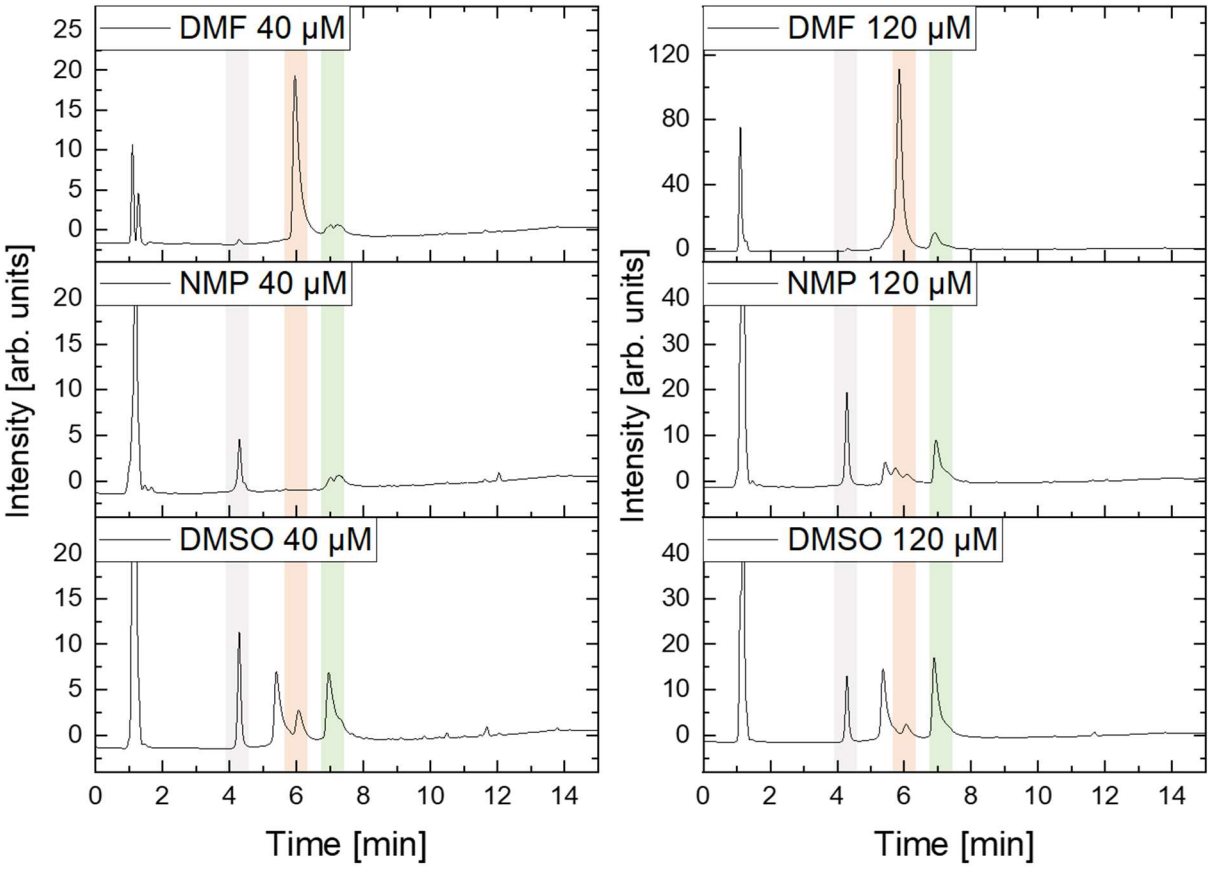

Figure 77: LC-MS measurements for the variation of solvent (top to down) at two different concentrations (left/right) from Figure 42. The colored bars indicate the retention time of **10a** (grey), **26** (red) and **12a** (green). LC-MS method II was used.

MALDI-MS Spectra for Chapter 3.1

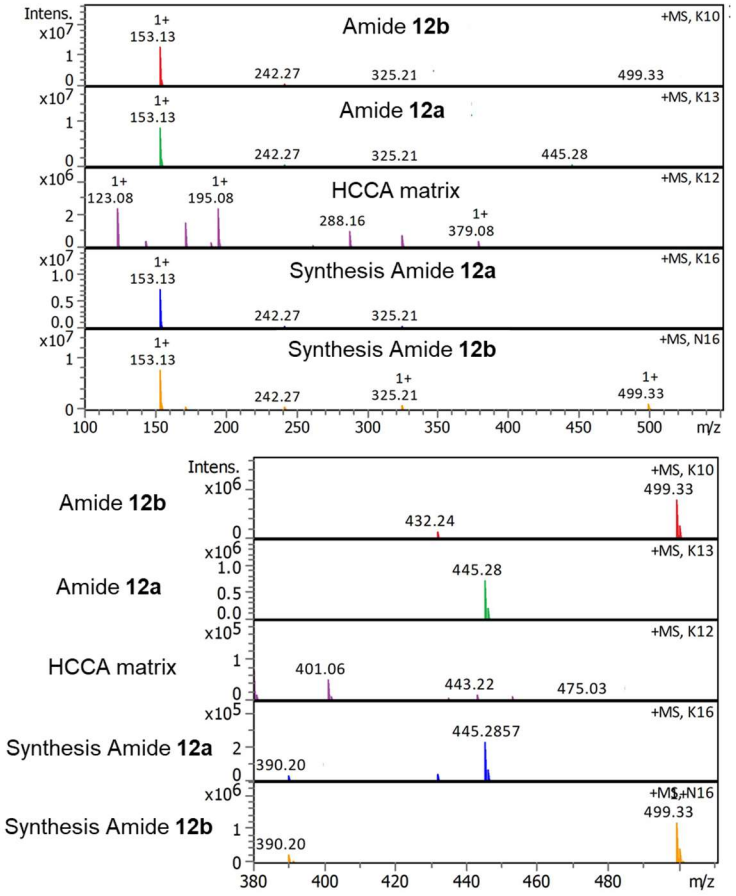

Figure 78: Mass spectra from first MALDI-MS measurements (3.1.6). The whole (top) and zoomed (right) spectra are shown for representative spots for amide **12b**, **12a**, HCCA, synthesis of **12a** and synthesis of **12b** (top to bottom).

MALDI-MS-screening (Chapter 3.1.7)

		208	15	8	20	16	8	4	1	2	18	19	25	15	208		
		207	12	19	18	17	5	22	17	8	26	24	14	27	195		
		181	29	16	9	11	19	12	13	25	5	13	11	23	196		
		182	24	10	2	29	13	20	24	14	21	1	9	4	181		
		203	21	11	28	9	1	24	28	4	22	7	5	28	182		
		25	7	26	181	6	23	18	181	7	30	9	17	8	22		
		14	13	1	182	10	7	30	182	12	16	20	12	3	2		
		23	4	17	204	21	25	15	209	23	15	19	18	29	30		
		6	22	27	193	26	27	14	208	11	27	3	20	6	10		
		5	3	30	194	28	2	3	197	10	6	29	26	21	16		
		50	34	49	42	51	40	187	59	33	54	183	49	43	40		
		48	35	44	60	32	38	188	36	50	52	184	56	44	31		
		36	58	59	59	57	41	208	56	43	40	210	53	34	39		
		47	45	46	36	33	47	194	41	31	46	198	37	45	33		
		38	43	33	48	43	34	195	45	60	42	199	32	36	60		
		183	41	56	32	49	53	35	57	34	58	42	54	50	183		
		184	37	42	52	37	52	44	37	47	44	46	47	35	184		
		206	31	53	57	54	50	56	49	35	48	55	51	57	209		
		195	51	60	40	31	45	39	39	51	53	59	48	41	208		
		196	54	39	55	58	55	46	55	38	32	38	58	52	200		
		63	78	74	191	65	84	62	185	63	84	68	80	63	79		
		67	66	79	192	87	74	76	186	89	61	70	65	89	81		
		89	73	90	208	82	89	75	210	88	78	83	77	71	90		
		85	70	64	200	73	64	79	201	76	85	79	78	86	82		
		80	76	84	201	72	90	83	202	65	66	67	87	68	67		
		75	81	62	63	71	69	185	69	64	82	185	85	61	76		
		82	86	65	68	67	85	186	73	86	87	186	84	66	74		
		68	87	61	80	77	61	204	90	75	74	209	73	88	62		
		83	77	72	86	70	81	197	72	81	71	208	64	75	70		
		69	71	88	66	78	88	198	80	62	77	193	83	72	69		
		187	99	104	102	111	97	113	120	116	91	95	91	94	183		
		188	111	96	108	95	99	105	113	119	114	96	116	102	184		
		205	119	95	114	104	109	100	106	112	109	93	108	110	205		
		208	118	113	110	106	102	112	96	105	104	113	103	98	208		
		207	91	117	97	107	96	119	94	103	108	120	100	97	207		
		116	92	109	187	93	118	114	187	110	102	93	117	114	105		
		107	93	112	188	116	103	92	188	111	115	100	106	118	92		
		103	94	101	206	120	91	117	210	118	99	92	112	107	101		
		98	100	120	199	94	101	110	208	117	107	95	109	111	99		
		105	106	115	200	98	108	115	196	97	98	101	115	104	119		
		140	128	123	134	141	133	189	125	140	143	189	121	146	143		
		142	138	149	145	149	127	190	128	129	148	190	138	128	144		
		127	124	143	135	125	126	203	147	146	121	209	130	131	141		
		146	150	141	124	148	123	208	131	136	126	197	136	125	132		
		131	134	136	136	131	132	207	150	141	134	198	145	124	139		
		126	130	145	189	147	140	144	189	144	133	127	137	129	142		
		137	139	135	190	138	142	150	190	135	139	122	140	149	147		
		122	133	121	210	122	137	143	204	123	142	138	135	134	150		
		125	129	148	208	146	121	139	201	132	124	145	126	127	123		
		132	144	147	199	128	129	130	202	149	130	137	133	122	148		
		165	156	161	166	167	152	191	156	174	172	185	175	155	171		
		175	157	172	165	163	161	192	167	169	178	186	167	157	166		
		158	168	162	160	170	172	206	176	161	162	203	163	151	153		
		176	155	159	154	164	159	193	175	152	163	208	158	154	178		
		178	173	160	158	151	178	194	159	165	168	207	174	176	169		
		207	154	166	170	175	155	177	153	173	160	162	161	152	191		
		191	177	180	153	176	162	156	158	179	154	160	180	170	192		
		192	174	179	163	157	179	173	171	157	155	173	179	156	208		
		205	167	152	169	169	171	168	166	170	177	165	177	159	202		
		208	151	164	171	153	180	174	164	180	151	172	168	164	208		

Figure 79: Printing scheme for the reaction screening with MALDI-MS-readout (Chapter 3.1.7.). White spots were filled with DMF only for reduction of evaporation effects. colored spots were used for controls, grey spots were used for the synthesis. The reaction IDs are listed in the table below. Green highlighted spots without numbers were used as matrix control spots for MALDI-MS.

Table 6: List of all reaction conditions tested in Chapter 3.1.7. [1]Ratio 1: 1.50 equiv. amine, 5.00 equiv. DIPEA; 2: 1.50 equiv. amine, 10.0 equiv. DIPEA; 3: 3.00 equiv. amine, 10.0 equiv. DIPEA.

Reaction ID	Acid	Amine	Ratio[1]	Product	concentration
1	10a	18b	1	12a	120 µM
2	10a	18b	1	12a	20 µM
3	10a	18b	2	12a	120 µM
4	10a	18b	2	12a	20 µM
5	10a	18b	3	12a	120 µM
6	10a	18b	3	12a	20 µM
7	10a	19b	1	12b	120 µM
8	10a	19b	1	12b	20 µM
9	10a	19b	2	12b	120 µM
10	10a	19b	2	12b	20 µM
11	10a	19b	3	12b	120 µM
12	10a	19b	3	12b	20 µM
13	10a	20	1	12c	120 µM
14	10a	20	1	12c	20 µM
15	10a	20	2	12c	120 µM
16	10a	20	2	12c	20 µM
17	10a	20	3	12c	120 µM
18	10a	20	3	12c	20 µM
19	10a	21	1	12d	120 µM
20	10a	21	1	12d	20 µM
21	10a	21	2	12d	120 µM
22	10a	21	2	12d	20 µM
23	10a	21	3	12d	120 µM
24	10a	21	3	12d	20 µM
25	10a	22	1	12e	120 µM
26	10a	22	1	12e	20 µM
27	10a	22	2	12e	120 µM
28	10a	22	2	12e	20 µM
29	10a	22	3	12e	120 µM
30	10a	22	3	12e	20 µM
31	10a TFA	18b	1	12a	120 µM
32	10a TFA	18b	1	12a	20 µM
33	10a TFA	18b	2	12a	120 µM
34	10a TFA	18b	2	12a	20 µM
35	10a TFA	18b	3	12a	120 µM
36	10a TFA	18b	3	12a	20 µM
37	10a TFA	19b	1	12b	120 µM
38	10a TFA	19b	1	12b	20 µM
39	10a TFA	19b	2	12b	120 µM
40	10a TFA	19b	2	12b	20 µM
41	10a TFA	19b	3	12b	120 µM
42	10a TFA	19b	3	12b	20 µM
43	10a TFA	20	1	12c	120 µM
44	10a TFA	20	1	12c	20 µM
45	10a TFA	20	2	12c	120 µM
46	10a TFA	20	2	12c	20 µM
47	10a TFA	20	3	12c	120 µM
48	10a TFA	20	3	12c	20 µM
49	10a TFA	21	1	12d	120 µM
50	10a TFA	21	1	12d	20 µM
51	10a TFA	21	2	12d	120 µM

52	10a TFA	21	2	12d	20 µM
53	10a TFA	21	3	12d	120 µM
54	10a TFA	21	3	12d	20 µM
55	10a TFA	22	1	12e	120 µM
56	10a TFA	22	1	12e	20 µM
57	10a TFA	22	2	12e	120 µM
58	10a TFA	22	2	12e	20 µM
59	10a TFA	22	3	12e	120 µM
60	10a TFA	22	3	12e	20 µM
61	10a HCl	18b	1	12a	120 µM
62	10a HCl	18b	1	12a	20 µM
63	10a HCl	18b	2	12a	120 µM
64	10a HCl	18b	2	12a	20 µM
65	10a HCl	18b	3	12a	120 µM
66	10a HCl	18b	3	12a	20 µM
67	10a HCl	19b	1	12b	120 µM
68	10a HCl	19b	1	12b	20 µM
69	10a HCl	19b	2	12b	120 µM
70	10a HCl	19b	2	12b	20 µM
71	10a HCl	19b	3	12b	120 µM
72	10a HCl	19b	3	12b	20 µM
73	10a HCl	20	1	12c	120 µM
74	10a HCl	20	1	12c	20 µM
75	10a HCl	20	2	12c	120 µM
76	10a HCl	20	2	12c	20 µM
77	10a HCl	20	3	12c	120 µM
78	10a HCl	20	3	12c	20 µM
79	10a HCl	21	1	12d	120 µM
80	10a HCl	21	1	12d	20 µM
81	10a HCl	21	2	12d	120 µM
82	10a HCl	21	2	12d	20 µM
83	10a HCl	21	3	12d	120 µM
84	10a HCl	21	3	12d	20 µM
85	10a HCl	22	1	12e	120 µM
86	10a HCl	22	1	12e	20 µM
87	10a HCl	22	2	12e	120 µM
88	10a HCl	22	2	12e	20 µM
89	10a HCl	22	3	12e	120 µM
90	10a HCl	22	3	12e	20 µM
91	10b HCl	18b	1	12f	120 µM
92	10b HCl	18b	1	12f	20 µM
93	10b HCl	18b	2	12f	120 µM
94	10b HCl	18b	2	12f	20 µM
95	10b HCl	18b	3	12f	120 µM
96	10b HCl	18b	3	12f	20 µM
97	10b HCl	19b	1	12g	120 µM
98	10b HCl	19b	1	12g	20 µM
99	10b HCl	19b	2	12g	120 µM
100	10b HCl	19b	2	12g	20 µM
101	10b HCl	19b	3	12g	120 µM
102	10b HCl	19b	3	12g	20 µM
103	10b HCl	20	1	12h	120 µM
104	10b HCl	20	1	12h	20 µM
105	10b HCl	20	2	12h	120 µM

106	10b HCl	20	2	12h	20 µM
107	10b HCl	20	3	12h	120 µM
108	10b HCl	20	3	12h	20 µM
109	10b HCl	21	1	12i	120 µM
110	10b HCl	21	1	12i	20 µM
111	10b HCl	21	2	12i	120 µM
112	10b HCl	21	2	12i	20 µM
113	10b HCl	21	3	12i	120 µM
114	10b HCl	21	3	12i	20 µM
115	10b HCl	22	1	12j	120 µM
116	10b HCl	22	1	12j	20 µM
117	10b HCl	22	2	12j	120 µM
118	10b HCl	22	2	12j	20 µM
119	10b HCl	22	3	12j	120 µM
120	10b HCl	22	3	12j	20 µM
121	10c TFA	18b	1	12k	120 µM
122	10c TFA	18b	1	12k	20 µM
123	10c TFA	18b	2	12k	120 µM
124	10c TFA	18b	2	12k	20 µM
125	10c TFA	18b	3	12k	120 µM
126	10c TFA	18b	3	12k	20 µM
127	10c TFA	19b	1	12l	120 µM
128	10c TFA	19b	1	12l	20 µM
129	10c TFA	19b	2	12l	120 µM
130	10c TFA	19b	2	12l	20 µM
131	10c TFA	19b	3	12l	120 µM
132	10c TFA	19b	3	12l	20 µM
133	10c TFA	20	1	12m	120 µM
134	10c TFA	20	1	12m	20 µM
135	10c TFA	20	2	12m	120 µM
136	10c TFA	20	2	12m	20 µM
137	10c TFA	20	3	12m	120 µM
138	10c TFA	20	3	12m	20 µM
139	10c TFA	21	1	12n	120 µM
140	10c TFA	21	1	12n	20 µM
141	10c TFA	21	2	12n	120 µM
142	10c TFA	21	2	12n	20 µM
143	10c TFA	21	3	12n	120 µM
144	10c TFA	21	3	12n	20 µM
145	10c TFA	22	1	12o	120 µM
146	10c TFA	22	1	12o	20 µM
147	10c TFA	22	2	12o	120 µM
148	10c TFA	22	2	12o	20 µM
149	10c TFA	22	3	12o	120 µM
150	10c TFA	22	3	12o	20 µM
151	10c HCl	18b	1	12k	120 µM
152	10c HCl	18b	1	12k	20 µM
153	10c HCl	18b	2	12k	120 µM
154	10c HCl	18b	2	12k	20 µM
155	10c HCl	18b	3	12k	120 µM
156	10c HCl	18b	3	12k	20 µM
157	10c HCl	19b	1	12l	120 µM
158	10c HCl	19b	1	12l	20 µM
159	10c HCl	19b	2	12l	120 µM

160	10c HCl	19b	2	12l	20 µM
161	10c HCl	19b	3	12l	120 µM
162	10c HCl	19b	3	12l	20 µM
163	10c HCl	20	1	12m	120 µM
164	10c HCl	20	1	12m	20 µM
165	10c HCl	20	2	12m	120 µM
166	10c HCl	20	2	12m	20 µM
167	10c HCl	20	3	12m	120 µM
168	10c HCl	20	3	12m	20 µM
169	10c HCl	21	1	12n	120 µM
170	10c HCl	21	1	12n	20 µM
171	10c HCl	21	2	12n	120 µM
172	10c HCl	21	2	12n	20 µM
173	10c HCl	21	3	12n	120 µM
174	10c HCl	21	3	12n	20 µM
175	10c HCl	22	1	12o	120 µM
176	10c HCl	22	1	12o	20 µM
177	10c HCl	22	2	12o	120 µM
178	10c HCl	22	2	12o	20 µM
179	10c HCl	22	3	12o	120 µM
180	10c HCl	22	3	12o	20 µM
181	10a				120 µM
182	10a				20 µM
183	10a TFA				120 µM
184	10a TFA				20 µM
185	10a HCl				120 µM
186	10a HCl				20 µM
187	10b HCl				120 µM
188	10b HCl				20 µM
189	10c TFA				120 µM
190	10c TFA				20 µM
191	10c HCl				120 µM
192	10c HCl				20 µM
193		18b	2		120 µM
194		18b	2		20 µM
195		19b	2		120 µM
196		19b	2		20 µM
197		20	2		120 µM
198		20	2		20 µM
199		21	2		120 µM
200		21	2		20 µM
201		22	2		120 µM
202		22	2		20 µM
203			1		120 µM
204			1		20 µM
205			2		120 µM
206			2		20 µM
207					
208					
209				12a	120 µM
210				12a	20 µM

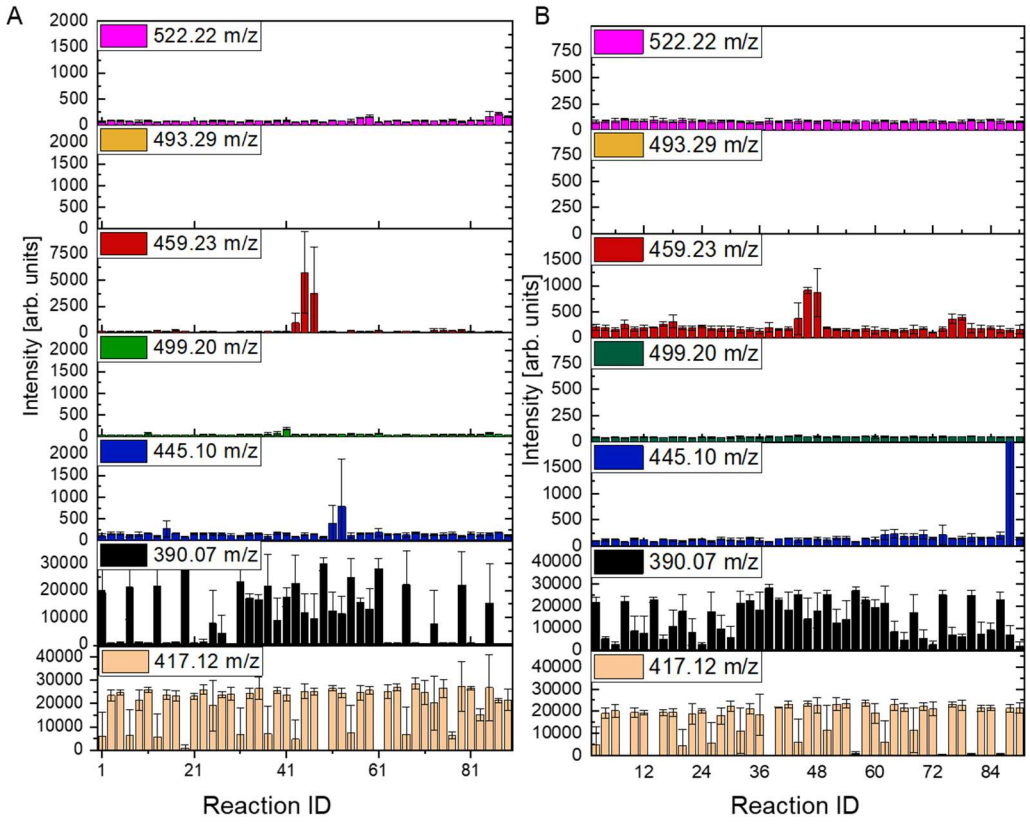

Figure 80: MALDI-MS results for Acid **10a** in 120 µM (A) and 20 µM (B) reaction concentration. The signal intensity is given for different mass signals, assigned by color code to the respective amide and acid.

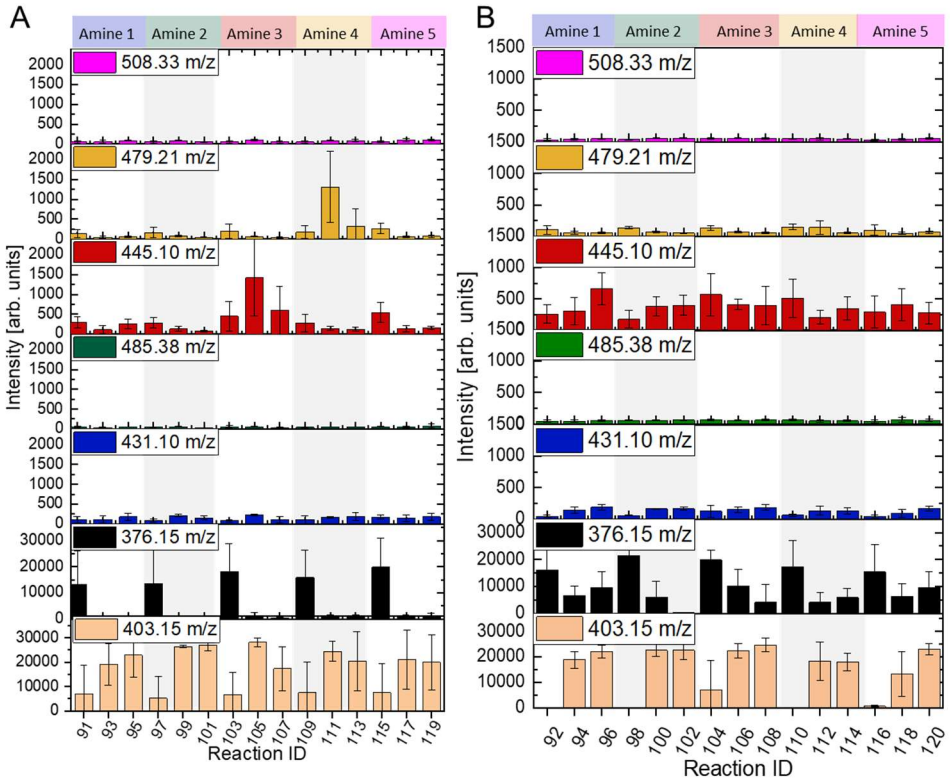

Figure 81: MALDI-MS results for Acid **10b** in 120 µM (A) and 20 µM (B) reaction concentration. The signal intensity is given for different mass signals, assigned by color code to the respective amide and acid.

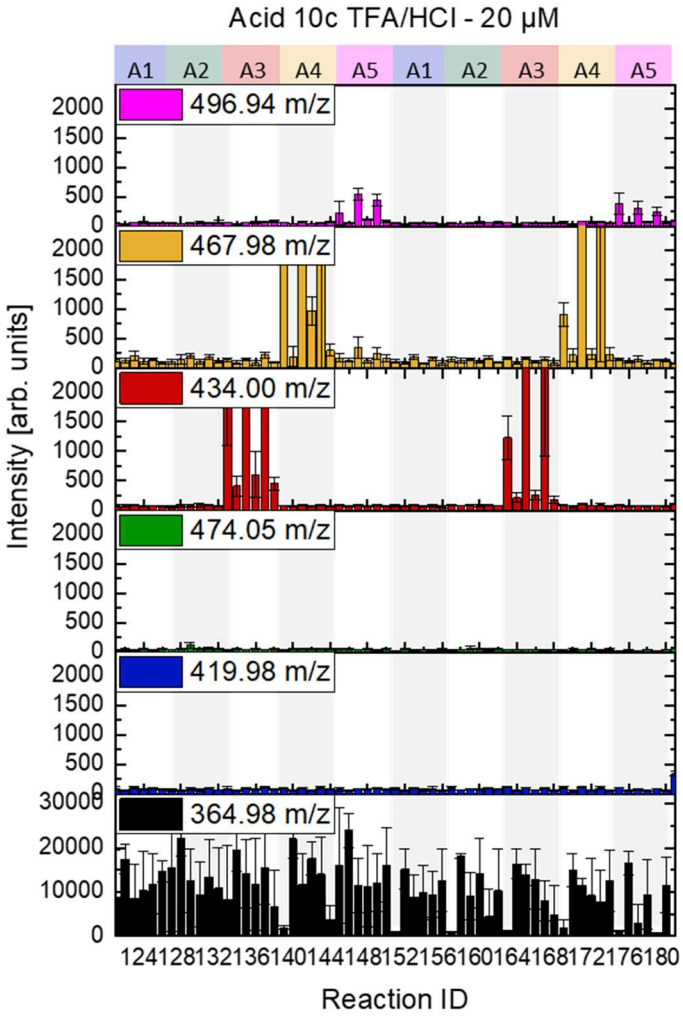

Figure 82: MALDI-MS results for Acid **10c** in 20 µM reaction concentration. The signal intensity is given for different mass signals, assigned by color code to the respective amide and acid.

Extraction with Environmental Impact (Chapter 3.2.2)

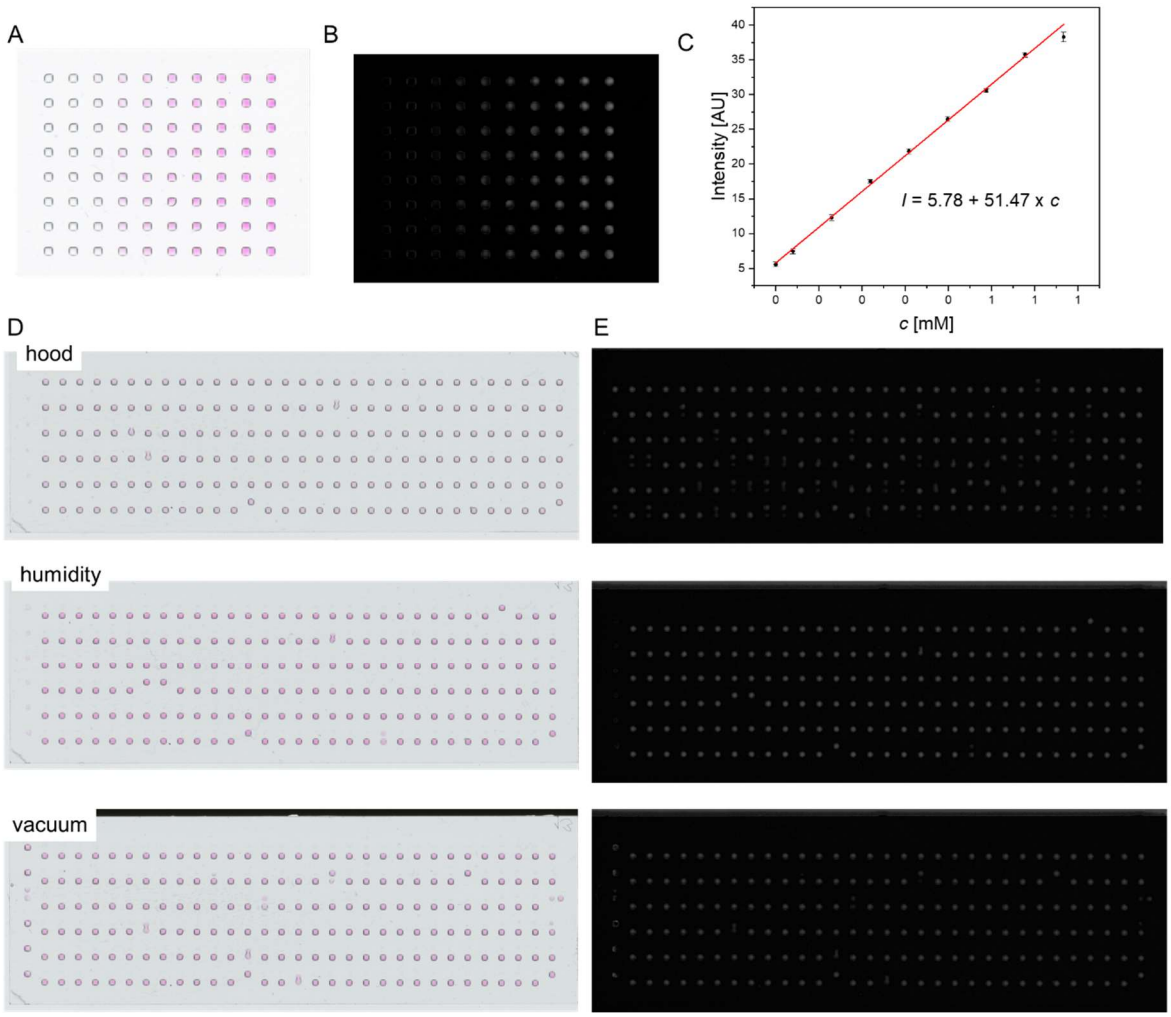

Figure 83: Calibration of Rhodamine B in 1-octanol as scanned (A), saturation value *S* from HSV stack (B) and the resulting calibration (C). D) Original scanned image and E) *S*-value and of a whole slide after extraction with 1-octanol with different environmental conditions.

Dip-Extraction (Chapter 3.2.7)

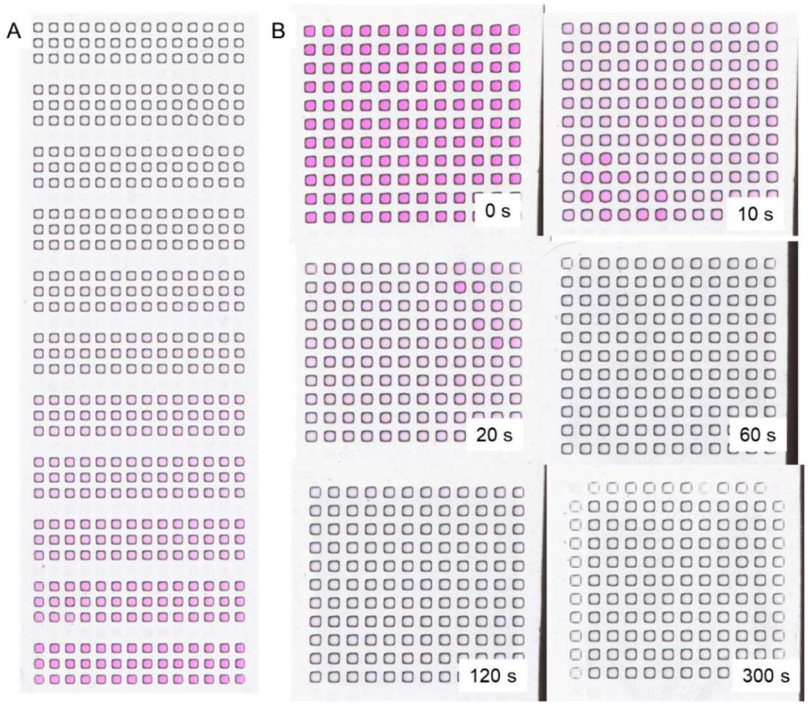

Figure 84: Scanned DMAs from Rhodamine B extraction from 1.00 mm square spots. A) Calibration curve with dilution series of Rhodamine B. B) 0.40 mM Rhodamine B solution after different extraction times. The spots have a side length of 1.00 mm. The DMA was imaged with a document scanner.

Curriculum Vitae

Personal Information

Name Janne Jasmin Wiedmann

Tel. (office) +49-721 608-24985

Languages

German (native)

English (proficient)

French (good commands)

Education

03/2020 – 07/2023 **PhD Candidate at Karlsruhe Institute of Technology,**

Karlsruhe, Germany, Institute for Biological and Chemical Systems

Topic: Miniaturized Synthesis

10/2017 – 12/2019 **Master Chemical Biology at Karlsruhe Institute of Technology,**

Karlsruhe, Germany

M.Sc. (final grade: 1.0, with distinction)

10/2014 – 09/2017 **Bachelor Chemical Biology at Karlsruhe Institute of Technology**,

Karlsruhe, Germany,

B. Sc. (final grade: 1.7)

09/2006 – 06/2014 Abitur

Hölderlin-Gymnasium, Lauffen am Neckar (final grade: 1.5)

Work Experience

12/2019 – 02/2020 Scientific Assistant

Karlsruhe Insitute of Technology, IBCS-FMS

Publication:

Nanoliter Scale Parallel Liquid-Liquid Extraction for High-Throughput Purification on a Droplet Microarray, J. J. Wiedmann, Y. N. Demirdögen, S. Schmidt, M. A. Kuzina, Y. Wu, F. Wang, B. Nestler, C.Hopf, P. A. Levkin, *Small* **2023**, *19*, e2204512.

Conferences:

02/2022 **SLAS2022 INTERNATIONAL CONFERENCE & EXHIBITION** (Boston, USA),

Conference Talk, winner of Tony B. Travel Grant

10/2022 **ELRIG DRUG DISCOVERY 2022** (London, UK),

Poster Presentation

Acknowledgments

First of all, I want to thank Prof. Pavel Levkin for giving me the opportunity to create this work under his supervision. Thank you for continuous constructive feedback and believing in me and my work. I really learned a lot about planning, performing and presenting scientific projects.

Next, I want to thank Prof. Carsten Hopf from CeMOS for the great collaboration during the last three years. Thank you for all MALDI-screenings performed in your lab as well as the feedback and discussions about my projects, also for the non-MALDI-related topics.

I also want to thank Prof. Stefan Bräse, the third member of my Thesis Advisory Committee, for discussions and feedback throughout the last three years.

Thanks goes also to the *Ministerium für Wissenschaft, Forschung und Kunst Baden-Württemberg* for the funding of this work, as well as to Dr. Maximilian Benz for establishing the base of this work.

In addition, I want to thank Dr. Thomas Maier and the whole Sanofi-Team for the collaboration, including the support of compounds used in this work as well as many fruitful discussions to solve the upcoming challenges in the project.

A huge thanks goes to Dr. Stefan Schmidt for coordinating all MALDI-MS-measurements at CeMOS performed for this work, as well as the evaluations of the results and many fruitful discussions during the planning phase and during the evaluation. I also want to thank Christian Croissant for our discussions about our projects.

For all evaluations in the beginning, the discussions about possibilities to evaluate my colorful spots for different projects and a great support after the GridScreener was established, I want to thank Marcel Schilling and Prof. Markus Reischl from the Institute for Automation and Applied Informatics.

Furthermore, I want to thank Konstantin Demir from Aquarray, for all the fruitful discussions, emergency-borrowing of pentenoic-acid and a huge amount of kind and helpful advices, even after leaving our group in the beginning of my PhD.

Big thanks go also to Sylvia Vanderheiden-Schroen and Dr. Patrick Hodapp from ComPlat for all the help with borrowed chemicals and your analytical devices.

I also want to thank the whole Levkin Lab for a great (working) atmosphere in the last years. I especially want to thank two former group members, Dr. Marius Brehm and Dr. Johannes Scheiger from whom I learned a lot when I joined the group about taking myself not too

seriously and that it is not my responsibility to solve everyone's problems, even if I did not realize it at that moment. Furthermore, I want to thank Yelda Demirdögen for starting a great new project, which I could continue to a joint publication. In addition, there goes a special thanks to Michelle Iwohn for final experiments, Jovana Topalovska for a lot of DMA slides and Michelle Christ for tests with the cells, as well as "my" students Viktor Guschin, Nils Holz, Pragya Parihar and Roxana Grömmer. I want to thank Dr. Anna Popova for a lot of biological advice as well as your support at my first flight and first conference talk in Boston. A huge thanks goes to the Chemistry-subgroup with Maximilian Seifermann and Julius Höpfner for all the discussions about upcoming problems and possible solutions. Thank you, Julius for the LC-MS measurements and Max for your feedback to this thesis.

Last but not least, I want to thank Mariia Kuzina for the last three and a half years, where we went together through all stages of our PhD, including moving a building. I learned a lot about scientific images from you and could always rely on your advice and help. Since the beginning, when due to the pandemics the only chance of social interactions was meeting colleagues at work, it was a precious gift to have a best friend sitting directly at the neighboring desk.

As this work is the result of a long journey, which started already before I came to this working group, I want to thank my former flat mate Johannes Wenz for a lot of advice and your contagious fascination about chemistry as well as my biology teacher Peter Spechtenhauser, who set the base for my interest and capability of scientific problem solving. For continuous support during all the time, I want to thank my parents and my sister. I learned a lot from all of you.

And finally, there goes an incredibly huge thanks to Lukas Langer, who was always there for me, with emotional and scientific support. This would have not been possible without you. Thank you for always believing in me.

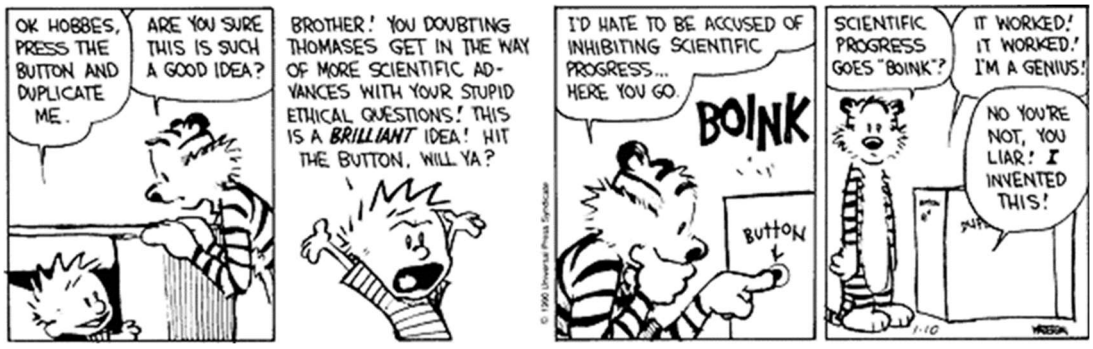

Bill Watterson: Calvin and Hobbes – Wednesday January 10, 1990.
Reprinted with permission of Andrews McMeel syndication.